ISSN 8755-6839

SCIENCE OF TSUNAMI HAZARDS

The International Journal of The Tsunami Society
Volume 27 Number 3 Published Electronically 2008

THE TSUNAMI SOCIETY
P. O. Box 2117, Ewa Beach, HI 96706-0117, USA,
WWW.TSUNAMISOCIETY.ORG

OBJECTIVE: The Tsunami Society publishes this journal to increase and disseminate knowledge about tsunamis and their hazards.

DISCLAIMER: Although these articles have been technically reviewed by peers, the Tsunami Society is not responsible for the veracity of any statement, opinion or consequences.

Submit manuscripts of articles, notes or letters to the Editor. If an article is accepted for publication the author(s) must submit a scan ready manuscript, a Doc, TeX or a PDF file in the journal format. Issues of the journal are published electronically in PDF format. Recent journal issues are available at:
http://www.TsunamiSociety.org
http://www.sthjournal.org

Tsunami Society members will be advised by e-mail when a new issue is available. There are no page charges for one paper per calendar year for authors who are members of the Tsunami Society. Permission to use figures, tables and brief excerpts from this journal in scientific and educational works is hereby granted provided that the source is acknowledged.

Issues of the journal from 1982 thru 2005 are available in PDF format at http://epubs.lanl.gov/tsunami/ and on a CD-ROM from the Society to Tsunami Society members. ISSN 8755-6839 http://www.sthjournal.org

Energy flux as a tool in locating tsunami secondary sources

Kowalik Zygmunt

Institute Marine Science, School of Fishery and Ocean Science, University of Alaska Fairbanks

Email:ffzk@ims.uaf.edu

Abstract

The sea levels recorded in the wake of Indian Ocean Tsunami of December 2004 and of the Kuril Island Tsunami of November 2006 show strong tsunami signal enhancement of the late arriving secondary waves. Using these tsunami events we demonstrate that sudden changes caused by higher energy pulses in the intermittent tsunami wave trains can be assessed by energy fluxes. Therefore, to delineate the regions of tsunami wave amplification and travel time we propose to use energy flux.

A series of numerical experiments defined in explicit way the bathymetric features which scatter tsunami signal towards ports, like Crescent City. Identification of the distant bathymetric features was achievable since the energy flux vector delineated the energy pathways that coupled distant bathymetric features to ports located thousands of kilometers apart. Calculations of the energy flux vector involves simple formulas based on two components of velocity and sea level. The maximum of the energy flux (which has no directional properties) can be evaluated from the sea level amplitude, hence both observed and computed sea level can be used for this purpose. The main task of this paper is to suggest that tsunami warning and prediction services should use numerical-hydrodynamical models with wider scope of physical processes by incorporating the energy balance equation into presently used tools.

Introduction

Along with the primary source of tsunami, sea level uplift due to earthquake, secondary sources due to scattering and refocusing, complicate the process of tsunami propagation. As amplified tsunami signals along ridges travel much slower than the direct signal from the primary source and scattered waves by seamounts arrive after the direct signal as well, the interaction between wave fronts generated by primary and secondary sources leads to difficulties in prediction of arrival time for the tsunami with the largest amplitude.

The importance of seamounts and islands in tsunami trapping and scattering was recognized early in tsunami research by Van Dorn (1970) when he analyzed sea level change caused by the 1957 tsunami recorded at Wake Island. The tsunami of 1964 recorded at Macquarie Island showed a maximum energy at 6 min period which Longuet-Higgins (1967) explained as a trapped long wave by the local bathymetry. A number of theoretical investigations of isolated island/seamount, ridge response to the incoming tsunami signal (see, Murty 1977, Mei, 1989 and Mofjeld et al., 2000 for summary) lead to conclusion that trapped motion can significantly modify the sea level and the currents in the island/seamount proximity. Spectra examinations of the sea level oscillations recorded during tsunami events (Loomis, 1966; Van Dorn, 1984; Rabinovich, 1997, Munger and Cheung, 2008, Horrillo et al., 2008) reveal standing waves and strong resonance amplification related to the local bathymetry and to the frequency window of the arriving tsunami waves.

To investigate tsunami wave amplification and travel time we propose to use energy flux. The source of the tsunami energy is the bottom displacement which defines the total potential energy. This energy constitutes only a small portion of the total seismic energy (Kajiura, 1981; VanDorn, 1984), for example the energy released by the 2004 Indian Ocean earthquake was estimated at 1.1×10^5 TJ (Terra joules) while the potential energy of tsunami was only (Kowalik et al., 2005a) 5.39×10^3 TJ. How the tsunami energy is delivered from the source to subdomains of the global ocean can be investigated through the energy flux pathways. Energy fluxes through major passages between oceans determine the leakage of tsunami energy from the source to the adjacent oceans (Munk, 1963). Along with such integral estimates the energy flux can be used locally to estimate inflow and outflow of the energy at the given geographical location.

We have tested this tool to reveal various aspects of tsunami physics (Kowalik et al., 2005a, b; 2007a, b; 2008). Energy flux, in contrast to the noisy tsunami sea level, reveals uniform behavior in time and space. In addition, it contains information about directionality of the signal which is important for identification of prominent bathymetric features as potential sources of tsunami wave refocusing. We will demonstrate application of the energy flux to generate charts of arrival time of the initial wave and the wave carrying the maximum energy.

Numerical models may serve, not only to produce the extent of coastal inundation and travel time charts to various locations on the coastlines, but also to assess sudden changes caused by higher energy pulses in the late arriving tsunami waves, so that proper decisions can be made on evacuation of people in real tsunami events, as well as for long term planning of the coastal zone development.

Global Tsunami Model and energy balance equation

We will describe and analyze results obtained on the energy flux through the global tsunami model (GTM) constructed and tested by Kowalik et al. (2005b, 2007a, b, 2008). The model includes a high order of approximation for the spatial derivatives (Imamura, 1996; Lynett et al., 2002; Mader, 2004). The boundary condition at the shore line is controlled by the total depth and can be set either to run-up or to the zero normal velocity. The model has been calibrated and tested through comparison to analytical solutions and to laboratory experiments as well.
After extensive testing and comparison, this model, with spatial resolution of 1 arc-minute, was applied to the tsunami of 26 December 2004 in the World Ocean from 80^0S to 69^0N. Because the computational domain included approximately 200 million grid points, a parallel version of the code was developed and run on a supercomputer. The finer spatial resolution of one arc-minute applied to the World Ocean (Kowalik et al. 2005a, b, 2007a,b) produces very small numerical dispersion even when tsunami waves travel over large distances. GTM due to its high spatial resolution sets the possibility of bringing a wider scope of physical processes into tsunami warning and prediction services.
Results of the GTM comparison against Indian Ocean Tsunami (IOT) recorded information showed quite surprising outcome, namely: a) travel time computation based on Fermat's principle may lead to errors in predicting tsunami arrival, b) passing through the narrows between continents a tsunami signal may reorganize from noisy into coherent wave pattern, and c) Coriolis force can play an important role in the global tsunami propagation.
Application of GTM to numerical simulation of the Kuril Islands tsunami (KIT) of November 2006 (Kowalik et al., 2008) highlighted the behavior of the transoceanic tsunami and the special conditions which cause tsunami enhancement at Crescent City. This investigation demonstrated that the tsunami delay and amplification at Crescent City were caused by both the redirection of tsunami energy over long distances of propagation and by amplification due to the local coastal morphology.
A conclusion from the global modeling applied to Indian and Pacific Oceans is that tsunami waves traveling over global oceans are strongly modified by bathymetry through scattering, refraction and trapping. Enhancement of tsunami amplitude is observed over major oceanic ridges which act as waveguides for tsunami waves, transferring the tsunami energy from thousands kilometers apart without noticeable dissipation. Large seamounts scatter tsunami energy refocusing the tsunami signal more efficiently toward a particular location.
Proposed tools for location of the secondary sources and travel times are based on the energy flux for the non-linear shallow water equations. Equations of motion along E-W and N-S directions (Kowalik and Murty, 1993),

$$\rho\,(\frac{\partial u}{\partial t}+u\frac{\partial u}{\partial x}+v\frac{\partial u}{\partial y})=-g\rho\,\frac{\partial \zeta}{\partial x}-\tau_x^b/D \qquad (1)$$

$$\rho\,(\frac{\partial v}{\partial t}+u\frac{\partial v}{\partial x}+v\frac{\partial v}{\partial y})=-g\rho\,\frac{\partial \zeta}{\partial y}-\tau_y^b/D \qquad (2)$$

and equation of continuity,

$$\frac{\partial}{\partial x}uD + \frac{\partial}{\partial y}vD + \frac{\partial \zeta}{\partial t} = 0 \tag{3}$$

are used to construct the energy conservation equation. In the above set of equations, u and v are horizontal components of the velocity vector, directed along E-W and N-S respectively, ζ is the sea level variation around mean-sea level, τ_x^b and τ_y^b are the components of the bottom stress vector, expressed as $\tau_x{}^b = ru\sqrt{u^2+v^2}$, $\tau_x{}^b = rv\sqrt{u^2+v^2}$, r is the bottom friction coefficient equal to 0.003, ρ is the density of water, and g is the gravity acceleration. The total depth is $D = H + \zeta$. Here H is the depth measured from the mean-sea level (MSL). In order to derive energy balance equation let us multiply eq.(1) by Du, eq.(2) by Dv, and eq.(3) by $\rho g\zeta$. Adding the resulting equation on either side, we arrive at

$$\frac{1}{2}\frac{\partial}{\partial t}[\rho D(u^2+v^2) + \rho g\zeta^{\,2}] + \frac{\partial}{\partial x}\{\rho uD[(u^2+v^2)/2 + g\zeta\,]\} + \frac{\partial}{\partial y}\{\rho vD[(u^2+v^2)/2 + g\zeta\,]\} = -\tau_x^b u - \tau_y^b v \tag{4}$$

The various terms in the above equation can be defined as follows:

1. $e_k = \rho D(u^2+v^2)/2$ denotes the surface density of the kinetic energy; it is defined by the velocity and the total depth.

2. $e_p = \rho g\zeta^2/2$ denotes surface density of the potential energy; it is defined by the sea level oscillations around MSL.

3. The second and the third terms in eq.(4) represent the components of an energy flux vector. This vector characterizes the flux of energy through a unit width surface extended from the ocean surface to the bottom. The components of the vector along latitude and longitude are

$$\mathbf{E_h} = \{\rho uD[(u^2+v^2)/2 + g\zeta], \rho vD[(u^2+v^2)/2 + g\zeta]\} \tag{5}$$

4. The tsunami energy dissipation takes place through the bottom stress: $-\tau_x^b u; -\tau_y^b v$.

The full definition of the energy flux vector (eq.5) includes two terms related to potential and kinetic energy. The flux of the kinetic energy $(u^2+v^2)/2$ in tidal computations and measurements is very small as compared to the flux of the potential energy (Henry and Foreman, 2001). Calculations in the Indian and Pacific Oceans show that the above conclusion is valid for tsunamis as well.

The first order approximation (possibly not valid in the very shallow water)

$$\mathbf{E_{h1}} = \{E_{hx}, E_{hy}\} = \{\rho g H u\zeta, \rho g H v\zeta\} \tag{5a}$$

will serve to describe the tsunami energy flux from the source to various locations.
To demonstrate the concept let's consider the progressive wave along the x-direction (Kowalik and Murty, 1993) for the sea level

$$\zeta = \zeta_a \cos(\omega t - \kappa x) \tag{6}$$

and for the velocity

$$u = \zeta_a \sqrt{\frac{g}{H}} \cos(\omega t - \kappa x) \tag{7}$$

Introducing above expressions into eq. (5a) for the energy flux and neglecting the kinetic energy term, the energy flux reads (Nekrasov, 1992)

$$E_{h1} = \frac{1}{2}\rho g \sqrt{gH}\,\zeta_a^2 [1 + \cos 2(\omega t - \kappa x)] \tag{7a}$$

The energy flux of the progressive wave is always positive and it changes from zero to the maximum value $\rho g \sqrt{gH}\,\zeta_a^2$. Its period of propagation is 2 times shorter than that of the sea level or velocity. It is aligned with the direction of propagation, but not with the direction of the velocity which can be positive and negative. Thus plotting the velocity would not yield the same pattern of directions as the energy flux will show, since velocity (eq.7) changes from positive to negative values.
The above formula for the energy flux can be also used to track the maximum energy flux. To achieve this we assume that u is normal to the wave front and when $\omega t - \kappa x = 0$ it follows from eq.(7a) that the energy flux is at maximum. For such simplified case the energy flux is expressed as

$$E_{h2} = \rho g \sqrt{gH}\,\zeta_a^2 \tag{7b}$$

This formula estimates the energy flux by the sea level only. Hence, along with numerical solutions which require both sea level and velocity for the full calculation using eq.(5a) we can apply observational sea level from buoys or coastal gauges (Koshimura et al., 2008) to calculate energy flux by eq.(7b). Unfortunately eq.(7b) estimates the energy flux maximum only, it does not defines the components of the energy flux vectors as eq.(5a) does, therefore it has no directional properties which are important for the identification of the tsunami energy sources.

Simple experiment – continuous source of tsunami waves

Consider a domain in proximity of the Crescent City (CC) as depicted in Fig. 1.
From the western open boundary a continuous wave train of 20 min period and 10 cm amplitude is forced into the domain. At the northern and southern open boundaries the radiating conditions are set. The energy balance equation will be considered inside the box depicted by dashed lines.

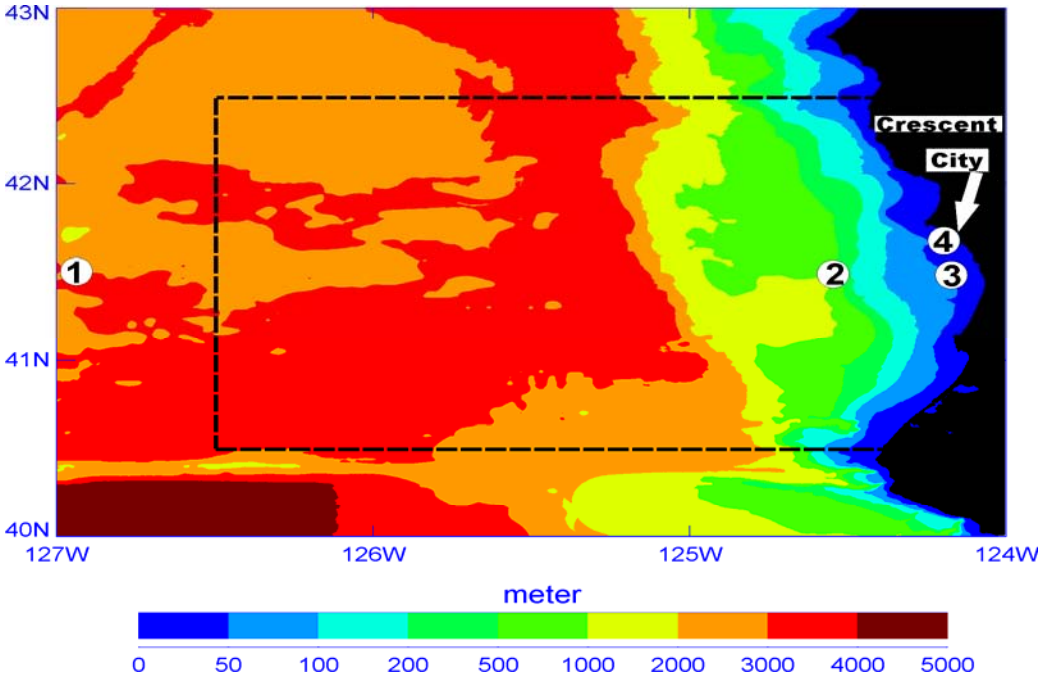

Figure 1. Bathymetry in proximity to Crescent City. Dashed lines denote box for considering energy fluxes. Points 1-4 indicate locations of numerical gauges where sea level and velocity are recorded.

The full stationary state inside the domain has been reached after about 20 periods of incoming wave, although the velocity and sea level are close to the stationary state after approximately 3 periods (cf. Fig.2). The time-history of velocity (east-west component) and the sea level is plotted in Fig. 2. Point 1, located in proximity of the open boundary (depth=2970m), has maximum particle velocity of 0.84cm/s and sea level amplitude of 9.7cm. Waves are strongly amplified in the nearshore region (in point 4 the depth is 0.7m). From point 1 to point 4 the velocity is amplified approximately 155 times while the sea level only 12 times.
The conservation of energy (eq.4) states that in every grid point the change in time of the total energy (i.e. sum of kinetic and potential energy) should be balanced by the energy fluxes (through the walls of the elementary volume $D\delta x\delta y$) and dissipation. If the sea level and velocity change is stationary in time (i.e. repeats itself over wave period) the integration over the wave period should lead to the conclusion that the total energy does not change from one period to the next, and therefore the energy balance will require that the fluxes of energy in/out of the domain should be balanced by the dissipation.

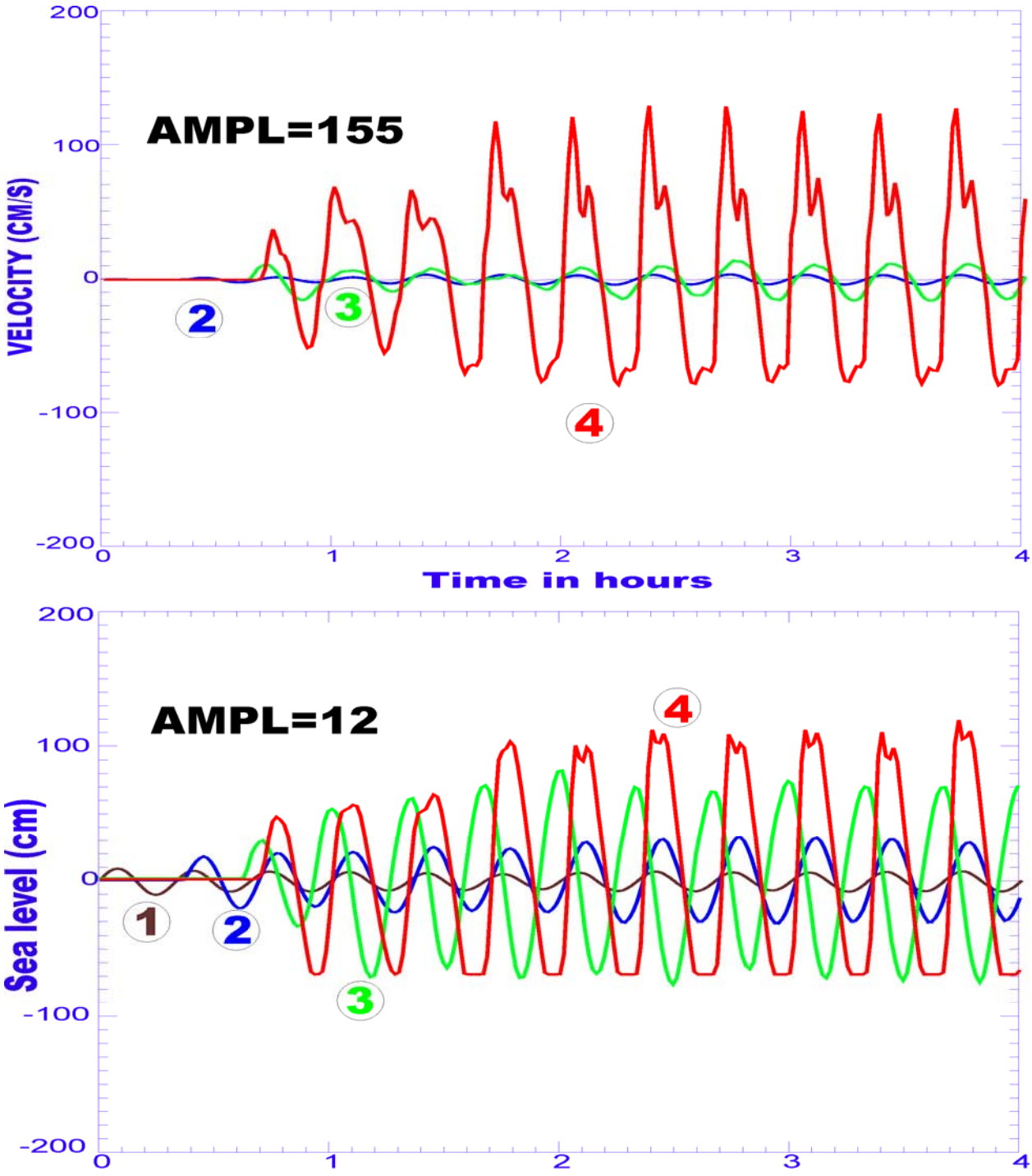

Figure 2. East-west velocity and sea level as a function of time. Recording points are depicted in Fig.1. Amplification coefficient (maximum value at P.4 divided by value at P.1) for velocity (155) is much larger than the amplification for the sea level (12).

The energy inside the domain after 20 periods is quite steady. The double precision calculation shows that the average over 20 min period for the total potential energy (EP) is EP= 4.67579×10^{19} watts, while for the kinetic energy (EK) is EK=4.55895×10^{19} watts. Thus the potential and kinetic energy is approximately equal (equi-partitioned), but a very small discrepancy points towards slight dominance of EP.

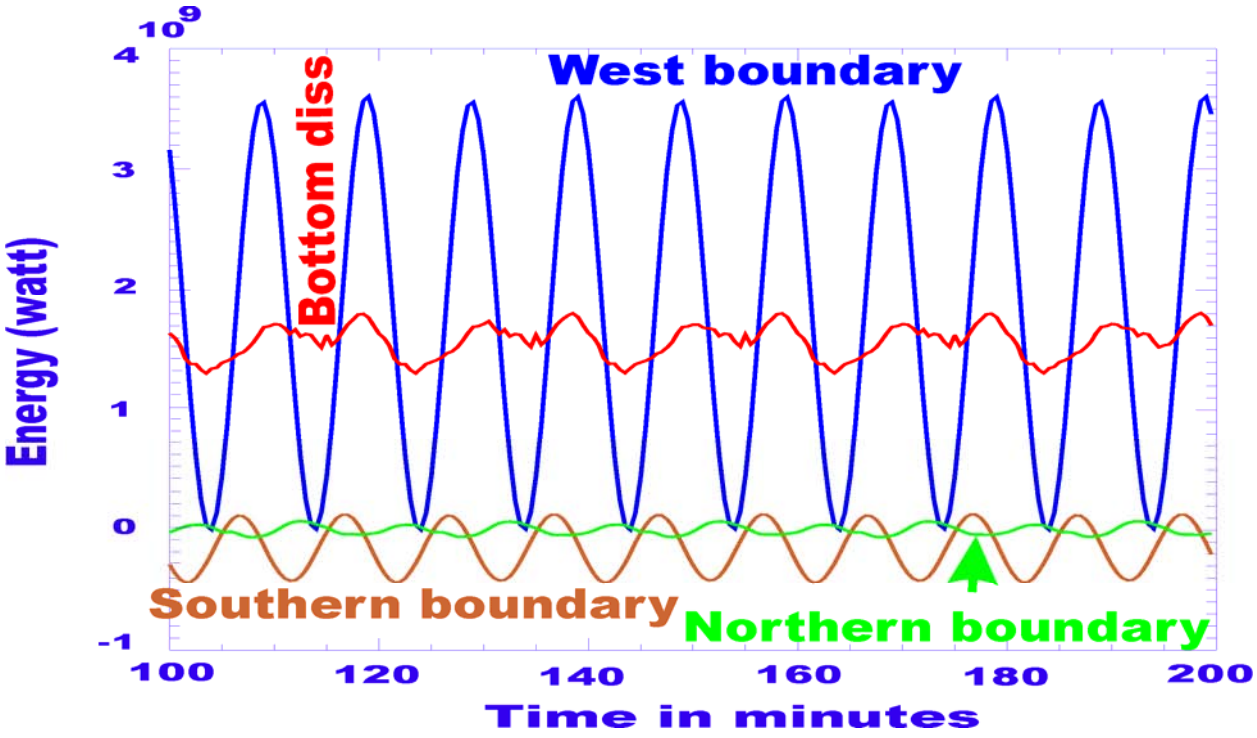

Figure 3. Energy balance for the 20 minute period incident wave in the control box surrounding Crescent City shelf. Energy influx through the western boundary is not completely balanced by the outflowing energy from the northern and southern boundaries and the energy dissipated by the bottom friction.

To investigate the energy fluxes through the open boundaries and the dissipation due to the bottom friction, the major constituents of the energy balance are plotted for 5 periods (between period 25 and 30) in Fig. 3. The inflowing potential energy through the western face of the box, and the outflowing energy through the northern and southern boundaries are periodical in time with the period of 10 min (since amplitude is squared, the period for energy is two times shorter). The bottom dissipation term has the same periodicity but it has unequal amplitudes during each half of the 20 min period wave. The run-up and rundown shown in Fig.2 is the cause of this inequality. The average energy over period (after computed 20 periods) is approximately constant. The inflowing energy (EI) is equal to 1.87162×10^{9} watts and the outflowing energy is =-1.56555×10^{8} watts. The energy dissipated due to the bottom friction is equal to - 1.61626×10^{9} watts and plays the main role in the balancing inflowing energy. The outflowing and dissipated energy (EO) result in -1.77282×10^{9} watts, thus not completely

balancing the inflowing energy. The difference between these two numbers is small; nonetheless it introduces an important question, namely what is happening to the undissipated inflowing energy since the total energy inside the control box is constant, but due to undissipated energy ought to grow in time. This problem is discussed in detail in the Appendix.

Energy flux application for tsunami physics

To demonstrate that the energy flux will be a valuable addition to the science of tsunami hazards we focus on the results obtained by application of the global tsunami model (GTM). A GTM was applied to investigate the Indian Ocean Tsunami (IOT) of December 26, 2004 and Kuril Islands Tsunami (KIT) of November 15, 2006 (Kowalik et al., 2005a,b, 2007a,b, 2008; Horrillo et al., 2008). The major result from these computations was an enhanced understanding of the tsunami wave trains origin arriving at the distant locations sometimes a few hours after an initial (forerunner) wave. Tsunami waves traveling over the global ocean are strongly modified by bathymetry through scattering, refraction and trapping. Enhancement of tsunami amplitude was observed over major oceanic ridges which act as wave guides for tsunami waves, transferring the tsunami energy from thousands kilometers apart without noticeable dissipation (Koshimura et al., 2001; Kowalik et al., 2005a, 2007b, 2008; Titov et al., 2005; Lay et al., 2005; Hirata et al., 2005).

The GTM for the IOT demonstrated how tsunami propagated over the entire World Ocean. In the Indian Ocean the tsunami properties were related to the source function, i.e., to the magnitude and direction of the sea bottom displacement. The leakage of energy into the Atlantic Ocean (between Africa and Antarctic) showed a unidirectional pattern since the energy was pumped into this domain through the directional properties of the source function. Nonetheless both observations and models showed strong tsunami in Pacific as well. The main questions were: How the energy was redirected into Pacific? What are mechanisms for redirection and how much energy entered the Southern Pacific Ocean?

To answer above questions, an energy flux is considered (Kowalik et al., 2005b, 2007a) through the three cross-sections located between Antarctica and the major continents. The cross-section (blue color in Fig. 4) along the longitude 20^{o}E from Antarctica to South Africa (AS) shows the time variation of the energy flux between Indian and Atlantic Oceans (eastward is the positive direction). This flux remains negative for the entire period of 50 h, thus confirming that the inflow is directed into the Atlantic Ocean. On the other hand, the energy flow through a cross-section along 140^{o}E (green color) extended from Antarctic to Australia (AA) is at all times positive (from the Indian to Pacific Oceans). The flux through the cross-section located between South America and Antarctica at 70W (red color), reveals a small inflow from the Atlantic into the Pacific.

Fig. 4 clearly demonstrates that the magnitude and the time variability of energy fluxes through cross-sections AA and AS are quite different in character. The flux passing AS has a large value and the maximum energy inflow to the Atlantic is located close to the initial wave front, even though the first arriving signal is not related to the maximum energy.

The energy flow into the Atlantic is a result of the source orientation. The energy flow through AA demonstrates that tsunami arrives to this cross-section about 10 h from the onset of the earthquake; it initially has small amplitude which slowly increases in time from 18 to 21 h to achieve a few maxima.

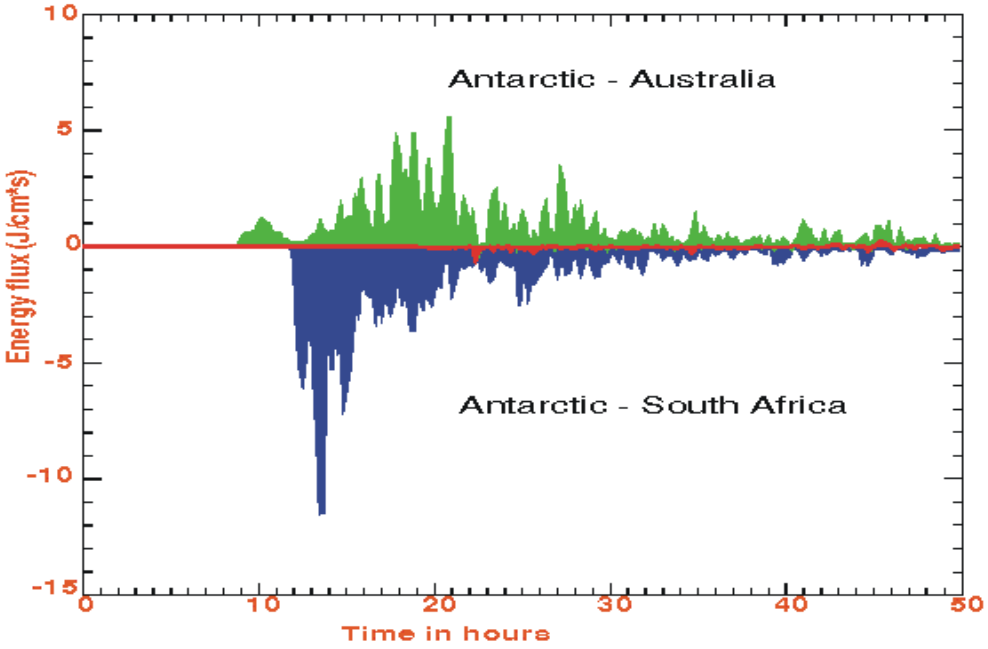

Figure 4. Energy flux through the cross-sections located between Antarctic and major continents. Along 20E from Antarctic to South Africa (AS), blue color, along 140E, from Antarctic to Australia (AA), green color, along 70W from South America to Antarctic, red color (after Kowalik et al., 2005b).

Analysis made by Kowalik et al., (2005b, 2007b) demonstrated that the maxima from 18 to 21 h in Fig. 4 were related to the energy flux arriving by the various routes from the Indian Ocean. The arrival time of these signals depends on the depth and on the traveled distance. Signals which travel from the generation area to the section AA through the deep ocean travel faster, in about 10 h, but transfer less energy. The large inflow of energy shown in Fig. 4, is related to the reflected signals off the Seychelles, Maldives and Africa, and to a slow wave which traveled along ridges that was originated through reflections in the Bay of Bengal. To compare the total energy flux entering Pacific and Atlantic Oceans over the first 50 h of process, the energy fluxes given in Fig. 4 have been integrated in time. The total energy leakage into the Pacific Ocean is approximately 75% of the total leakage to the Atlantic Ocean. This large value is quite remarkable considering that the source directs energy into the Atlantic Ocean and the energy is re-routed into the Pacific by reflections. As pointed out by Murty et al., (2006), the Indian Ocean resembles an elliptical shape which has a tendency to multiple reflections and focusing. Fig. 4 is closely related to the time-history of the tsunami energy in the Indian Ocean. Van Dorn (1984) and Candella et al.(2008) deduced from the coastal observations that the tsunami energy

has an exponential decay in time. The energy leakage to the Atlantic and Pacific (Fig. 4) shows a similar pattern in time. After an initial build up, the energy started to decay in time but the decay pattern is dominated by strong energy pulses, due to multiple reflections and energy trapping along the ridges, islands and seamounts.

The energy time-history in the oceans adjacent to the Indian Ocean will be even more complicated due to the fact that the tsunami temporal and spatial variability is restructured while tsunami travels through the narrow passages between oceans (cf. Kowalik et al., 2007b, Fig.10.11, p. 109). The tsunami signals in the Northern Atlantic and Southern Pacific have been strongly reorganized into coherent wave trains after passing through the narrows between Africa and South America, and Australia and Antarctica. To the lesser extent the same process was taking place for the tsunami entering into the Atlantic (between Africa and Antarctica) and for the waves entering the Pacific from the Atlantic (between South America and Antarctica).

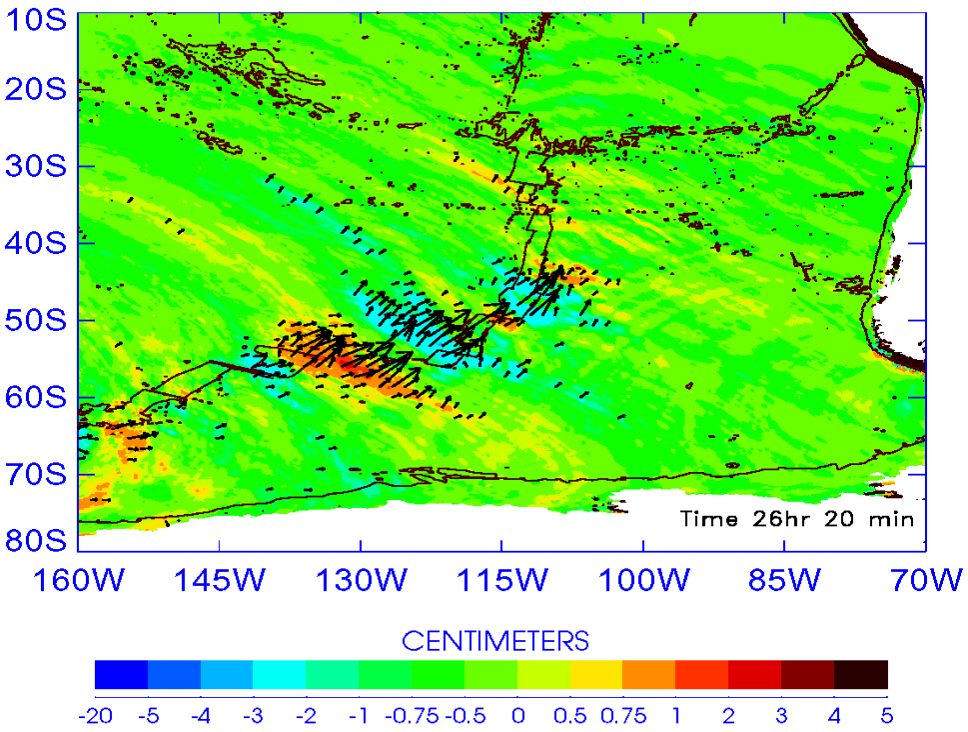

Figure 5. Energy flux vectors over the South Pacific Ridge at time 26h 20min from IOT onset. The colors denote the sea level. The dark-brown lines denote the ridge depth - 3000m depth contour.

The energy flux vectors in Fig. 5 demonstrate that the slower signal travels along oceanic ridges and transfers more energy. In this figure, the energy flux vectors are shown in the south-western part of the Pacific Ocean. The larger tsunami amplitudes are located above the oceanic ridge and the energy flux vector is directed along the ridge (notice that vector does not change direction over positive or negative sea level). This small group of higher amplitude waves does not belong to the first tsunami signal to arrive in this region. Its average wavelength is about 1350 km, as the depth of the ridge is close to 3 km, the wave period is about 2 h. The tsunami enhancement is partly related to the presence of the South Pacific Ridge but this strong and coherent group of

waves was generated out of the chaotic signal while passing through the strait between Australia and Antarctic (Kowalik et al., 2005a, b; 2007b).
In the wake of Kuril Islands Tsunami (KIT) of November 15, 2006, the sea level at Crescent City (CC) initially changed up to 20 cm and 2-3 hours later the highest wave of about 90 cm amplitude was recorded. Numerical experiments using GTM (Kowalik et al., 2008) identified the bathymetric features which scatter the tsunami signal towards CC via the Mendocino Escarpment (Fig. 6). This escarpment seems to be efficient in delivering enhanced tsunami energy if the approaching tsunami signal travels from the west along the escarpment.

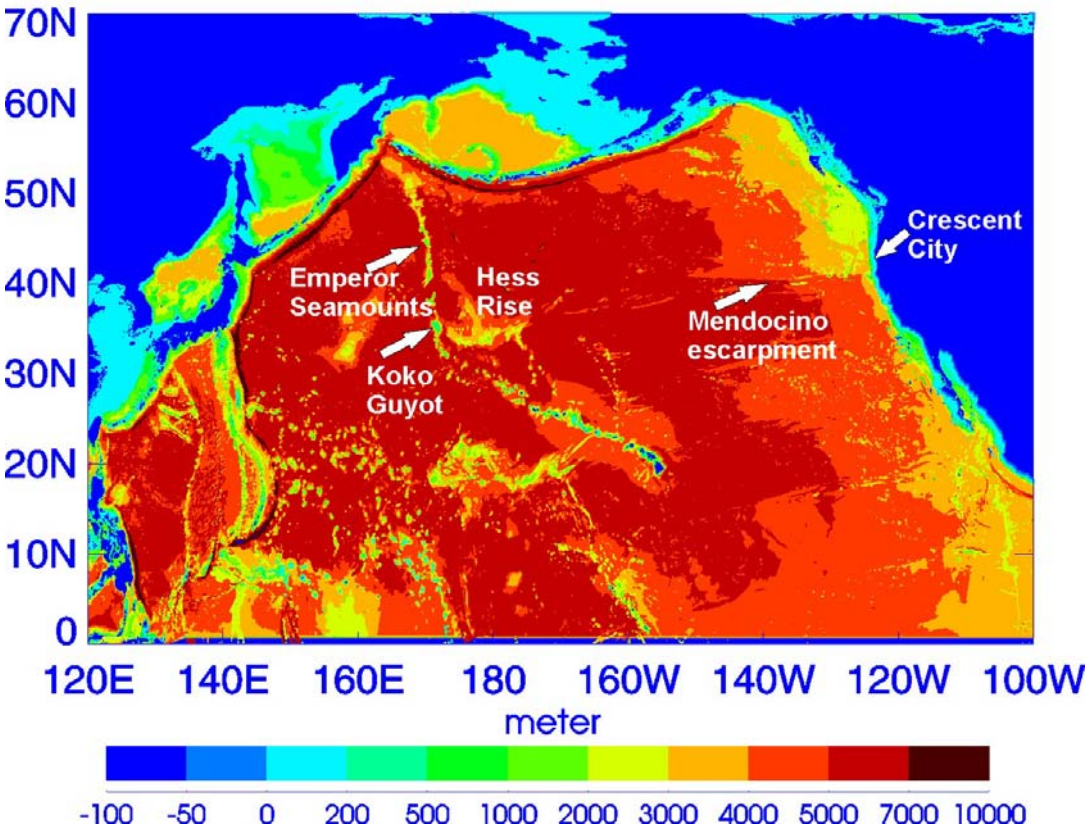

Figure 6. Bathymetry based on the one-minute grid. Shown are main bathymetric features important for the tsunami arriving at Crescent City.

To investigate the pattern of the energy trapped over Mendocino Escarpment the energy flux was used. A simple experiment was performed to demonstrate the wave trapping by this bathymetric feature. Three waves of 16 minutes period each and 10 cm amplitude were sent towards the west coast of North America from the open boundary located at 150W (Fig. 7, left panel). In Fig. 7 (right panel) the wave pattern 160 minutes later is shown. The energy flux vectors in these figures demonstrate the strong local amplification of energy during wave propagation towards CC. The wave amplitude shows a corresponding strong local amplification as well. The wave front curvature focuses the energy flux vectors slightly up north from the Mendocino Escarpment.

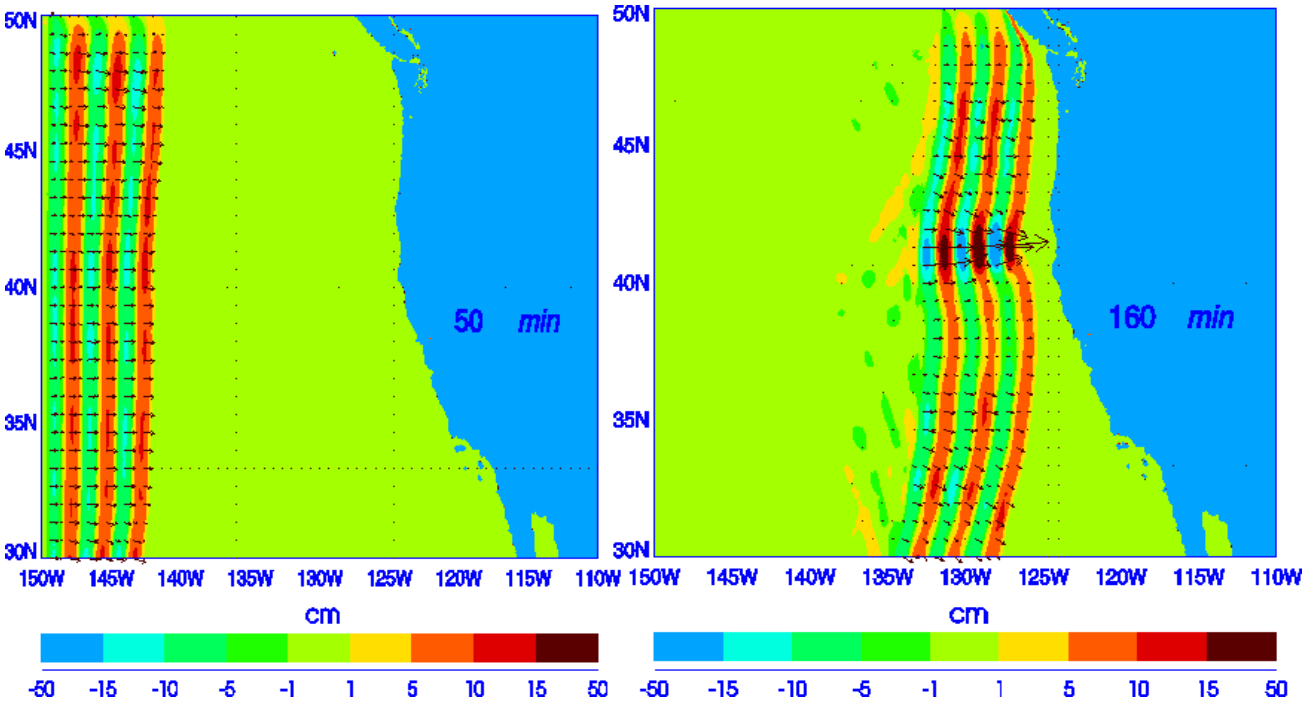

Figure 7. Three waves of 10 cm amplitude and 16 min period travel parallel to the Mendocino Escarpment. Amplitude given by colors. Vectors denote energy flux (after Kowalik et al., 2008a)

The time-history of the energy flux traveling towards CC during the Kuril Islands tsunami of 2004 was analyzed by considering a similar box as in Fig. 1. The box around CC was constructed as follows. The west boundary is located at 129W, the north boundary at 44.5N, the south boundary at 39.5N and the east boundary is on land. The time dependent energy flux was averaged over the length of each boundary.

The results given in Fig. 8 show two distinct pulses of energy crossing the western face of the box towards CC. Within the second pulse, 2 maxima occur separated by 20 minutes time interval. It is interesting to see that there is very little reflected energy coming back across the faces of the box. This must mean that most of the incident energy is dissipated by the near shore bottom friction.

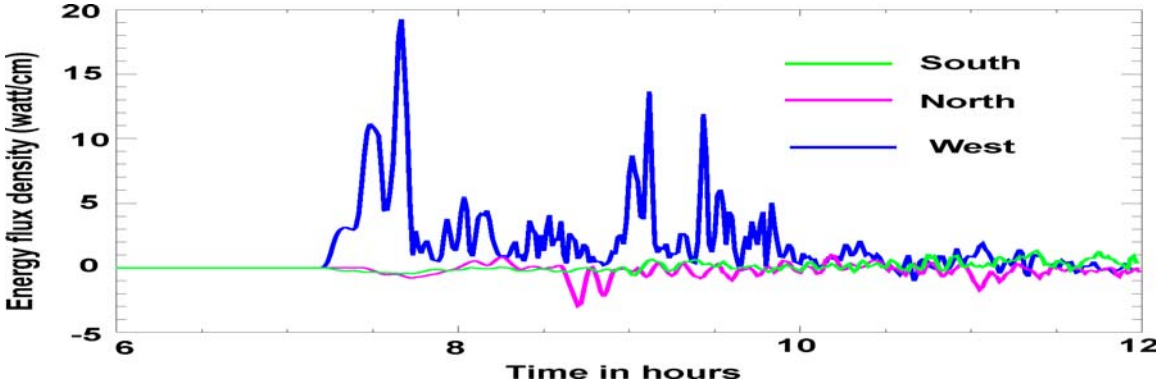

Figure 8. Energy flux through the western (blue), northern (red) and southern (green) walls of a 5 degree box around Crescent City (adapted from Kowalik et al., 2007a).

Energy flux through the faces of the box around CC can be easily applied to pinpoint the source of the second wave packet. First, we simply remove from the bathymetry the Hess Rise by setting it to the depth of 5000 m. Next, the Koko Guyot is removed in the same manner (both located at the southern end of Emperor Chain, see Fig. 6).

In Fig. 9 the energy flux crossing the western wall is plotted; in the upper panel the Hess Rise is removed but the Koko Guyot stays unchanged and in the lower panel the Koko Guyot has been removed while the Hess Rise remains unchanged. For comparison the energy flux across the western face from Fig. 8 is also given.

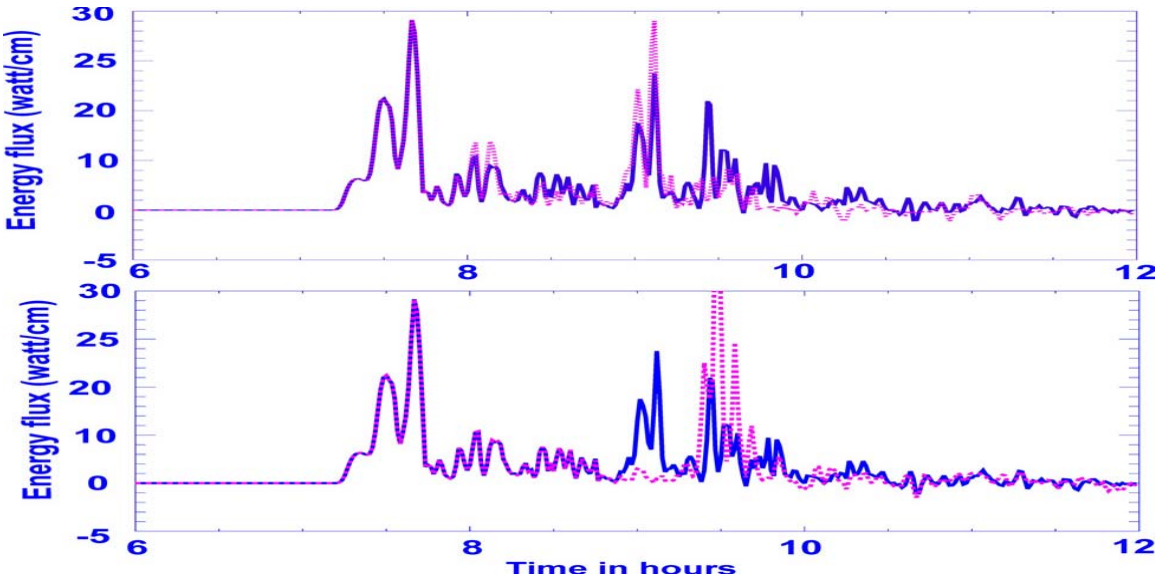

Figure 9. Energy flux through the western wall of a 5-degree box around Crescent City. Blue line: regular bathymetry. Red line: a) upper panel: Hess Rise is removed from bathymetry; b) lower panel: Koko Guyot is removed from bathymetry (adapted from Kowalik et al., 2008a)

The absence of Koko Guyot resulted in a restructuring of the energy flux through the western face of the box in such a way that the first maximum in the second wave group practically disappeared (Fig. 9, lower panel). The second maximum in this later arriving wave group, as the upper panel shows, is related to the Hess Rise. The absence of the Hess Rise leads to energy amplification from the Koko Guyot. As the first group of waves in Fig. 9 does not change in the above experiments we can also conclude that the first group of waves to arrive at CC must travel a route unobstructed by either Koko Guyot or the Hess Rise.
The immense influence of the Koko Guyot on tsunami signal scattering is due to its size and strong contrast between shallow and deep waters. It rises from the depth of 4750 m to within 250 m of the ocean surface (Davies et al., 1972).

Identification secondary sources by tracking energy flux in the Northern Pacific

We have used energy fluxes to elucidate the amplification processes during KIT propagation towards Crescent City. We continue investigation of the same tsunami to work out an approach for identification of the sources of the high amplitude secondary signals and to illustrate the

time delay between initial tsunami wave and secondary signals. The bathymetric features which are important for tsunami arriving at Crescent City have been described in Fig. 6.

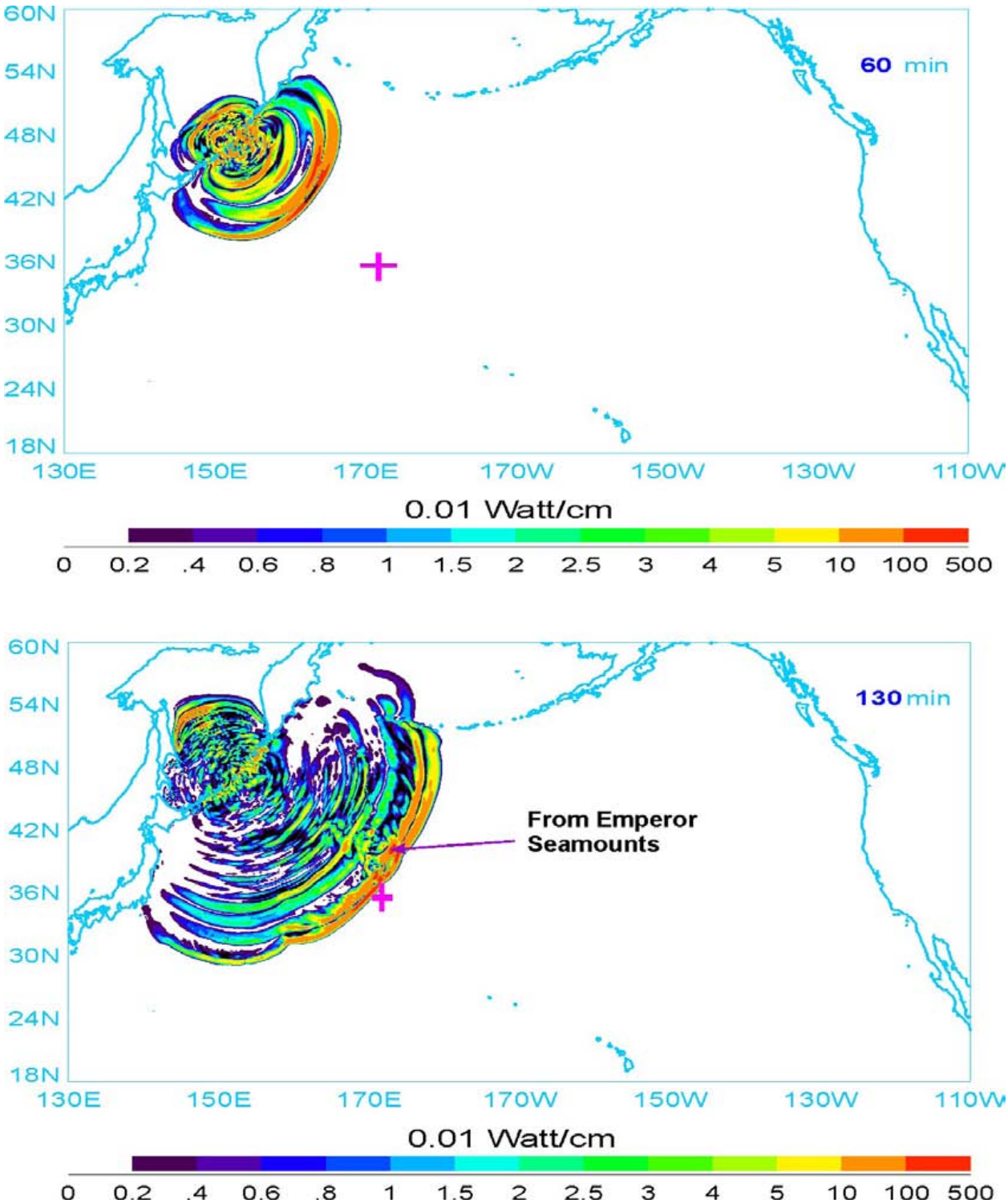

Figure 10. Energy flux contours, 60 min (upper panel) and 130 min (lower panel) after tsunami onset. Red plus marker points to location of Koko Guyot seamount.

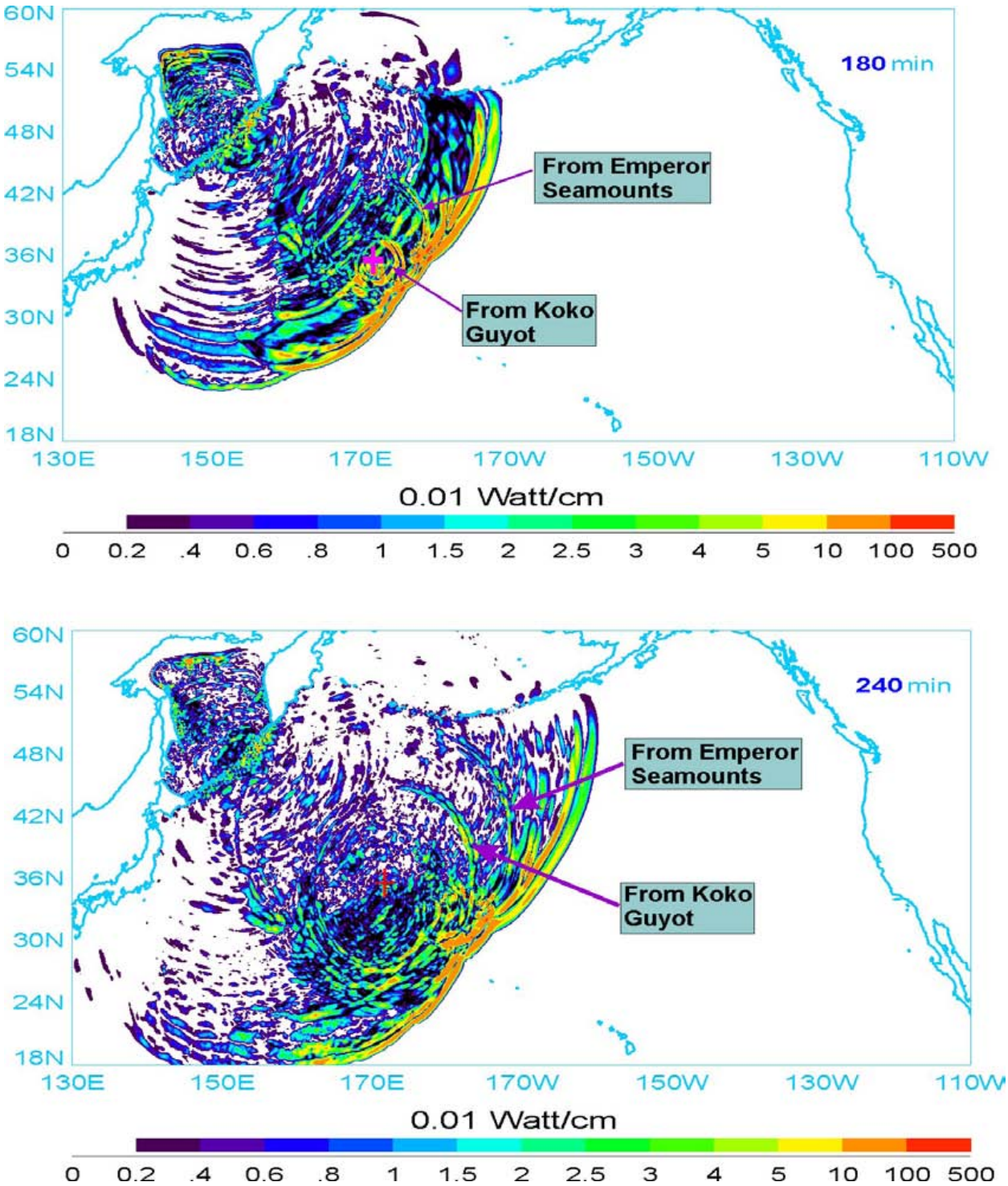

Figure 11. Energy flux contours, 180 min (upper panel) and 240 min (lower panel) after the tsunami onset. Two signals of higher energy have been identified as scattered from the Emperor Seamounts and the Koko Guyot. Note that only the second stronger front is centered on the Koko Guyot. Red plus marker points to location of the Koko Guyot seamount.

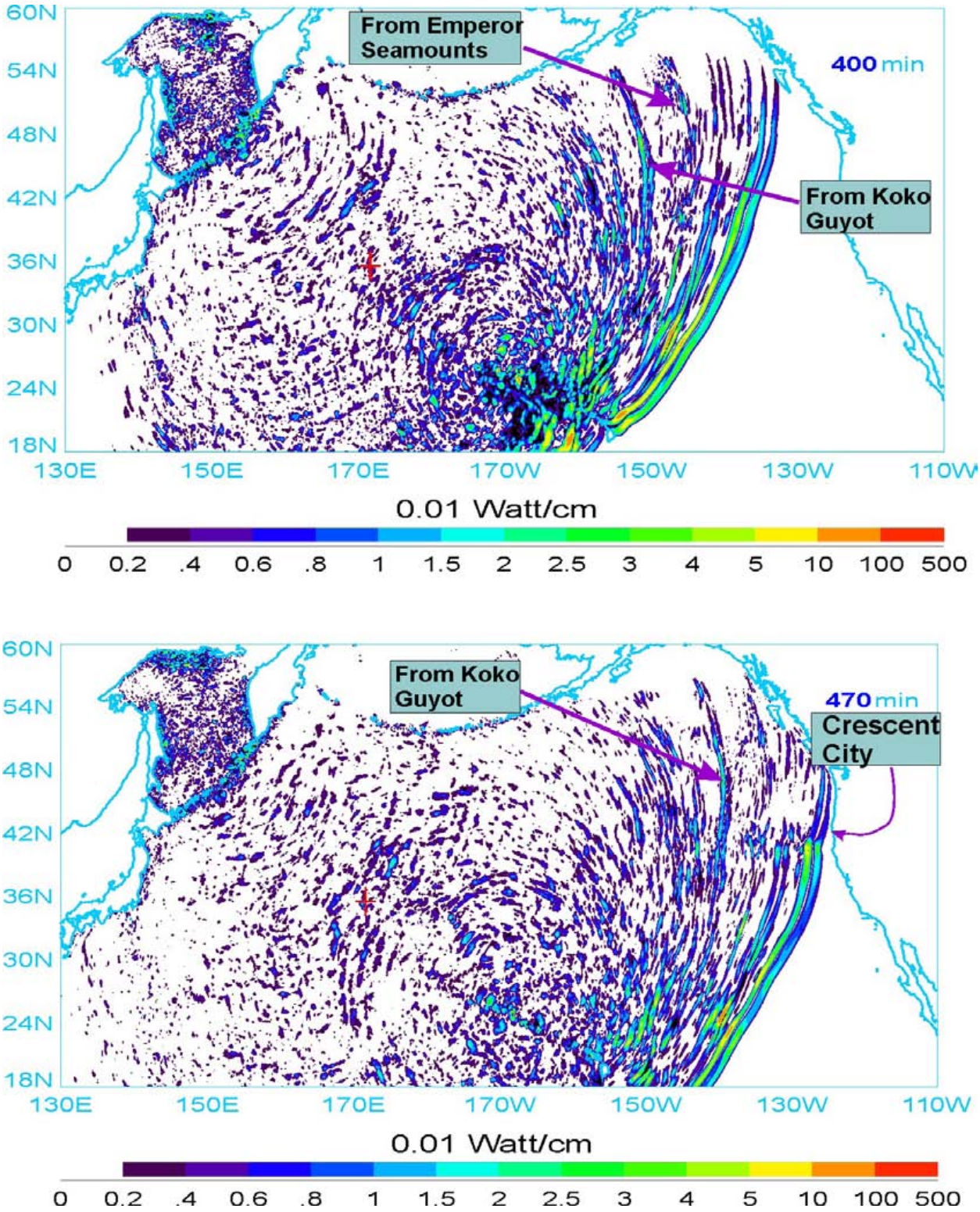

Figure 12. Energy flux contours, 400 min (upper panel) and 470 min (lower panel) after the tsunami onset. Note: a) The signals from Emperor Seamounts have dissipated, b) The first wave arriving to the proximity of Crescent City shows enhancement by the Mendocino Escarpment. Red plus marker points to location of the Koko Guyot seamount.

To further identify important stages in the KIT development the time history of energy flux contours is given in Figs. 10-12. The contours are given by $\mathbf{E}_c = \sqrt{E^2_{hx} + E^2_{hy}}$. Here the energy flux components are defined by eq.(5a). Sixty minutes after the tsunami onset (Fig.10, upper panel) the tsunami front in the Northern Pacific shows two closely spaced maxima. Notice that these maxima are related to the initial wave's positive and negative amplitudes. The two maxima can be easily tracked in all figures up to the arrival at Crescent City (Fig. 12, lower panel).

Important bathymetric feature in tsunami scattering is Emperor Seamount chain, its influence is depicted 130 min after the tsunami onset by distortion of the primary and secondary wave fronts.

To identify the Koko Guyot as an important bathymetric feature, we plot in Fig. 11, upper panel, the energy flux contours immediately following passage of the main energy lobe past Koko. Note that only the second front is centered on the Koko Guyot, the first front has been generated by the Emperor Seamount Chain and it is not centered on Koko Guyot. Further time history given in Fig. 12 shows that the energy maximum due to the Emperor Seamounts has been significantly dissipated and the stronger energy fluxes are associated with the primary wave and the wave scattered from the Koko Guyot. Not only tsunamis on the US shores were influenced by these bathymetric features, as Koshimura et al. (2008) showed the tsunami scattered from the Emperor seamounts strongly influenced the maximum tsunami energy along the Pacific coast of Japan, as well.

Above experiments by using energy flux defined in the explicit way the bathymetric features which scatter tsunami signal towards Crescent City, via the Mendocino Escarpment. Identification of the distant bathymetric features was achievable since the energy flux delineates the energy pathways that couple bathymetric features (Koko Guyot and the Hess Rise) to the Crescent City located thousands of kilometers apart.

Tsunami travel time

Application of energy fluxes for tracking the large amplitude tsunami waves will result in the prediction of arrival time for these waves. Both observations and numerical models show that, during IOT in many locations along the Pacific and Atlantic coasts, the first arriving signal, forerunner had lower amplitude than the main signal, which often was much delayed (Rabinovich et al., 2006; Kowalik et al., 2005a, 2007a,b). Understanding this temporal distribution of tsunami characteristics is important for the application to tsunami warning and prediction procedures and technology. Fig. 4 shows that the signal from the tsunami source directed into Atlantic Ocean arrives practically unobstructed carrying maximum amplitude close to the arrival time of the first wave. The situation is quite different for the tsunami entering into Pacific Ocean. The path through the deep Indian ocean carried miniscule energy and the signal arrives at 9 h from the tsunami onset, while the stronger signal arrived to the cross-section at approximately 16 h. A similar processes occurred while the tsunami signal traveled over the Southern Pacific towards the Americas. The path through the deep ocean to western North America again carried miniscule energy, while the stronger signal traveled a much longer distance via South Pacific ridges (cf. Fig. 5). As tsunami travel time from the source region to the given location is an important parameter in the tsunami prediction and warning we intend to investigate in detail this parameter based on our computation of the IOT. The IOT arrival times

have been determined for many locations (Merrifield et al, 2005; Rabinovich et al., 2006). We performed numerical experiments to delineate the tsunami arrival time in IOT by using GTM at every grid point for a signal of 0.1 cm amplitude. The computed tsunami travel time chart is depicted in Fig. 13. The chart shows that even at such small limiting amplitude the tsunami signal arriving at Alaska and North America did not pass through the Indonesian Straits but rather around Australia and New Zealand.

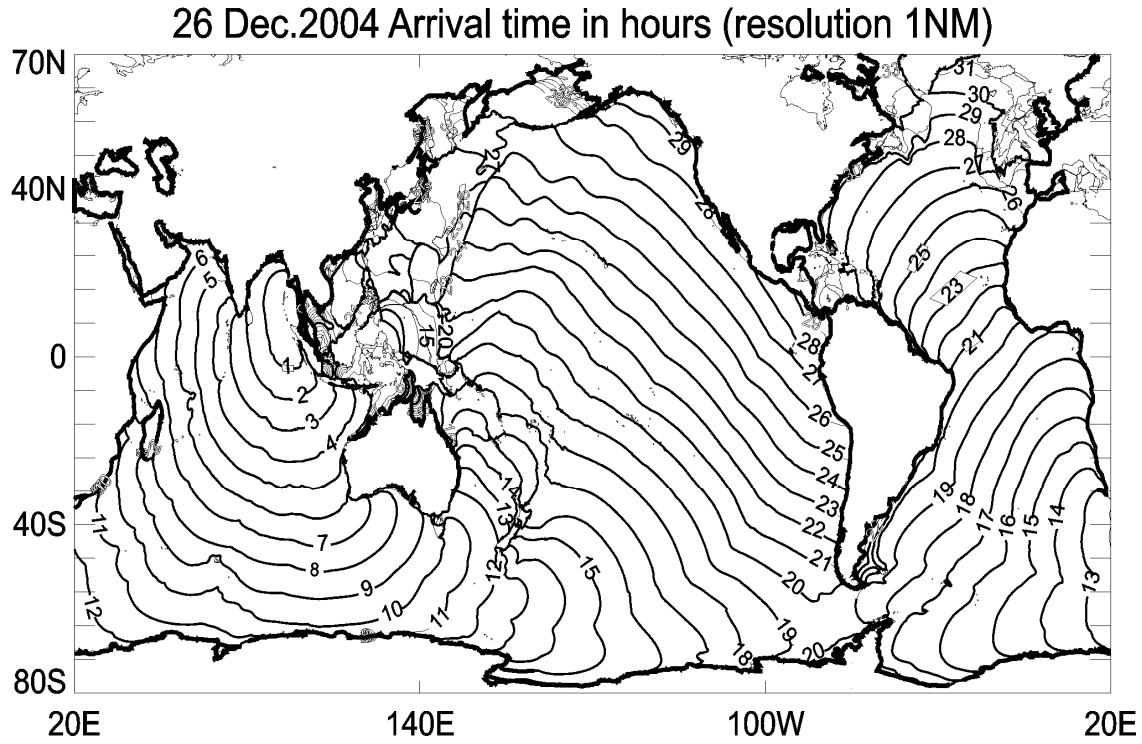

Figure 13. Travel time (in hours) for arrival of the tsunami of 0.1cm amplitude during the IOT of Dec. 2004.

The next numerical experiment computes isolines of arrival time for the tsunami signal of 0.5 cm amplitude (Fig. 14). In the vast regions of the Northern and Central Pacific this figure does not show a consistent arrival time. We may conclude that the main premise used to construct these figures, namely that the first train of tsunami waves is associated with the 0.5 cm amplitude, does not hold true.

We were able to construct isolines of arrival time in the regions of larger amplitudes, i.e. in the Indian Ocean, in the South Pacific (especially along the South Pacific Ridge) and in the South Atlantic. By checking results of computations at the coastal locations we found that a tsunami of 0.5 cm amplitude arrived at every location in the Pacific Ocean. This wave did not arrive at the western North America by refracting around New Zealand; it traveled closer to South America via energy ducts located over South Pacific ridges. This is a much longer travel time compared to the travel time depicted in Fig. 13.

The observations define travel times uniquely when the amplitude of the signal is above the noise level. The mixed signal of meteorological/oceanographic and tsunami origin is difficult to differentiate. Probably the tsunami amplitude of a few centimeters is strong enough to be seen

above the meteorological noise. Therefore, the observed arrival time is usually much longer than the calculated, for example, at Jackson Bay NZ the arrival time was 18 h 18 min, while according to the travel time computed by the first perturbation of 0.1 cm at this location, the arrival time for the first wave was 12 h 30 min.

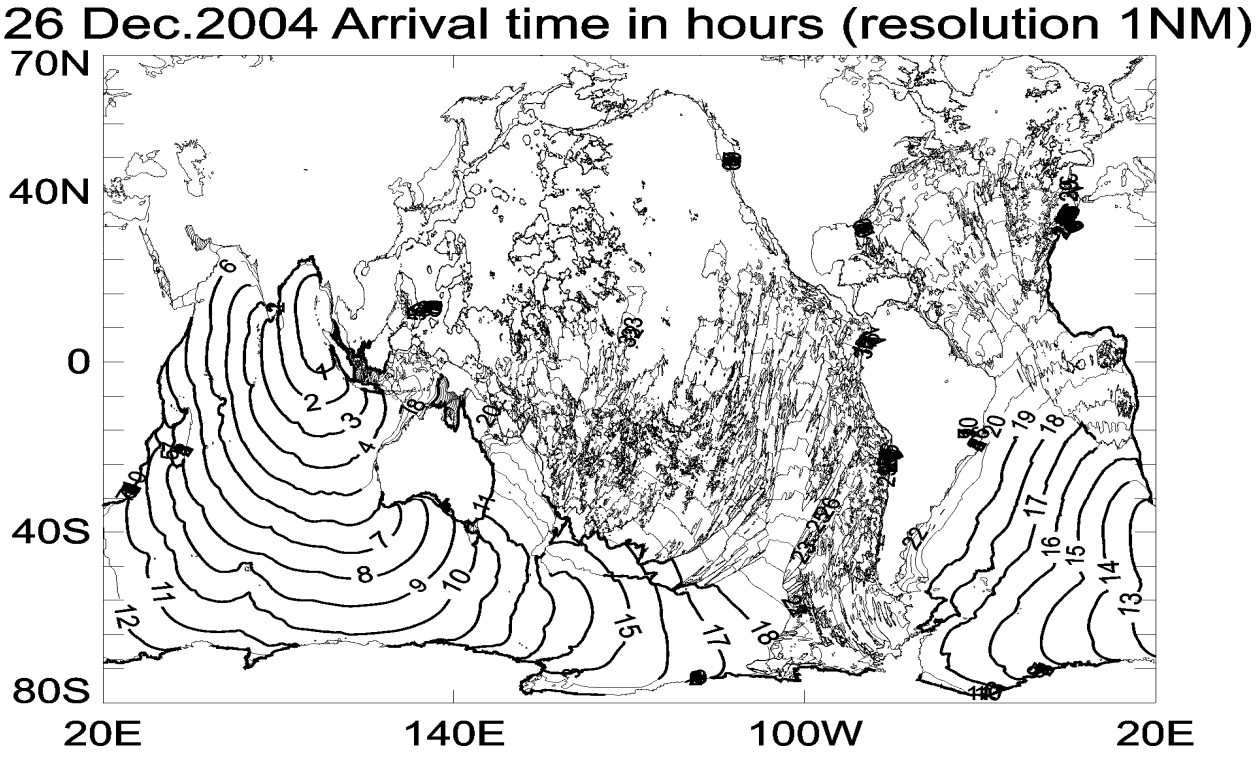

Figure 14. *Travel time (in hours) for arrival of the tsunami of 0.5cm amplitude during the IOT of Dec. 2004.*

Stations located in the Northern Pacific showed the largest differences between the calculated and observed travel time (Kowalik et al., 2005a, 2007a,b). This is caused either by small tsunami signal-to-noise ratio, or by multiple paths between the source and gauge locations. The higher energy tsunami signals arriving at distant locations are usually those which travel slowly over oceanic ridges.

In the Southern Pacific, wave energy ducting marked tsunami propagation over oceanic ridges. Travel times obtained from computations as arrival of the first significant wave show a clear and consistent pattern only in the region of high tsunami amplitudes and in the simply connected domains, such as in the case of the tsunami which traveled from Indonesia, around New Zealand, and into the Pacific Ocean. Described wave behavior indicates that the computations of tsunami travel time based on the ray theory of wave propagation and on Fermat's principle of least time might lead to large errors in predicting travel time for tsunamis large enough to propagate into contiguous oceans. Therefore, to identify the travel times for the large amplitude tsunamis we propose to use the time dependent energy flux contours as shown in Figs. 10-12.

Conclusions and discussions

It is important to recognize that the failure to predict the arrival time of the maximum tsunami in the wake of Kuril Islands Tsunami is due to lack of the proper tools being used by Tsunami Warning Centers. To investigate tsunami wave amplification and time delay we use energy flux. This tool, when tested against IOT of 2004 and KIT of 2006, shows that strong secondary signals are generated by scattering, reflection and refocusing of the primary tsunami wave.

The tsunami scattering by seamounts and trapping along ridges and escarpments needs to be further investigated to understand how the signal is changed during the tsunami/bathymetry interactions. We cannot solely relay on experiments like those done for the Koko Guyot in Figs. 11 and 12. Although the bathymetric features responsible for the tsunami scattering have been identified, we did not arrive at a complete understanding of the generation, scattering and trapping by the Koko Guyot. One of the important results from Figs. 11 and 12 is that the scattering from the Koko Guyot has extended the duration of the Kuril Islands tsunami and scattered signal showed directional modulation which resulted in stronger tsunami in the distant locations. Directional and temporal properties of the tsunami signal in proximity to the bathymetric features depend on the superposition of two waves; a primary wave arriving from the tsunami source and a secondary wave generated by the bathymetry. One can straightforwardly assume that such superposition (cf. Lautenbacher, 1970, Fujima et al., 1995; Liu et al., 1995) generates larger amplitudes at the island's perimeter by refraction process, however there is no straightforward approach to deduce temporal changes in the wave trapped around the island/seamount. The question is how the trapped energy decay in time? Often decay is relatively short in time when caused by the nonlinear frictional dissipation. However, sometimes such waves have been observed to last for a long period of time, pointing towards the existence of trapped and partially leaky modes of oscillations (Yanuma and Tsuji, 1998; Nirupama et al., 2006), interaction between oscillations trapped at the coast and the continental slope (Nekrasov, 1970; Horrillo et al., 2008) and possibly to generation of the dispersive, coastally trapped edge waves (Kurkin and Pelinovsky, 2002).

The search for the resonance periods which are responsible for the tsunami energy trapping is often based on an assumption of stationary oscillations in the primary wave arriving from the source. The short and variable in time tsunami train impinging on a bathymetric feature does not develop the full resonance response (Munk et al., 1956; Horrillo et al., 2008). Examination of tsunami signals (Kowalik et al., 2008) scattered from the bathymetric features also shows stronger energy of shorter wave periods when compared with the primary tsunami signal arriving from a source. As Mofjeld et al., 2000 have noticed these short period waves also contribute to the random appearance of tsunami time series when waves reflected from various bathymetric features interact with each other.

An intermittent behavior of the tsunami train seems to be the crux of all problems related to response calculation of tsunami impinging on seamounts and ocean ridges: shorter and longer tsunami trains result in different enhancement and trapping (Munk et al., 1956; Horrillo et al., 2008). In the above applications to the Indian Ocean Tsunami of 2004 and the Kuril Islands Tsunami of 2006, we have demonstrated that sudden changes caused by higher energy pulses in the intermittent tsunami wave trains can be assessed by energy fluxes. These experiments defined in explicit way the bathymetric features which scatter tsunami signal towards ports, like Crescent City. The identification of the distant bathymetric features was

achievable since the energy flux delineated the energy pathways that coupled bathymetric features (like Koko Guyot) to ports located thousands of kilometers apart.

APPENDIX

Tsunami energy balance and numerical dissipation

As we found in the domain adjacent to the Crescent City the total energy balance which seems to account for all sources and sinks did not balance (Fig. 3). Since the energy inflowing into the domain was not completely dissipated by the frictional forces and at the same time the total energy or sea level did not increase in time, therefore, this fact points towards an numerical dissipation. We shall demonstrate that the additional energy dissipation usually occurs in the short spatial or temporal scales where numerical schemes are unable to resolve wave propagation. Processes of destruction of the tsunami waves due to the short wave dissipation/dispersion are well observed when the wave travels in an upsloping channel (Kowalik, 2003).
To investigate the role of numerical friction, the wave propagation experiment in the 3000km long channel closed at both ends is considered. The shape of the channel is given in Fig. 15.

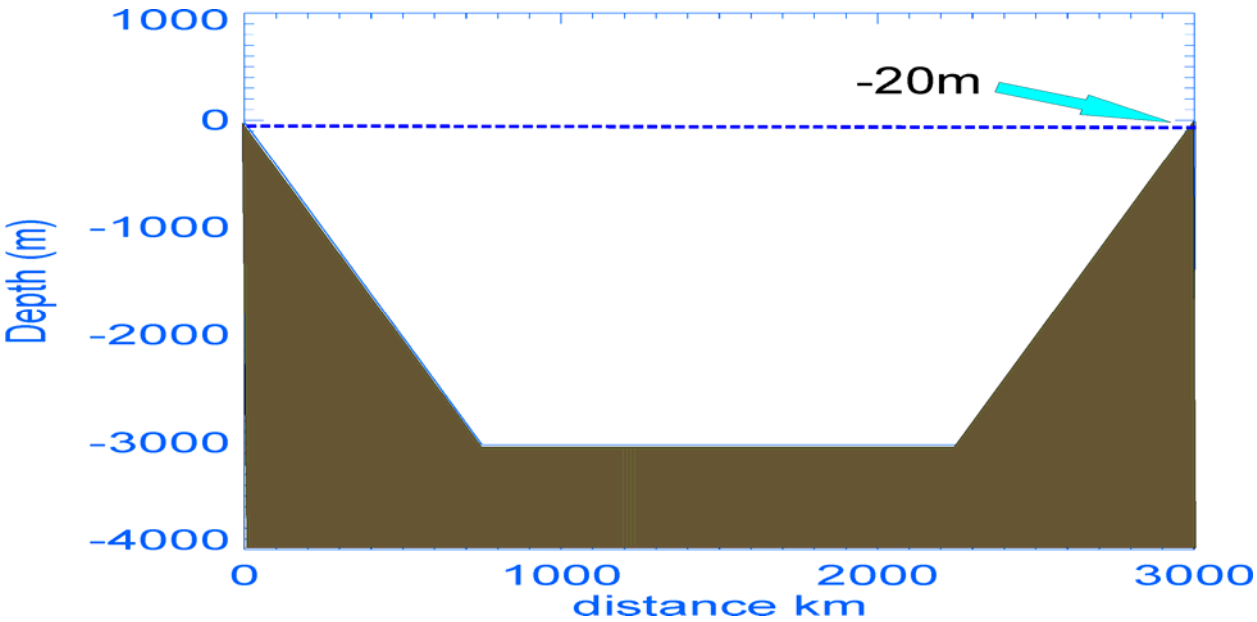

Figure 15. Bathymetry of a channel. Constant depth of 3km at the central part. At the distance of 750km apart from the shores, sea-bottom slopes change linearly to achieve 20m depth at the shores.

The tsunami wave is generated by the bottom displacement in the center of the channel. The high spatial resolution is achieved by the 10m-space step. The time step of 10^{-2} s is used.
In the first experiment, a rectangular bottom displacement of 100km length and 2m height generates the sea level change in the center of the channel which propagates both to the left and the right shores as shown in Figure 16.

As the waves propagate towards the shores, even in the deep water, the rectangular signal starts to change by generating short numerical dispersive waves in the front and in the tail of the sea level displacement. Such behavior demonstrates that the numerical scheme with finite resolution is not able to reproduce a square wave without loosing energy either through dissipative or dispersive numerical processes.

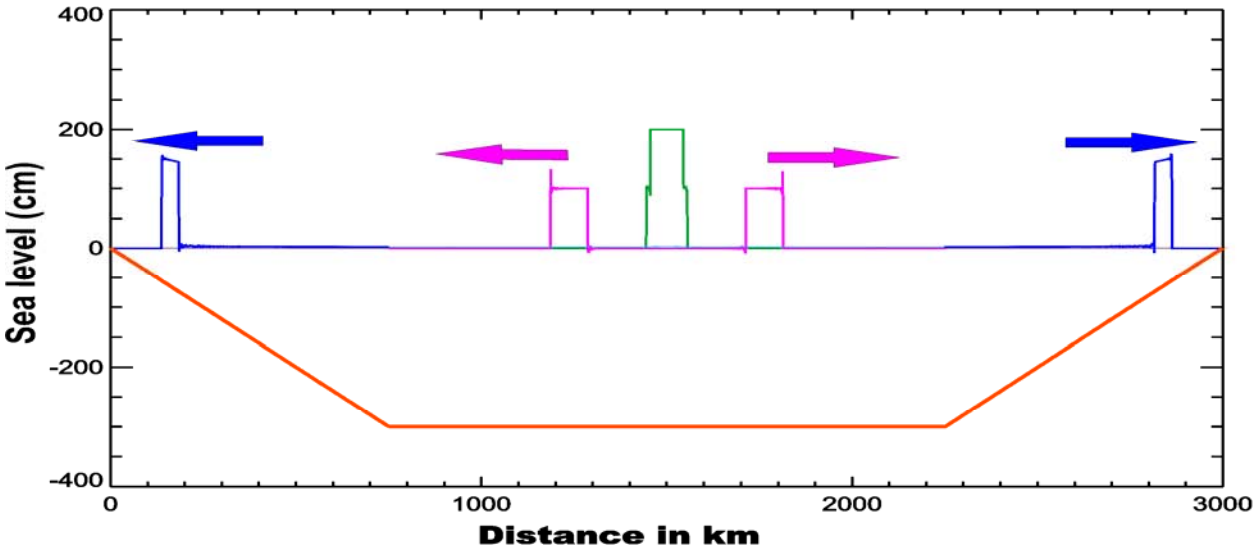

Figure 16. A rectangular bottom displacement of 100 km long generates two waves propagating towards the left and right shores. Notice dispersive waves in the front and tail of the main displacement.

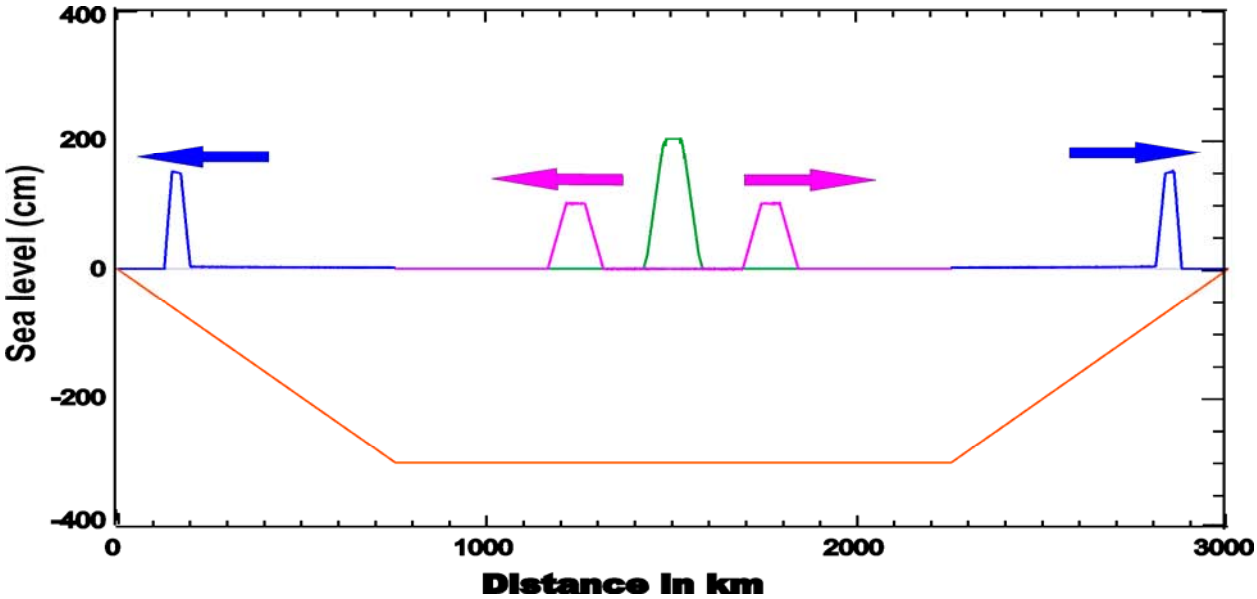

Figure 17. A trapezoidal bottom displacement of 100 km long generates two waves propagating towards the left and right shores. Notice the lack of numerical dispersive waves in the front and tail of the main displacement.

The time-history of a trapezoidal bottom displacement is shown in Fig. 17.

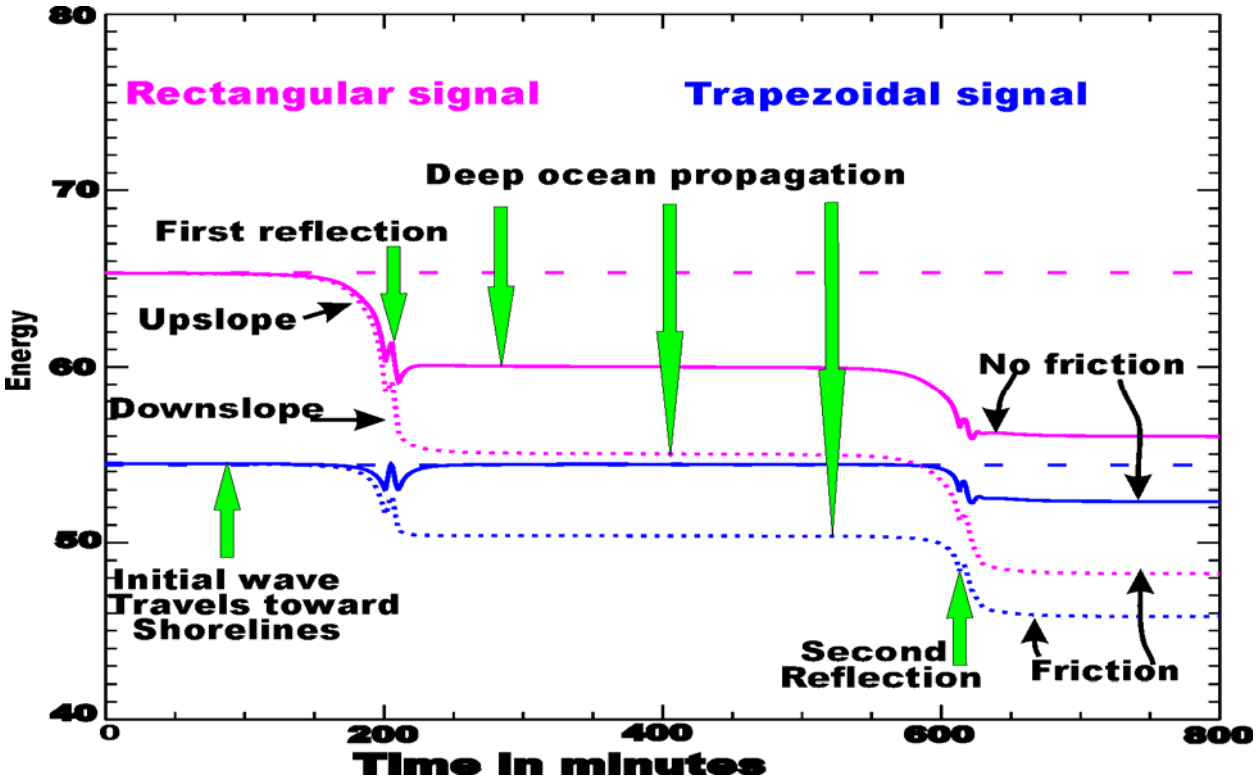

Figure 18. Total energy (kinetic and potential) averaged over computational domain.

The total energy as a function of time has been plotted in Fig. 18. As signal enters the shallow water domain it starts to loose energy both in case when the bottom friction term is included (dotted lines) and when the bottom friction term is set to zero (continuous lines). The latter result confirms the energy dissipation due the spatial and temporal resolution of the numerical schemes.

In our computations the nonlinear advective term has been rendered into a numerical form through the upstream/downstream method, therefore to explain the energy loss we can invoke numerical friction due to the first order of approximation. For this purpose in eq. (1) only advection along the x direction is considered

$$\frac{\partial u}{\partial t} + u\frac{\partial u}{\partial x} = 0 .$$

Its numerical form is

$$\frac{u_j^{m+1} - u_j^m}{T} + u_{j,p}^m \frac{u_j^m - u_{j-1}^m}{h_x} = 0 \qquad (8)$$

Here: m is the time stepping index, T is the time step, j the spatial index, h_x is the space step.

The formula above has been written for the positive velocity $u_{j,p}^m$ only. It can be linearized by considering $u_{j,p}^m$ as the constant coefficient. The numerical error introduced by spatial and temporal approximations in (8) is expressed by the second derivative (Kowalik and Murty, 1993, p. 53), as

$$\frac{u_{j,p}^m h_x}{2}\frac{\partial^2 u^m}{\partial x^2} \tag{9}$$

This numerical term is actually similar to the horizontal friction with viscosity coefficient being a function of the space step h_x and velocity $u_{j,p}^m$. Such numerical viscosity coefficient, because of its dependence on the velocity, produces the strongest dissipation in the shallow water region. Unfortunately, this numerical viscosity coefficient does not explain the deep-water dissipative processes, as the deep-water velocity is very small.

Spectral properties of the numerical dissipation can be further elucidated by considering an amplification which numerical scheme introduces to the unit amplitude sinusoidal signal when computation are advanced from the time step *m* to *m+1*. If again, eq.(8) can be considered as a linear equation with coefficient $u_{j,p}^m$, an amplification factor (λ) is calculated as (Kowalik and Murty, 1993, p. 46),

$$\lambda = \sqrt{[1+2q(q-1)(1-a)]} \tag{10}$$

Here $q = u_{j,p}^m T / h_x$ is the Courant number and $a = \cos \kappa h_x$. The latter parameter defines spatial resolution of a wave length L through the wave number $\kappa = 2\pi / L$. The shortest wave in the system is equal to $2h_x$. Obviously eq.(10) defines the signal amplification as a function of two dimensionless parameters q and a.

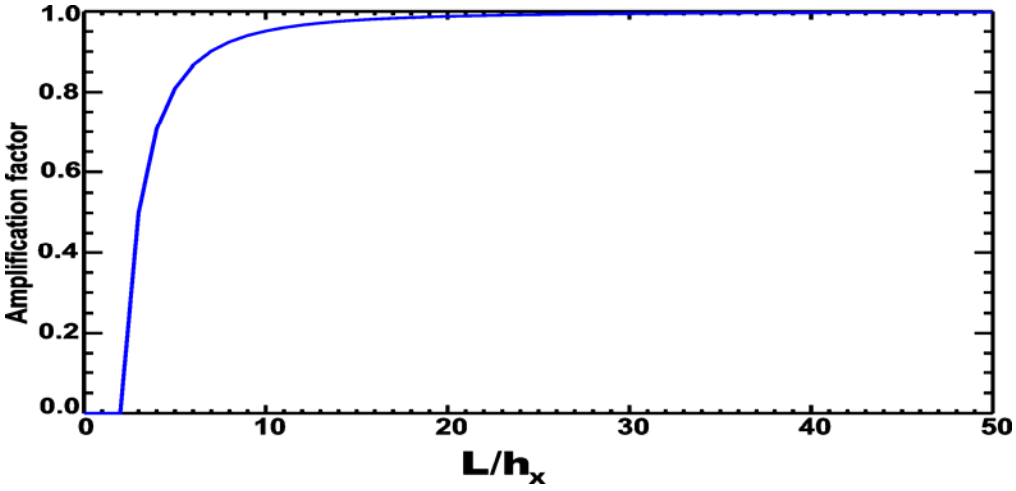

Figure 19. Amplification factor (λ) for the numerical scheme given by eq.(8) as a function of wavelength resolution. L denotes the wavelength, h_x is the space step.

We intend to demonstrate that in the numerical scheme given by eq.(8) the amplification factor suppresses short waves, thus dissipation of energy will take place in the short wave range. For the longer waves when $\kappa \to 0$ the damping will be negligible. Fig. 19 shows λ as a function of the wave number. In this figure, the Courant number is $q = 0.5$. Argument of the cosine function $\kappa h_x = \frac{2\pi}{L} h_x$ defines how well is the wavelength resolved by the spatial step. It changes as a function of the wavelength, starting from the shortest wave $L = 2h_x$, $\kappa h_x = \frac{2\pi}{2h_x} h_x = \pi$ and continues increasing towards the longer waves as shown in Fig. 19. The amplitude of the shortest wave $L = 2h_x$ is completely suppressed in this numerical system. Even if the wavelength is resolved ten times $L/h_x = 10$, the amplification factor is equal $\lambda = 0.95$. The wave described by the rectangular sea level change (Fig. 16) consists of multiple short waves; therefore the numerical scheme will quickly dissipate the short wave energy.

The total energy in the near shore region in Fig. 18 depicts a small kink as the wave reflects from the shore. The wave energy instead of being dissipated is growing in this region, thus pointing towards instabilities of the numerical scheme (Phillips, 1959). The source of this energy is not related to physics but to numerics. As eq.(8) is not completely linear, the nonlinear effects will grow in the shallow water due to the sea level and velocity enhancement. A numerical nonlinear instability usually starts at the shortest wavelength in the system since a cascade of motion which arrives from the large scales to the small scales is blocked by the lack of finer resolution. The result is the build up of energy at the short wavelengths which induces instability. Often this type of instability is referred to as aliasing, which points out to the fact that the finite numerical grid cannot discern certain wavelength (see Roache, 1976, p. 81). An example how the new wavelength can be generated through the nonlinear interaction has been given by Kowalik and Murty (1993, p. 179).

Acknowledgment

I would like to express my deep gratitude to George Pararas-Carayannis, President of Tsunami Society, Juan Horillo, University of Alaska Fairbanks and William Knight, West Coast/Alaska Tsunami Warning Center for their comments and suggestions which enhanced this manuscript.

References:

Candella, R. N., A. B. Rabinovich and R. E. Thomson. 2008. The 2004 Sumatra tsunami as recorded on the Atlantic coast of South America. Adv. Geosci., 14, 117–128.

Davies, T. A., P. Wilde and D. A. Clague . 1972. Koko Seamount: A major guyot at the southern end of the Emperor Seamounts, Mar. Geol., 13, 311--321.

Fujima, K., Y. Dede, Goto, C. Hayashi, K., Shigemura, T. 1995. Characteristics of long waves trapped by conical island. Coastal Engineering Journal, 38(2), 111-132

Henry, R. F. and M. G. G. Foreman, 2001. A representation of tidal currents based on energy flux, Marine Geodesy, 2493, 139-152.

Hirata, K., K. Satake, Y. Tanioka, T. Kuragano, Y. Hasegawa, Y. Hayashi, and N. Hamada. 2005. The Indian Ocean Tsunami: Tsunami Source Model From Satellite Altimetry. Proceedings of the International Tsunami Symposium, eds., G.A. Papadopoulos and K. Satake, Chania Greece, 2005, 72-76.

Horrillo, J., W. Knight, and Z. Kowalik. 2008. Kuril Islands tsunami of November 2006: 2. Impact at Crescent City by local enhancement, J. Geophys. Res., 113, C01021, doi:10.1029/2007JC004404.

Imamura, F.: 1996, Review of tsunami simulation with a finite difference method. In Long-Wave Run-up Models, H.Yeah, P. Liu and C. Synolakis, Eds, World Scientific, 25-42.

Kajiura, K.. 1981. Tsunami energy in relation to parameters of the earthquake fault model. Bull. Earthquake Res. Inst., 56,415-440.

Koshimura, S., Y. Hayashi, K. Munemoto and F. Imamura. 2008. Effect of the Emperor seamounts on trans-oceanic propagation of the 2006 Kuril Island earthquake tsunami. Geophysical Research Letters, vol. 35, L02611, doi:10.1029/2007GL032129.

Koshimura, S., F. Imamura, and N. Shuto. 2001. Characteristics of Tsunamis Propagating over Oceanic Ridges, Natural Hazards, 24(3), 213–229.

Kowalik, Z., 2003. Basic relations between tsunamis calculation and their physics-II, Science of Tsunami Hazards, 21(3), 154-173.

Kowalik, Z., J. Horrillo, W. Knight, and T. Logan. 2008. Kuril Islands tsunami of November 2006: 1. Impact at Crescent City by distant scattering, J. Geophys. Res., 113, C01020, doi:10.1029/2007JC004402.

Kowalik, Z., Knight, W. Logan, T. and P. Whitmore, 2007a. The tsunami of 26 December 2004: Numerical Modeling and energy considerations-II. In: Tsunami and Its Hazard in Pacific and Indian Oceans,Eds: Satake,K., Okal, E. A., Borrero, J. C., Pure and Applied Geophysics (PAGEOPH),vol. 164, No. 2/3,379-393.

Kowalik Z., W. Knight, T. Logan, and P. Whitmore. 2007b. Numerical Modeling of the Indian Ocean Tsunami. In: The Indian Ocean Tsunami. Co-editors: T. Murty, U. Aswathanarayana and N. Nirupama. Taylor and Francis, London, pp. 97-122.

Kowalik Z., W. Knight, T. Logan, and P. Whitmore, 2005a. Numerical Modeling of the Global Tsunami: Indonesian Tsunami of 26 December 2004. Science of Tsunami Hazards, Vol. 23, No. 1, 40- 56.

Kowalik, Z., Knight, W. Logan, T. and P. Whitmore, 2005b. The tsunami of 26 December 2004: Numerical Modeling and energy considerations, Proceedings of the International Tsunami Symposium, Eds.: G.A. Papadopoulos and K. Satake, Chania, Greece, 27-29 June, 2005, 140-150.

Kowalik, Z. and T. S. Murty. 1993. Numerical Modeling of Ocean Dynamics. World Scientific Publ., 481 pp.

Kurkin, A., and E. Pelinovsky. 2002. Focusing of edge waves above a sloping beach, European Journal of Mechanics B/Fluids 21, 561–577

Lautenbacher, C. C. 1970. Gravity wave refraction by islands. J. Fluid Mech. 41, 655-672.

Lay, T., H. Kanamori, C. J. Ammon, M. Nettles, S. N. Ward, R. C. Aster, S. L. Beck, S. L. Bilek, M. R. Brudzinski, R. Butler, H. R. DeShon, G. Ekstrom, K. Satake, S. Sipkin. 2005. The Great Sumatra-Andaman Earthquake of 26 December 2004. Science, v. 308, 1127-1139.

Liu PLF, Cho YS, Briggs MJ, Kanoglu U, Synolakis CE. 1995. Runup of solitary wave on a circular island. Journal of Fluid Mechanics. 302:259-285.

Longuet-Higgins, M.S. 1967. On the Trapping of Wave Energy Round Islands. Jour. Fluid Mech., Vol. 29, Part 4, pp 781-821.

Loomis, H. G. 1966. Spectral analysis of tsunami records from stations in the Hawaiian Islands, Bull. Seismol. Soc. Am., 56, 697– 713.

Lynett, P. J.,T.-R. Wu and P.L.-F.Liu. 2002. Modeling wave run-up with depth-integrated equations, Coast. Engrg. 46(2), 89-107.

Mader, C. L.: 2004, Numerical Modeling of Water Waves, CRC Press, 274 pp.

Mei, C. C.: 1989, The Applied Dynamics of Ocean Surface Waves, World Scientific, 740 pp.

Merrifield, M.A., Y.L. Firing, G. Brundrit, R. Farre, B. Kilonsky, W. Knight, L. Kong, C. Magori, P. Manurung, W. Mitchell, F. Shillington, E.M.S. Wijeratne, J. Jardin, S. Nakahara, F.-Y. Porter, and N. Turesky. 2005. Tide Gauge Observations of the Indian Ocean Tsunami, December 26, Geophysical Research Letters. 32, , L09603, doi:10.1029/2005GL022610.

Mofjeld, H.O., V.V. Titov, F.I. Gonzalez, and J.C. Newman. 2000.
Analytic Theory of Tsunami Wave Scattering in the Open Ocean with Application to the North Pacific. NOAA Technical Memorandum OAR PMEL-116, 42pp.

Munger S. and K. F. Cheung. 2008. Resonance in Hawaii waters from the 2006 Kuril Islands Tsunami. Geophysical Research Letters, 35, L07605, doi:10.1029/2007 GL032843.

Munk, W.H. 1963. Some Comments Regarding Diffusion and Absorption of Tsunamis. In Proc. Tsunami Meetings Associated with the Tenth Pacific Science Congress, Honolulu, Hawaii, Aug.- Sept. 1961, ed. Doak C. Cox, IUGG, Paris, IUGG Monograph No. 24, pp 53-72.

Munk, W., F. Snodgrass, and G. Carrier. 1956. Edge waves on the continental shelf, Science, 123(3187), 127– 132.

Murty, T.S., 1977. Seismic Sea Waves - Tsunamis, Bulletin 198, Fisheries Research Board of Canada, Dept. of Fisheries, Ottawa, Canada, 337 pp.

Murty, T., Rao, A.D, Nirupama, N., and Nistor, I. and. (2006).Tsunami warning systems for the hyperbolic (Pacific), parabolic (Atlantic) and elliptic (Indian) oceans, J. of Ind. Geophysical Union,, Vol. 10, No. 2, 69-78.

Nekrasov, A. V. 1970. Transformation of tsunamis on the continental shelf. In: Tsunamis in the Pacific Ocean, W.M. Adams, ed, East_West Center Press, Honolulu, 337-350.

Nekrasov, A. V. 1992. On tidal energy horizontal circulation. The Journal of the Korean Society of Coastal and Ocean Engineers, 4(3), 168--177.

Nirupama, N., T.S. Murty, I. Nistor and A.D. Rao. 2006. Persistent high water levels around Andaman & Nicobar Islands following the 26 December 2004 Tsunami, Science of Tsunami Hazards, Vol. 24, No. 3, 183-193.

Phillips, N. A. 1959. An example of Non-Linear Computational Instability. The Atmosphere and the Sea in Motion, The Rockefeller Institute Press, New York, N.Y., pp. 501-504.

Rabinovich, A. B. 1997. Spectral analysis of tsunami waves: Separation of source and topography effects, J. Geophys. Res., 102, 12,663– 12,676.

Rabinovich A.B., R.E. Thomson and F.E. Stephenson. 2006. The Sumatra tsunami of 26 December 2004 as observed in the North Pacific and North Atlantic oceans, Surv. Geophys., 27, 647–677.

Roache, P. J. 1976. Computational Fluid Dynamics. Hermosa Publishers, 446 pp.

Titov, V., A. B. Rabinovich, H. O. Mofjeld, R. E. Thomson and F. I.Gonzales. 2005. The Global Reach of the 26 December 2004 Sumatra Tsunami, Science, 309, 2045–2048.

Van Dorn W. G. 1970. Tsunami Response at Wake Island: a Model Study. 1970. Journal of Marine Research, v.28, no.3, 336-344.

Van Dorn, W.G. 1984. Some Tsunami Characteristics Deducible from Tide Records. Jour. Physical Oceanography, Vol. 14, No. 2, 353-363.

Yanuma, T., and Y. Tsuji. 1998. Observation of edge waves trapped on the continental shelf in the vicinity of Makurazaki Harbor, Kyushu, Japan, J. Oceanogr., 54, 9– 18.

ASSIMILATION OF REAL-TIME DEEP SEA BUOY DATA FOR TSUNAMI FORECASTING ALONG THAILAND'S ANDAMAN COASTLINE

Seree Supharatid

Natural Disaster Research Center, Rangsit University, Pathumtani 12000, Thailand

ABSTRACT

The occurrence of 2004 Indian Ocean tsunami enhanced the necessity for a tsunami early warning system for countries bordering the Indian Ocean, including Thailand. This paper describes the assimilation of real-time deep sea buoy data for tsunami forecasting along Thailand's Andaman coastline. Firstly, the numerical simulation (by the linear and non-linear shallow water equations) was carried out for hypothetical cases of tsunamigenic earthquakes with epicenters located in the Andaman micro plate. Outputs of the numerical model are tsunami arrival times and the maximum wave height that can be expected at 58 selected communities along Thailand Andaman coastline and two locations of DART buoys in the Indian Ocean. Secondly, a "neural" network model (GRNN) was developed to access the data from the numerical computations for subsequent construction of a tsunami database that can be displayed on a web-based system. This database can be updated with the integration from two DART buoys and from several GRNN models.

Key words: Numerical modeling, Neural network modeling, Web-based online, Data assimilation, GRNN, DART Buoy

Science of Tsunami Hazards, Vol. 27, No. 3, page 30 (2008)

1. Introduction

The 2004 Indian Ocean tsunami was responsible for the greatest damage in history and a death toll of more than 200,000 people. The highest number of victims (both confirmed dead and missing) was in Indonesia (163,795), followed by Sri Lanka (35,399), India (16,389) and Thailand (8,345)(International Federation of Red Cross and Red Crescent, 2005). In Thailand, many resorts in the low-laying coastal area of Kao Lak experienced serious destruction and more than 2,000 people lost their lives.

Because of the great damage and destruction caused by this 2004 disaster, it is necessary to review the present tsunami warning systems and examine three important aspects - specifically timing, accuracy and stability. Whitmore and Sokolowski (1996) developed the following approach in forecasting tsunami heights. They used a nonlinear long-wave numerical model to develop a database of water levels for 15 hypothetical tsunamigenic earthquakes in the northwest Pacific, for events ranging in moment magnitude from 7.5 to 9.0. According to this method, when a possible tsunamigenic earthquake occurs, a comparison of pre-computed and of measured water levels near the tsunamigenic source from the database helps identify the closest event and provides an estimate of tsunami heights for the Pacific. According to another numerical simulation technique introduced by the Japan Meteorological Agency (JMA) in April 1999(JMA, 2006), tsunami generation and propagation for 100,000 different cases (epicenter, depth, magnitude and fault geometry) are calculated in advance and the estimated tsunami heights and arrival times along the coast are stored in a database for use in the warning system. Still, another method for quick tsunami forecasting database for Korea (Lee et al., 2005), uses a superposition of a linear long wave solution which describes tsunami propagation from tsunami source units of 5.5 km. x 5.5 km. area and 1.0 height along the active fault zone in the Sea Japan/East Sea. Finally, NOAA's World Data Center A – Tsunami (WDC, 2005) has collected an updated tsunami database for the Atlantic, Indian, and Pacific Oceans, as well as the Mediterranean and the Caribbean Seas. This NGDC tsunami database - dating from 2000 B.C. to the present - includes a listing of historical tsunami source events and run-up locations throughout the world.

The first model simulation results of the Indian Ocean tsunami were obtained from the "MOST" (Method of Splitting Tsunamis) model (Titov and Synolakis, 1998) and were posted by Titov on the Internet Tsunami Bulletin Board (within 12 hours after the earthquake). MOST is part of the tsunami forecasting and warning system under development for the Pacific Ocean (Titov et al., 2005) that will provide fast real time estimates of tsunami amplitudes using preset models, real-time seismic data and, most importantly, deep-ocean tsunami amplitude data from a network of deep-ocean pressure sensors. Other researchers also ran models and posted results. Results of MOST and of other model runs have been widely used worldwide by the media for early planning of relief efforts and for post-tsunami field surveys. Unlike the Pacific, the Indian Ocean does not yet have a network of deep ocean pressure sensors, and so coastal tide gauges provide the only direct measurements of Indian Ocean tsunami amplitudes.

On May 30, 2005, five months after the December 26, 2004 tsunami, Thailand begun operating a National Disaster Warning Centre (NDWC, 2006) to monitor and relay critical information on all natural disasters. For the tsunami warning system, the NDWC begun using data on earthquake magnitude and depth for estimates of the potential risk from possible tsunamis. In November 2006, the NDWC, in cooperation with USAID, deployed the first DART buoy in the Indian Ocean. However, to establish an operating tsunami warning system, Thailand also required the development of a tsunami database along its Andaman Sea coastline.

The present study describes the development of a hybrid model that was developed by the integration of three techniques. First, a numerical model of linear and non-linear shallow water waves is introduced. Secondly, the neural network model is described in detail and the results of the database are displayed at an internet website. Thirdly, the database is updated with the assimilation from two DART buoys in the Indian Ocean, making use of several GRNN models.

2 Methodology

2.1 Numerical computation

A numerical model (similar to that of Shuto, 1997) was set up using linear and non-linear shallow water equations for estimation of tsunami propagation and of terminal effects. Equations. (1) – (3) are the linear equations without bottom friction in two-dimensional flow.

$$\frac{\partial \eta}{\partial t} + \frac{1}{R\cos\theta}\left(\frac{\partial M}{\partial \lambda} + \frac{\partial (N\cos\theta)}{\partial \theta}\right) = 0 \qquad (1)$$

$$\frac{\partial M}{\partial t} + \frac{gh}{R\cos\theta}\frac{\partial \eta}{\partial \lambda} = fN \qquad (2)$$

$$\frac{\partial N}{\partial t} + \frac{gh}{R}\frac{\partial \eta}{\partial \theta} = -fM \qquad (3)$$

Where η is the vertical displacement of the water surface above still water level, R is the earth's radius, t is time , g is the gravitational acceleration, M and N are discharge fluxes in the λ (along a parallel of latitude) and θ (along a circle of longitude) directions and f ($2\omega\sin\theta$) is the Coriolis coefficient.

Generally, a relatively smaller grid mesh is required to compute the tsunami along the coast where the water depth is shallow and variation of local topography has an important effect on tsunami behavior. However, it is difficult to use a smaller grid mesh in the total region of the large computational domain, such as the near shore of Thailand's Andaman coastline. Hence, the shallow water equations are applicable. The nonlinear shallow water equations in a Cartesian co-ordinate system consist of the continuity (Eq. (4)), and momentum equations in x (Eq. (5) and y (Eq. (6)):

$$\frac{\partial \eta}{\partial t} + \frac{\partial M}{\partial x} + \frac{\partial N}{\partial y} = 0 \qquad (4)$$

$$\frac{\partial M}{\partial t} + \frac{\partial}{\partial x}\left(\frac{M^2}{D}\right) + \frac{\partial}{\partial y}\left(\frac{MN}{D}\right) + gD\frac{\partial \eta}{\partial x} + g\frac{n^2}{D^{7/3}}M\sqrt{M^2+N^2} = 0 \qquad (5)$$

$$\frac{\partial N}{\partial t} + \frac{\partial}{\partial x}\left(\frac{MN}{D}\right) + \frac{\partial}{\partial y}\left(\frac{N^2}{D}\right) + gD\frac{\partial \eta}{\partial y} + g\frac{n^2}{D^{7/3}}N\sqrt{M^2+N^2} = 0 \qquad (6)$$

where “x” and “y” are horizontal coordinates, D is the total water depth, and n is Manning’s roughness. The application of the long-wave equations for tsunami modeling have also been described by Shuto et al. (1986), Kowalik and Murty (1993), and Titov and Synolakis (1998).

The computing domain covering the Andaman Sea coastline is shown in Fig. 1. The total region is bounded by latitude 2^{O} S longitude 85^{O} E to latitude 18^{O} N longitude 105^{O} E. Dynamic linking is accomplished in the boxed area. According to this method, larger grids in the deep sea are overlapped and dynamically linked with grids having 1/4 of the width in the shallower region (linking of 1.85 km to 462.5 m). During the computation, water level and discharge are exchanged satisfying a dynamic equilibrium along the boundary of these two regions. This process is repeated until the required grid resolution is obtained.

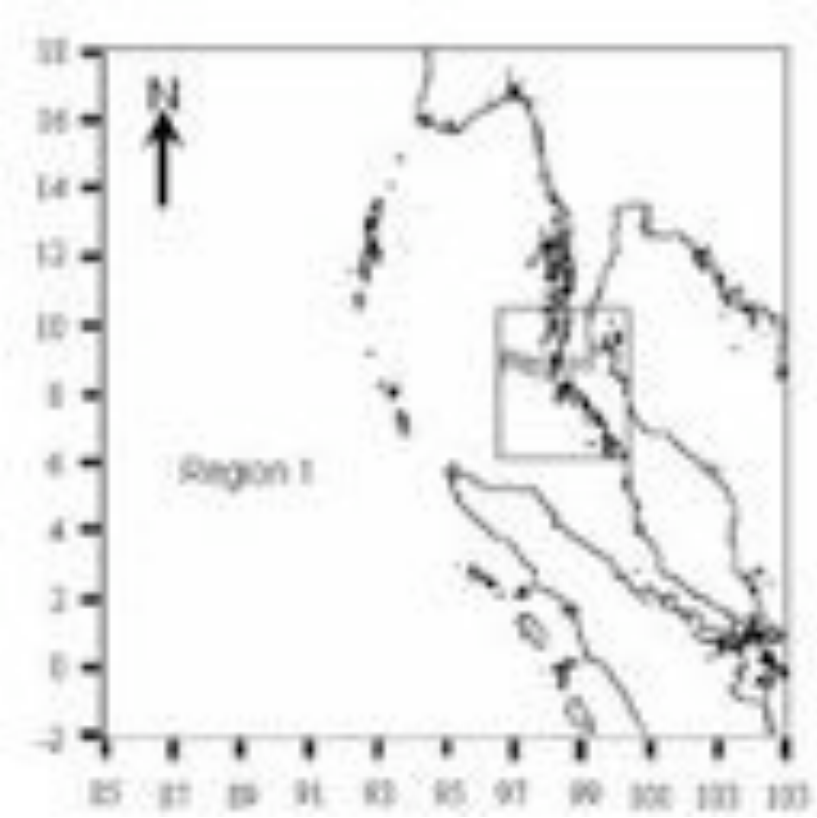

Fig. 1 Computing Domain

The initial condition corresponds to still water with the specified surface wave at the source of the earthquake. The algorithm of Mansinha and Smylie (1971) provides the initial surface wave through the seafloor deformation - based on input seismic parameters that include strike, dip and slip angles, the amount of the slip displacement and the location of the fault. The tsunami sources and earthquake epicenters for the Andaman micro plate were obtained from historic earthquakes (USGS) (Lay et al., 2005). Figure 2 shows the model region, which covers most of Thailand’s Andaman coastline with postulated earthquakes and tsunamis. Prior to the simulation, the model was calibrated with measurements of the tsunamis of 1881, 1941 and 2004.

The moment magnitude of postulated earthquakes was varied from 6.0 – 9.0. The relationship between moment magnitude and the fault dimensions were obtained from Donald and Kevin (1994) and Kanamori, H(1977). In total, there are 420 cases in the simulation.

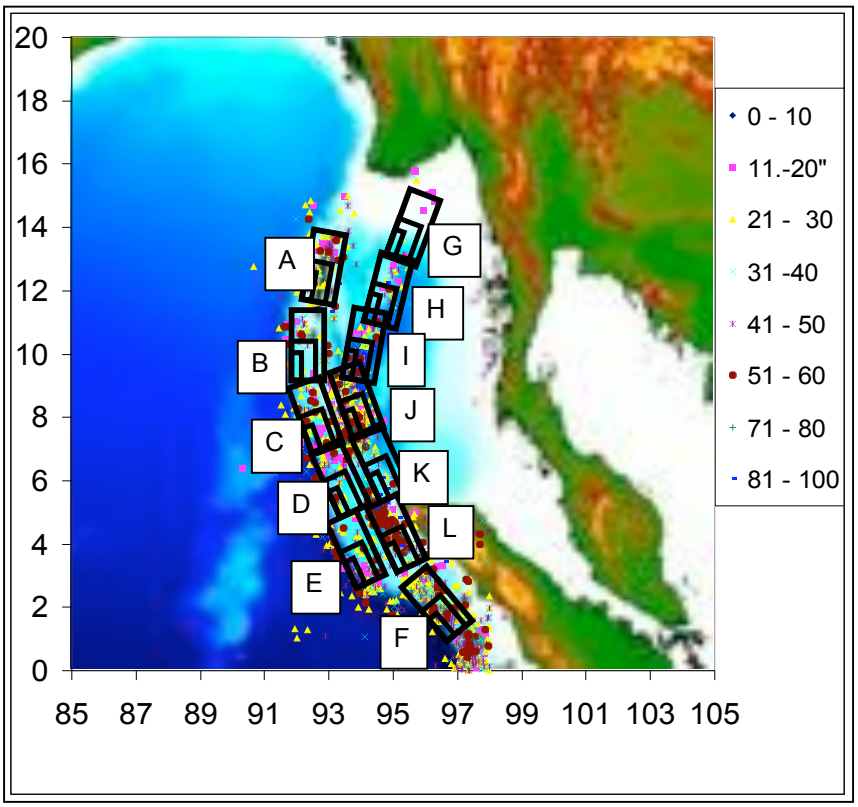

Fig. 2 Hypothetical earthquakes

2.2 Neural network

The neural network (NN) techniques used to solve problems in civil engineering began in the late 1980s (Flood and Kartam, 1994). Their applications in simulating and forecasting problems in oceanography are relatively recent (Hsieh and Pratt, 2001; Supharatid, 2003; Cigizoglu, 2005). Unlike other conventional-based models, the NN model is able to solve problems without any prior assumptions. As long as enough data is available, a neural network will extract any regularities or patterns that may exist and use it to form a relationship between input and output. Additional benefits include data error tolerance and the characteristic of being data-driven, thereby providing a capacity to learn and generalize patterns in noisy and ambiguous input data.

The General Regression Neuron Network (GRNN) proposed by Specht (1991) does not require an iterative training procedure as required in the back propagation method. It approximates any arbitrary function between input and output vectors, drawing the function estimate directly from the training data. In addition, it is consistent in that, as the training set size becomes large, the estimation error approaches zero with only mild restrictions on the function. The GRNN is used for the estimation of continuous variables, as in standard regression techniques. It is related to the

radial basis function network and is based on a standard statistical technique called kernel regression. The GRNN is a feed forward neural network best suited to function approximation tasks such as system modeling and prediction. It is a four-layer network with one hidden layer described in Fig. 3.

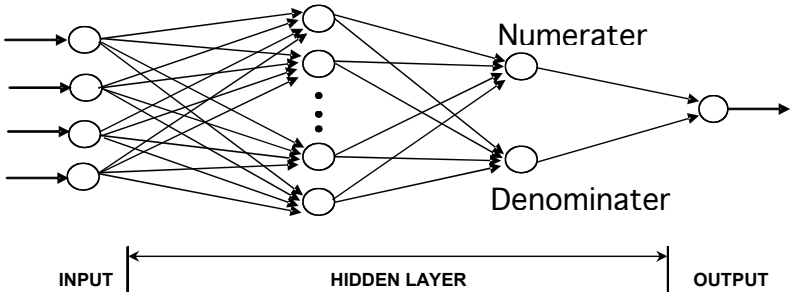

Fig. 3 Basic Procedure of GRNN

The input is a state space denoted by X (Epicenter, moment magnitude and earthquake depth). The estimated value ($\hat{Y}$) is calculated by Eq. (7) at 58 selected communities and 2 DART buoy locations (see Fig. 4). In this study, we used the cross training technique. Therefore, there are 210 hypothetical cases for training and 210 cases for testing the network. The input parameters are varied according to Table 1.

$$\hat{Y}(x) = \frac{\sum_{i=1}^{k} Y^i \exp(-D_i^2 / 2\sigma^2)}{\sum_{i=1}^{k} \exp(-D_i^2 / 2\sigma^2)} \qquad (7)$$

Where k is the number of input patterns is a scalar function representing the Euclidian square from the new input pattern to the training input pattern, and σ is a single smoothing parameter, which determines how tightly the network matches its prediction to the data in the training patterns. D_i^2

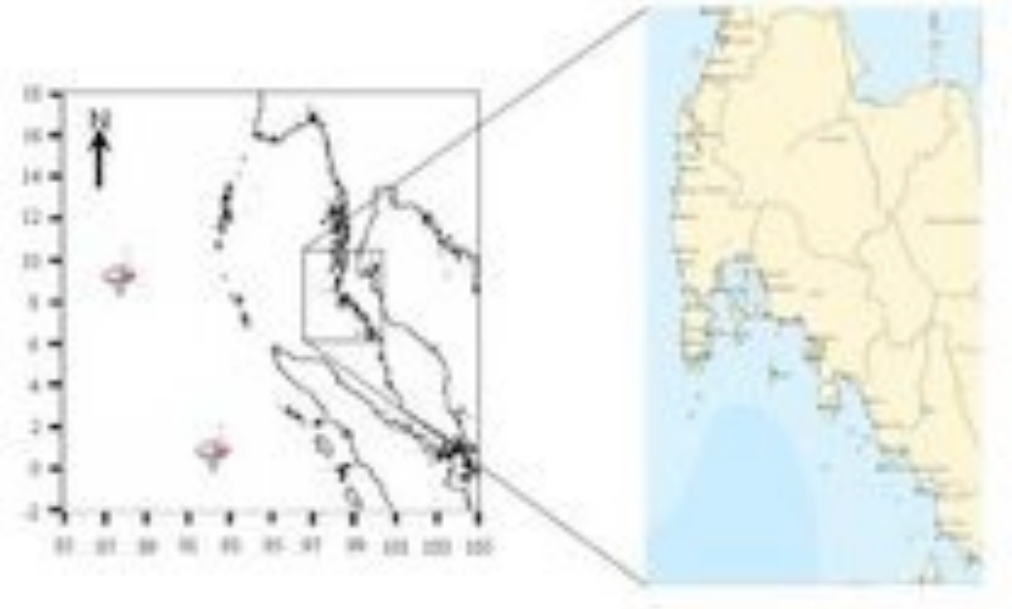

Fig. 4 Location of 58 selected communities and 2 DART buoys

Table 1 Input parameters and outputs for GRNN-1 model

Inputs		Outputs
Epicenter	Fixed at 12 locations	Maximum wave height in 58 risked communities along the coastline and 2 DART buoy locations
Earthquake magnitude (Mw)	6.0, 6.5, 7.0, 7.5, 8.0, 8.5 and 9.0	
Earthquake depth (D)	10, 20, 30, 40 and 50 km.	

By definition, the regression of a dependent variable y on an independent x, estimates the most probable value for y, given x and a training set. The regression method will produce the estimated value of y which minimizes the Mean-Squared Error (MSE). The GRNN is a method for estimating the joint probability density function (pdf) of x and y, given only a training set. Because the pdf is derived from the data with no preconceptions about its form, the system is perfectly general.

To evaluate the performance of GRNN, two common statistics, Efficiency Index (EI) and Root Mean Square Error (RMSE) are used as given in Eqs. (8) and (9).

$$EI = 1 - \frac{\sum_{k=1}^{k} (O_k - H_k)^2}{\sum_{k=1}^{k} (O_k - \overline{O})^2} \tag{8}$$

$$RMSE = \sqrt{\frac{\sum_{k=1}^{k} (O_k - H_k)^2}{k}} \tag{9}$$

where O_p and H_p are the target output and forecasted output, respectively. $\overline{O}$ is the mean value of the target output.

2.3 Data assimilation

In real operation, the initial warning decisions described in section 2.2 are based only on earthquake parameters. Without data assimilation from the direct measurement, results are susceptible to large errors of seismic source estimates. It has to be mentioned that the tsunami confirmation by coastal tide gages may come too late for timely evacuation measures. This can lead to a high false alarm rate and ineffective local emergency response. In this study, the arrival time of tsunami wave is detected by 2 DART buoys (see also Figure 4). The 1st and 2nd DART buoys were installed in the Indian Ocean at lat. 8.9^{O} N, long. 88.5^{O} E (No. 23401) and lat. 0.05^{O} N, long 81.88^{O} E (No. 54301), respectively. The previous GRNN-1 model was improved (GRNN-1.1, GRNN-1.2, GRNN-2). Difference in these models is the number and the position of DART buoys to be input to the model. Details of input are given in Tables 2 -4.

Table 2 Input parameters and outputs for GRNN–1.1 model

Inputs		Outputs
Epicenter	Fixed at 12 locations	Maximum wave height in 58 selected communities along the coastline
Earthquake magnitude (Mw)	6.0, 6.5, 7.0, 7.5, 8.0, 8.5 and 9.0	
Earthquake depth (D)	10, 20, 30, 40 and 50 km.	
DART buoy	No. 23401	

Table 3 Input parameters and outputs for GRNN–1.2 model

Inputs		Outputs
Epicenter	Fixed at 12 locations	Maximum wave height in 58 selected communities along the coastline
Earthquake magnitude (Mw)	6.0, 6.5, 7.0, 7.5, 8.0, 8.5 and 9.0	
Earthquake depth (D)	10, 20, 30, 40 and 50 km.	
DART buoy	No. 54301	

Table 4 Input parameters and outputs for GRNN–2 model

Inputs		Outputs
Epicenter	Fixed at 12 locations	Maximum wave height in 58 selected communities along the coastline
Earthquake magnitude (Mw)	6.0, 6.5, 7.0, 7.5, 8.0, 8.5 and 9.0	
Earthquake depth (D)	10, 20, 30, 40 and 50 km.	
DART buoy	Nos. 23401 and 54301	

2. Discussion of Results

Some examples of the maximum simulated tsunami wave height for Case study A, D, F and J are depicted in Fig. 5. They are shown only for the earthquake of magnitude Mw 9 and depth of 10 km. It was found that in all cases the main energy lobe is directed perpendicular to the elongated source in the deep water. These figures also display the wave height enhancement in the shallow water and especially in proximity to 6 provinces along Thailand's Andaman coastline. Regions in the northwest of Thailand show considerable energy concentration through refraction process.

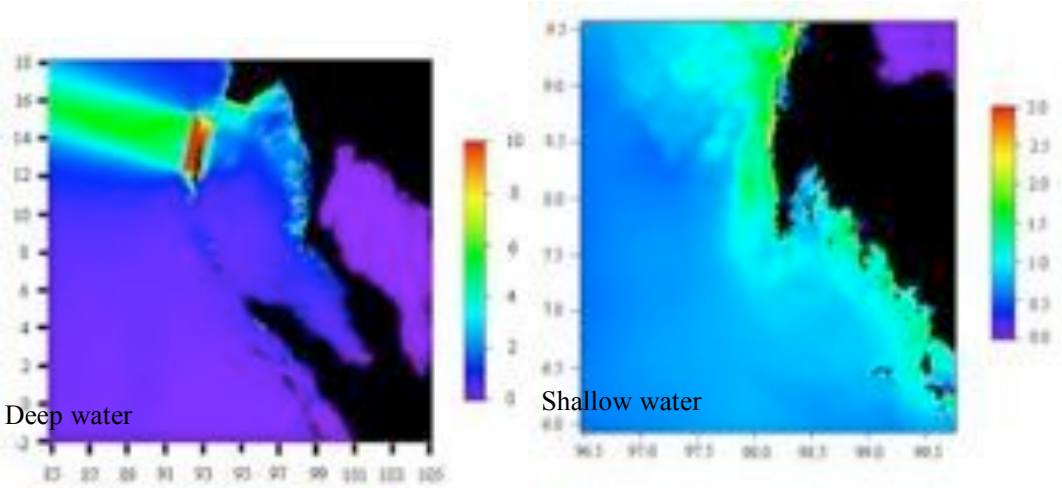

(a) Case A

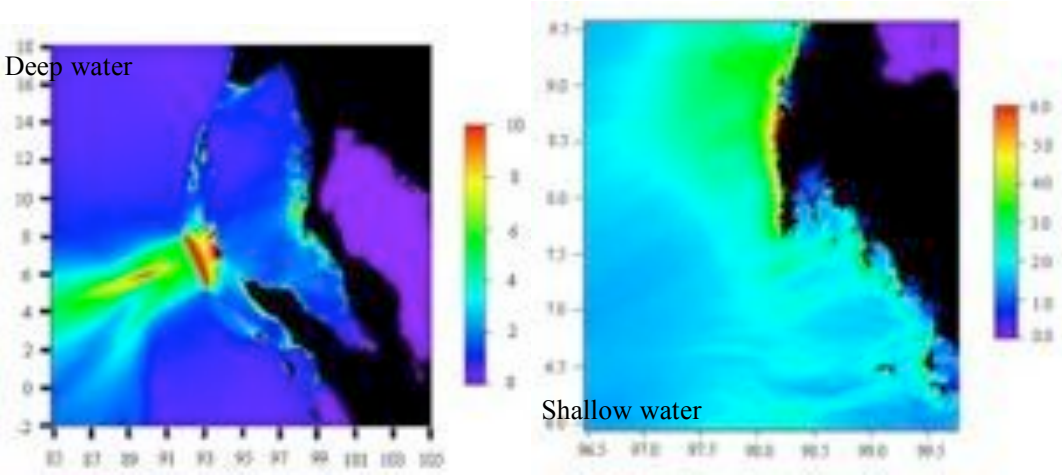

(b) Case D

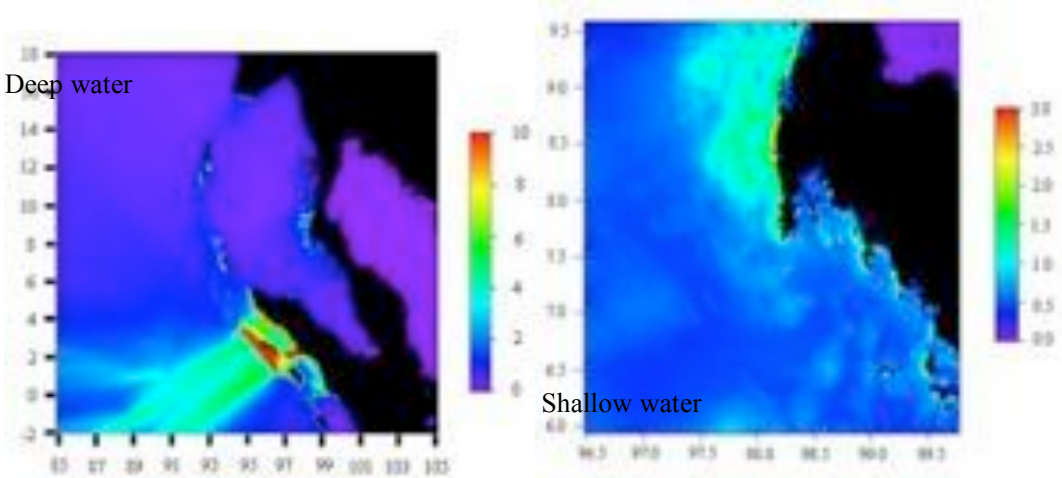

© Case F

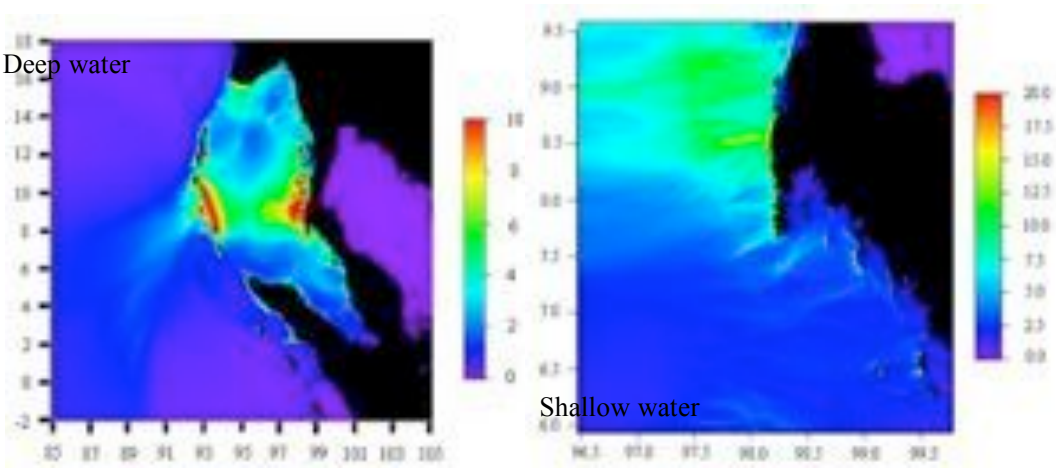

(d) Case J

Fig. 5 Maximum tsunami wave height

Figure 6 shows scatter plots of wave height at some communities (Talaenok, Namkem, Patong and Phiphi) and at 2 DART buoys in the Indian Ocean from the GRNN-1 model. Straight lines show perfect agreement. In general, agreements between the GRNN and numerical model are satisfactory with the EI more than 0.90 and RMSE less than 1 m. However, some deviations are found in medium to large wave heights (Most GRNN model gave underestimated results).

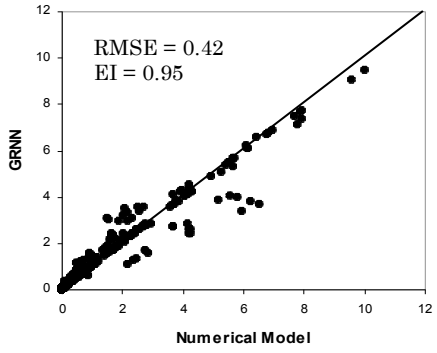

(a) Talaenok

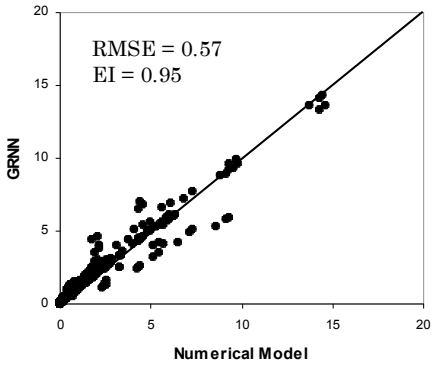

(b) Namkem

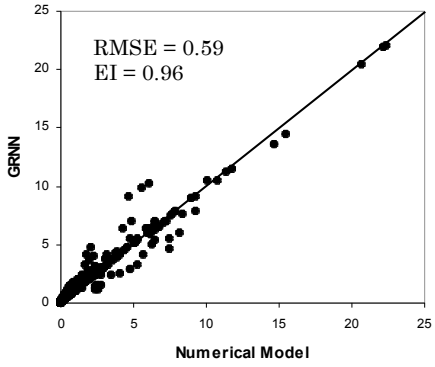

(c) Patong beach

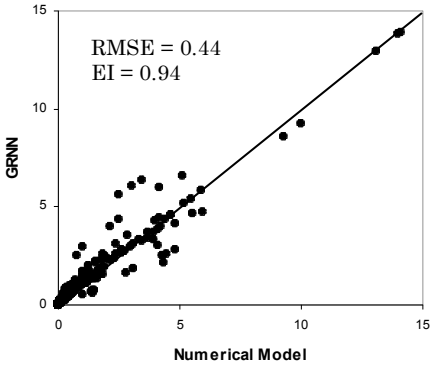

(d) Phiphi Island

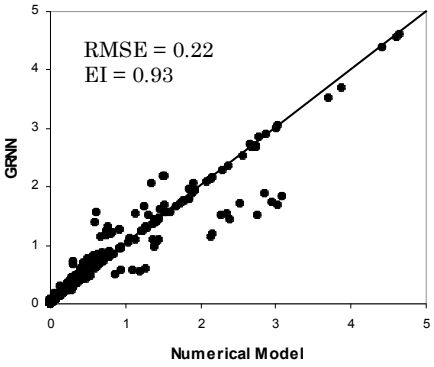

(e) Ao Makam

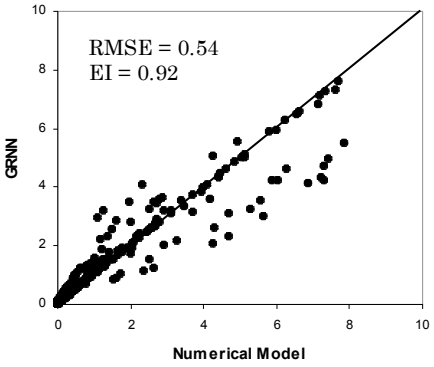

(f) Ko Sarai

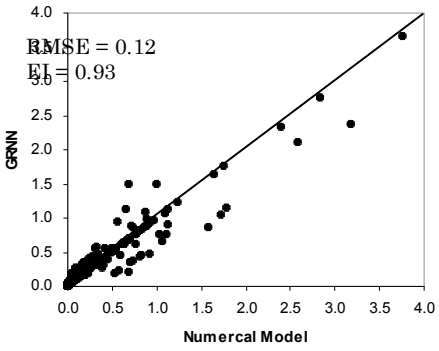

(e) 1st Buoy

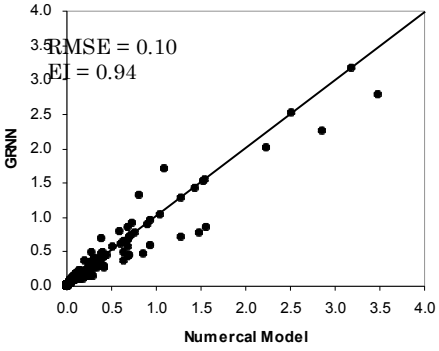

(f) 2nd Buoy

Fig. 6 Scatter plots of Tsunami wave height from GRNN – 1 Model

The outputs of GRNN-1 model in term of arrival time and wave height are stored and displayed on a website. By moving a cursor to the location where the earthquake occurred (Fig. 7a), 2 inputs (Earthquake magnitude and depth) are needed to fill (Fig. 7b). The program then selects a database corresponding to the event and displays the arrival time and wave height in 6 provinces along Thailand's Andaman coastline (Fig. 7c). Then, by moving the cursor to a location of where you are and press enter, the arrival time and wave height for communities at risk in that province will be displayed (Fig. 10d). Therefore, the people in several communities can understand their tsunami vulnerabilities within 5 minutes after the earthquake occurrence and can prepare themselves for safe evacuation according to the tsunami evacuation route map.

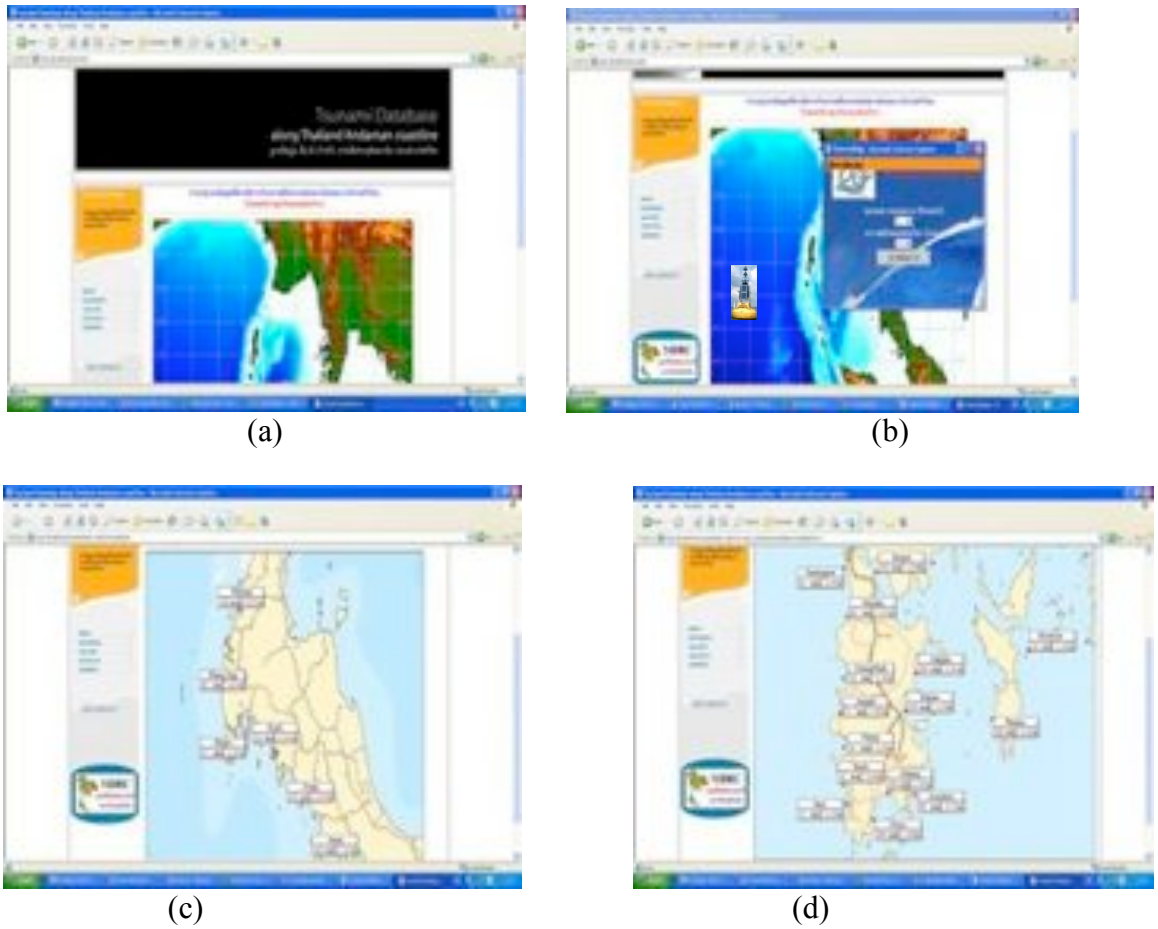

(a) (b)

(c) (d)

Fig. 7 Web-based online tsunami warning system for Thailand's Andaman Coastline

However, in real practice, the confirmation of tsunami wave arrival is one of interesting topics for researchers. Therefore, several false alarms may be expected. In this paper, we try to use the real-time deep sea buoy for making an assessment of the severity of the waves at the risked communities. Therefore, we improved the previous GRNN model (GRNN-1) by including wave height at the DART buoys (Nos. 23401 and 54301) that were installed in the Indian Ocean. The

forecasted outputs of tsunami height at the same 58 communities can be computed as given in Table 5. Scatter plots of tsunami waves at 6 communities same as Fig. 6 is also shown in Figs. 8 to 10.

Table 5 Statistical parameters comparison

Communities	GRNN-1 Model		GRNN-1.1 Model		GRNN-1.2 Model		GRNN-2 Model	
	EI	RMSE (m)	EI	RMSE (m)	EI	RMSE (m)	EI	RMSE (m)
Klongkong	0.92	0.40	0.97	0.27	0.97	0.27	0.98	0.24
Kaopayam	0.95	0.41	0.98	0.26	0.97	0.30	0.98	0.29
Bangben	0.92	0.39	0.97	0.27	0.97	0.27	0.97	0.24
BanChakle	0.94	0.09	0.97	0.06	0.97	0.06	0.98	0.06
Talaenok	0.93	0.51	0.98	0.32	0.97	0.34	0.98	0.30
Suksamlan	0.95	0.44	0.98	0.28	0.98	0.31	0.98	0.29
BanTream	0.96	0.41	0.98	0.27	0.98	0.28	0.98	0.27
Tunglaaon	0.95	0.17	0.98	0.11	0.98	0.11	0.98	0.12
Tungdab	0.96	0.54	0.98	0.42	0.98	0.44	0.98	0.47
Tungtuk	0.95	0.58	0.98	0.36	0.98	0.38	0.98	0.43
Namkem	0.94	0.60	0.98	0.40	0.98	0.41	0.98	0.38
Bandsak	0.96	0.63	0.98	0.43	0.98	0.44	0.98	0.41
Pakarang	0.97	0.66	0.98	0.47	0.98	0.48	0.98	0.47
Bangniang	0.97	0.73	0.98	0.57	0.98	0.60	0.98	0.59
Tablamu	0.97	0.52	0.98	0.44	0.98	0.48	0.98	0.48
Tabyang	0.98	0.56	0.98	0.49	0.98	0.53	0.98	0.56
Nairai	0.97	0.59	0.98	0.46	0.98	0.49	0.98	0.50
Natai	0.97	0.58	0.98	0.44	0.98	0.46	0.98	0.46
Klong Klain	0.92	0.14	0.97	0.09	0.97	0.09	0.98	0.08
Klongbon	0.93	0.22	0.97	0.16	0.97	0.16	0.97	0.15
Plunai	0.95	0.25	0.97	0.18	0.97	0.18	0.97	0.18
Bangpat	0.89	0.14	0.95	0.10	0.94	0.10	0.96	0.09
SaunMaprawe	0.97	0.56	0.98	0.42	0.98	0.42	0.98	0.45
Naiyang	0.97	0.66	0.97	0.62	0.97	0.63	0.97	0.59
Pasak	0.97	0.50	0.98	0.39	0.98	0.39	0.98	0.41
Kamala	0.97	0.56	0.98	0.43	0.98	0.45	0.98	0.46
Patong	0.96	0.59	0.97	0.51	0.97	0.52	0.96	0.56
Karon	0.97	0.70	0.97	0.66	0.97	0.67	0.98	0.58
Kata	0.97	0.71	0.97	0.65	0.97	0.66	0.98	0.64
Saiyuan	0.96	0.29	0.97	0.22	0.97	0.22	0.97	0.23
Palai	0.95	0.23	0.98	0.14	0.98	0.14	0.99	0.12
Aomakam	0.94	0.23	0.98	0.14	0.98	0.14	0.98	0.12
Bangku	0.91	0.21	0.96	0.13	0.96	0.14	0.97	0.12
Phaklok	0.93	0.24	0.98	0.14	0.98	0.14	0.98	0.12
Kaoaen	0.93	0.58	0.95	0.45	0.95	0.47	0.96	0.44
Leam Sak	0.87	0.19	0.94	0.14	0.93	0.14	0.95	0.12
Tatonglang	0.91	0.30	0.96	0.19	0.96	0.19	0.97	0.17
Khao Kuao	0.94	0.27	0.96	0.21	0.97	0.20	0.97	0.20
Ao Nang	0.92	0.37	0.97	0.24	0.97	0.23	0.97	0.22
Phiphi	0.94	0.43	0.96	0.35	0.96	0.35	0.96	0.36

Khlong Prasong	0.89	0.20	0.96	0.13	0.95	0.14	0.97	0.12
Khlongruao	0.87	0.27	0.95	0.18	0.95	0.18	0.96	0.16
Khaopu	0.94	0.38	0.97	0.27	0.98	0.25	0.98	0.25
Klongtop	0.94	0.45	0.97	0.30	0.97	0.29	0.98	0.27
Pak Klong	0.93	0.35	0.98	0.19	0.97	0.22	0.99	0.17
Musa	0.88	0.25	0.94	0.18	0.94	0.18	0.95	0.16
Dunun	0.90	0.24	0.96	0.16	0.96	0.16	0.97	0.14
Hang Lang	0.91	0.32	0.97	0.20	0.97	0.20	0.98	0.17
Khao Phul	0.92	0.29	0.97	0.18	0.97	0.18	0.98	0.16
Phla Muang	0.90	0.15	0.95	0.10	0.95	0.10	0.96	0.09
Lang Khao	0.93	0.36	0.97	0.24	0.98	0.22	0.98	0.21
Na Hedchum	0.91	0.20	0.96	0.14	0.96	0.14	0.97	0.12
Na Hedchum	0.92	0.22	0.97	0.14	0.97	0.14	0.98	0.12
Tong Kanan	0.88	0.23	0.95	0.16	0.94	0.17	0.95	0.15
Son Klang	0.92	0.36	0.97	0.23	0.97	0.22	0.98	0.19
Taolosai	0.91	0.20	0.96	0.14	0.96	0.14	0.97	0.12
Klongkike	0.87	0.21	0.94	0.15	0.93	0.15	0.95	0.13
Ko Sarai	0.93	0.49	0.97	0.31	0.97	0.31	0.98	0.26
Average	**0.93**	**0.38**	**0.97**	**0.28**	**0.97**	**0.29**	**0.97**	**0.28**

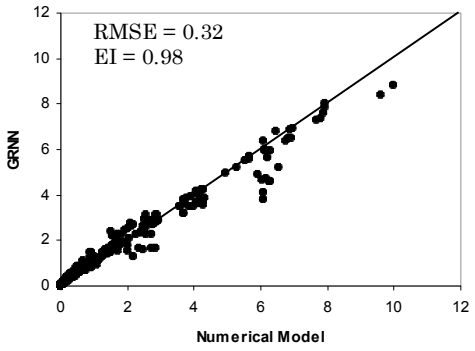

(a) Talaenok

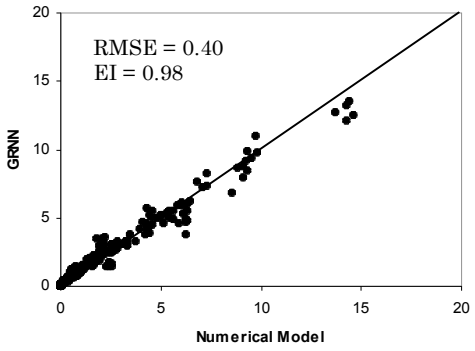

(b) Namkem

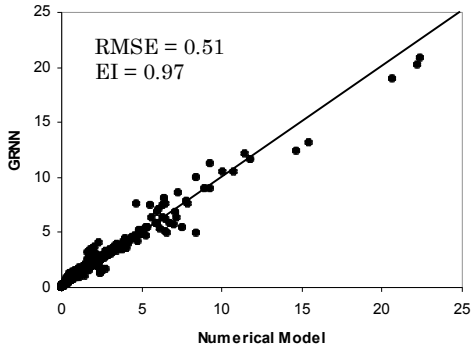

(c) Patong beach

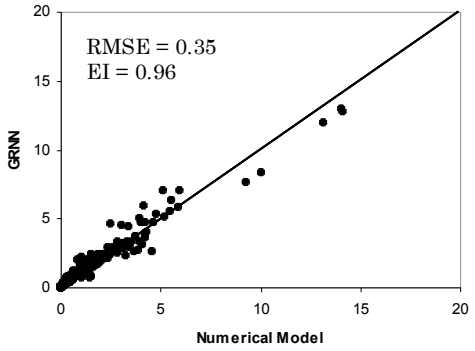

(d) Phiphi Island

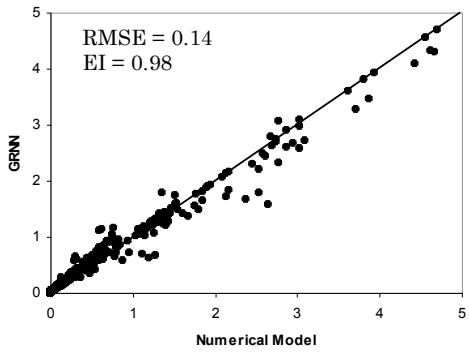

(e) Ao Makam

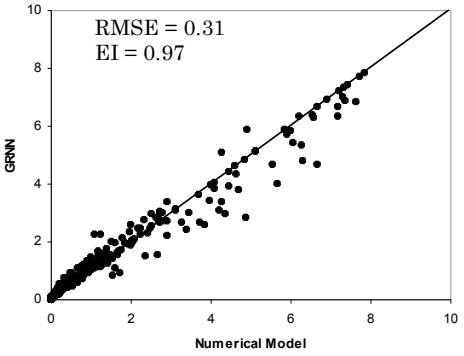

(f) Ko Sarai

Fig. 8 Scatter plots of Tsunami wave height from GRNN – 1.1 Model

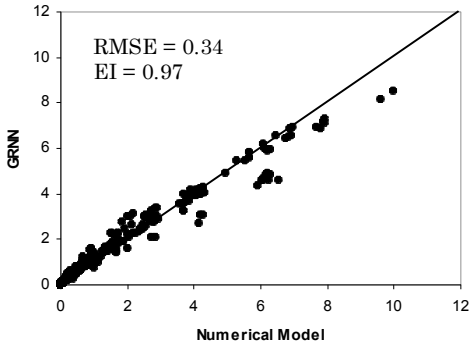

(a) Talaenok

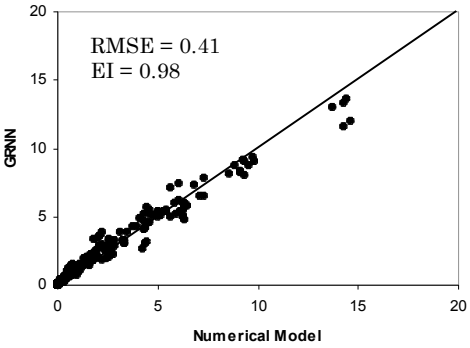

(b) Namkem

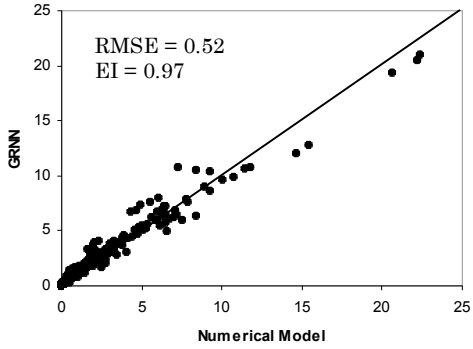

(c) Patong beach

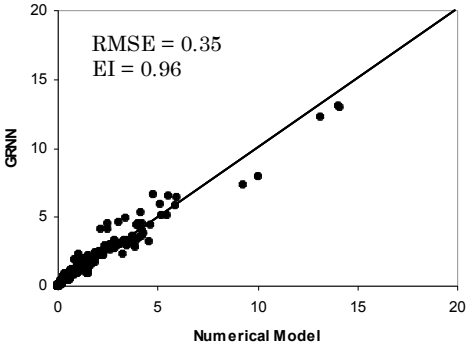

(d) Phiphi Island

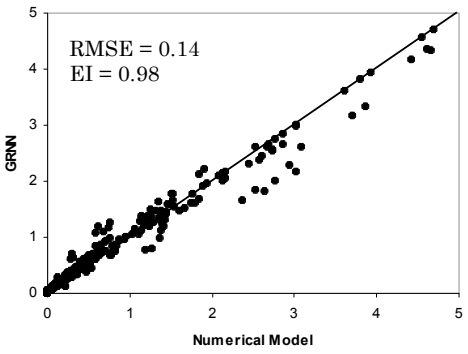

(e) Ao Makam

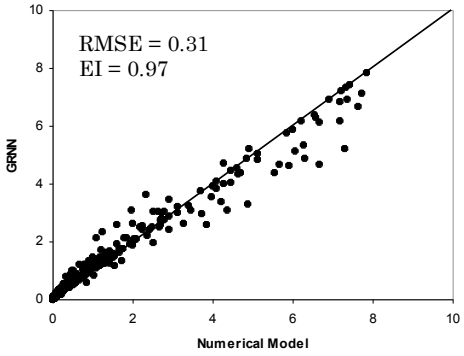

(f) Ko Sarai

Fig. 9 Scatter plots of Tsunami wave height from GRNN – 1.2 Model

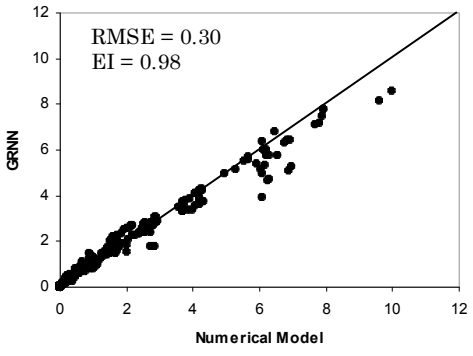

(a) Talaenok

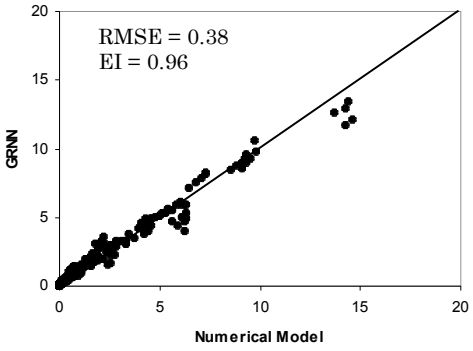

(b) Namkem

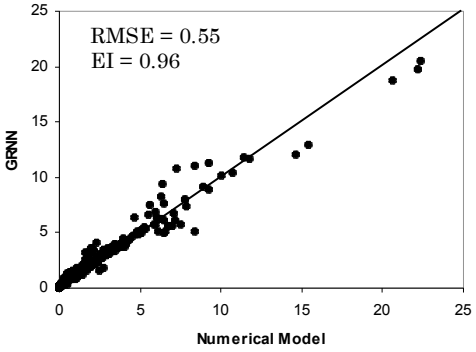

(c) Patong beach

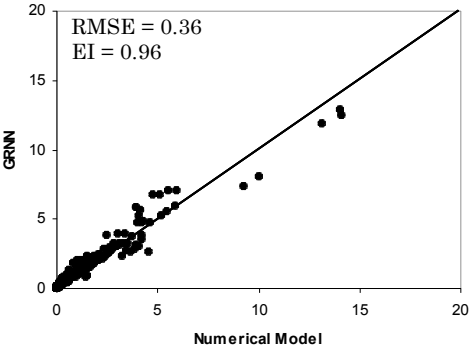

(d) Phiphi Island

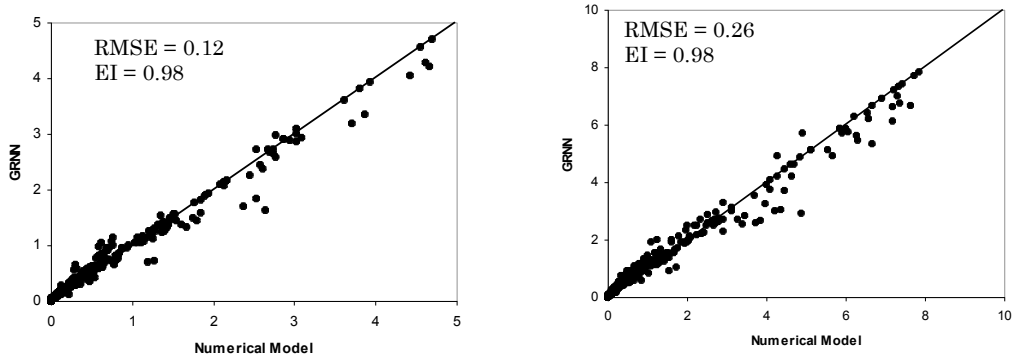

(e) Ao Makam (f) Ko Sarai

Fig. 10 Scatter plots of Tsunami wave height from GRNN -2 Model

It can be seen from Table 6 that, on the average, the EI increases 4 % while the RMSE decreases 26 % for all last 3 models (GRNN-1.1, GRNN-1.2, GRNN-2) compared to the first GRNN model (GRNN-1). These significant improvements of EI and RMSE indicate the essential requirement of real-time monitoring from these buoy data for the confirmation of tsunami warning massages to the people. We could not see significant difference among the last 3 models in Figs. 8 to 10. Therefore, the GRNN-1.1, GRNN-1.2, and GRNN-2 models can be used to compute the updated value of wave heights along 58 communities at risk, depending on the time arrival of wave at the buoys.

6. Conclusions

In this study, we present the development of the Tsunami Warning System for Thailand's Andaman Sea coastline by using 3 combination techniques; numerical simulation, GRNN and web base developing, and data assimilation from DART buoys. The numerical simulation (by the linear and non-linear shallow water equations) was carried out from the 420 hypothetical cases of postulated tsunamigenic earthquakes with epicenters on the Andaman micro plate in the Indian Ocean. The outputs are tsunami arrival time and the maximum tsunami wave height at 58 selected communities (along Thailand Andaman coastline) and at 2 locations of DART buoy in the Indian Ocean. The model was calibrated with the data of the tsunamis of 1881, 1941 and 2004. The computed results from the numerical model were used to train and test the GRNN model with only 4 input parameters (latitude, longitude and earthquake magnitude and depth) by the cross training technique. Good accuracy of the forecasted results by the GRNN (GRNN-1) model was found from the efficiency index (EI > 0.90) and the root mean square error (RMSE < .38 m). Then, the results were used to construct the tsunami database which could be displayed on the internet website. Finally, we assimilated the data from two DART buoys in the Indian Ocean to the previous model, thus deriving three additional GRNN (GRNN-1.1, GRNN-1.2, and GRNN-2) models. The additional GRNN models gave a higher performance (EI increases of 4 % and RMSE decreases of 26 %) compared to the GRNN-1 model. The selection of the models is dependent on the arrival time of a tsunami. Thus, thesr models can be used to confirm and update tsunami generation and potential tsunami heights near the epicenter and at Thailand's coastline.

7. References

Cigizoglu H. K., Generalized regression neural network in monthly flow forecasting, Civil Engineering and Environmental System, Vol.22, No.2, 71-84. 2005.

Donald L. and Kevin J., New Empirical Relationships among Magnitude Length, rupture width, rupture area and surface Displacement, Bulletin of the Seismological Society of America, Vol. 84, No.4, 997-1002. 1994.

Flood, I., and Kartam, N., Neural networks in civil engineering –I Principles and understanding, Journal of Computing in Civil Engrg., ASCE, Vol. 8, No.2, 131-148. 1994.

Kanamori, H.,1977, The energy release in great earthquakes, Journal of Geophys. Res., 82., pp 1981 – 1987

Hsieh, B. B. and Pratt, T. C., Counter-propagation network, Journal of Applied Optics, Vol. 23, No.6, 4979 – 4984. 2001.

International Federation of Red Cross and Real Crescent Societies, Worlds Disaster Report, Kumarian Press, Bloomfield, Connecticut, pp 246. 2005.

Japan Meteorological Agency, Japan Meteorological Agency - The national meteorological service of Japan, Japan. 2006.

Kowalik, Z. and Murty, T.S, Numerical simulation of two-dimensional tsunami runup. Marine Geodesy, Vol. 16, No.2, 87–100. 1993.

Lay, T., Kanamori, H., Ammon, C., Nettles, M., Ward, S., Aster, R., Beck, S., Bilek, S., Brudzinski, M., Butler, R., DeShon, H., Ekstrom, G., Satake, K. and Sipkin, S., The Great Sumatra-Andaman Earthquake of 26 December 2004, Science, Vol 308, No. 5725, 1127 – 1133. 2005.

Lee, H.-J., Cho, Y.-S.,and Woo, S.-B., Quick tsunami forecasting based on database. IN Satake, Kenji, editor, Tsunamis - Case studies and recent developments, Springer (Dordrecht, The Netherlands), 231-240. 2005.

Mansinha, L and Smylie, D.E, The displacement fields of inclined faults , Ball. Seism. Soc. Auer.61, 1433-1440. 1971.

National Disaster Warning Center, A document for the Tsunami alert rapid notification system (trans) system design and plan workshop, 24th -27th May, Sailom Hotel, Huahin Thailand. 2006.

NOAA's National Geophysical Data Center, http://www.ngdc.noaa.gov/seg/hazard/tsrnsrch_idb.shtml. 2005.

Shuto, N., T. Suzuki, K. Hasegawa, and K. Inagaki, A study of numerical techniques on the tsunami propagation and run-up, Science of Tsunami Hazard, Vol. 4, No.2, 111-124. 1986.

Shuto, N. and Imamura, F., IUGG/IOC time project, numerical method of tsunami simulation with the leap-frog scheme manuals and guides, UNESCO' s Workshop, Paris. 1997.

Specht, D.F., A General Regression Neural Network, IEEE trans on Neural Networks, Vol. 2, No. 6, 568 – 576. 1991.

Supharatid, S., Tidal-level forecasting and filtering by neural network model, Coastal Engineering Journal, Vol 45, No. 1, 119-138. 2003.

Titov, V.V. and C.E. Synolakis. Numerical modeling of tidal wave runup. Journal of Waterways, Ports, Coastal and Ocean Engineering Vol. 124, No.4, 157-171. 1998.

Titov, V.V., F.I. González, E.N. Bernard, M.C. Eble, H.O. Mofjeld, J.C. Newman, and A.J. Venturato. Real-time tsunami forecasting: Challenges and solutions, Natural Hazards Vol. 35, No. 1, 41-58. 2005.

Whitmore, P. M. and Sokolowski, T. J. Predicting tsunami amplitudes along the North American coast from tsunamis generated in the northwest Pacific Ocean during tsunami warnings, Science of Tsunami Hazards, Vol. 14, No. 3, 147-166. 1996.

TSUNAMI SCENARIO SIMULATOR: A TOOL FOR ENSURING EFFECTIVE DISASTER MANAGEMENT AND COASTAL EVACUATION IN A MULTILANGUAGE SOCIETY

Virginia Clerveaux
Toshitaka Katada
Department of Civil Engineering, Gunma University,
Gunma, Japan

Kyohei Hosoi
Institute of Social Technology, Japan

Email: v_clerveaux@yahoo.com

ABSTRACT

An emergent paradigm in disaster-risk reduction is the issue of Multilanguage societies within the context of risk information and communication. The primary mitigation measure for tsunamis is the development of effective warning systems and evacuation strategies. The scale of the earthquake, the level of maintenance of prevention structures, such as seawalls, efficiency of the information dissemination system and the residents' willingness to evacuate, influence the impact of a tsunami disaster. Therefore, the goal of tsunami disaster reduction is concerned not only with the use of prevention infrastructures but also with encouraging residents to evacuate quickly through the provision of disaster education and the relay of disaster information in a manner comprehendible by all groups in society. The simulator combines hydrodynamic simulation of tsunamis with warning and human-response simulations for evacuation. Additionally, because of its visual 3D/GIS presentation the simulator is an effective tool for educating the public.

Keywords: Tsunami Scenario Simulator, Risk Communication, Multilanguage Groups**,** Risk Information, Disaster Management, and Disaster Education

1. INTRODUCTION

The generation of risk information and its timely and effective communication to stakeholders in a disaster management jurisdiction is the essence of strategies for hazard/disaster loss reduction. However, the latter is a major challenge for disaster managers, especially in an increasingly globalized world characterized by higher levels of Multilanguage as more and more people migrate to locations outside their culture zones where not only language differs, but also perceptions of and attitudes towards hazard/disaster risk (Martin 2003). Disaster managers therefore have to design effective risk communication strategies that span language differences and are sensitive to the various language groups present in the society, so that warnings can be encompassing and inclusive. There is therefore a need for disaster management decisions to reflect an understanding of risk.

Over the years, several theories and models have been developed to explain the risk communication-disaster management interface and, in response to the failure of traditional practice theories, to address multicultural issues (Cross, T, et al 1989; Green, J.W. 1995; LaFromboise, T.D, & Foster, S.L 1992 ; Sue, D.W. & Sue, D. 1990 & Sue, D.W, 1992) such as language differences. Language is a defining criterion of culture and as such, differences in language can prove a formidable barrier to effective risk communication. Since learning a new language requires time and patience, recent immigrants as well as visitors to a country may experience information communication gaps. In fact, some elderly people may never develop the language skills required to effectively communicate in a new society. Therefore, emergency preparedness and response information will require effective translation to be fully understood by different cultural/language groups. Translations should convey the message clearly and be delivered in a manner respectful of cultural differences. In addition, during an emergency, language skills which are normally adequate may be impaired due to stress and pressure (Solis G. et al 1997).

Given the complexities of effectively communicating to mixed groups there is increasing suggestion that multiple media and tools be used to communicate with residents in emergency situations. To develop a single model or tool that would embrace all aspects of ethnical and cultural risk perceptions (beliefs, values, gender, and age) and all aspects of risk communication strategy is, to say the least, a formidable challenge. While there are many cultural issues that can affect risk perception and subsequently disaster management response, this paper will focus primarily on how to overcome challenges in communicating in a society where multiple languages are spoken and how the application of this model will allow disaster managers to effectively communicate risk information in a Multilanguage society.

In the Turks and Caicos Islands (TCI), approximately 65% of the population is foreigners

(Clerveaux 2005) and the majority is not competent in English, the national language. This situation poses a serious problem for disaster managers in the TCI especially as this relates to effectively communicating risk information and warnings. Like the rest of the Caribbean region, the TCI is unprepared to deal with a tsunami hazard. Warning systems are non-existent and the bulk of the resort facilities and non-English-speaking nationals are located in a zone vulnerable to tsunamis. It is in that regard that the tsunami scenario simulator model was designed to ensure that during the occurrence of a tsunami risk/warning information being communicated is understood by both English and non-native English speakers. This simulator can be used as an educational tool by disaster management decision-makers in the TCI and the general population, allowing them to become more accountable for their actions. This is because the model has the capacity to simulate different 3D scenarios that are determined by the actions taken by residents. Through the use of this simulator, disaster managers will be better able to effectively communicate risk information in a Multilanguage setting by using several media simultaneously. These will include sound, speech and text, thus ensuring that the dissemination of risk information is not biased towards any particular language group. In other words, the use of this simulator by disaster administrators can be an effective mitigation tool as it displays the complexities that are involved in communicating disaster risk information in a Multilanguage society.

2.0 METHODS

2.1 Multilanguage Perspective in the Design of the Model

One of the most important requirements for social life is communication. Every human culture includes a language; language is the primary means of linking members of a society together. During a disaster, communication between people may fail due to language differences. This could reduce the efficiency of the overall response system. For this reason, minority language groups in our society may be at a greater risk in a disaster. It is therefore the responsibility of emergency planners and responders to identify and work to overcome these barriers. Emergency planners must find alternative methods to reach out to ensure that all community members are aware of emergency procedures. The communication network developed to spread preparedness information may also be useful during emergency response. An effective means of communication could be a lifeline to victims of a disaster (Solis, G et al 1997).In designing the model the following were taken into consideration to enhance the communication of risk/warning information in a Multilanguage society:

1.
2. Identification of members of ethnic/language groups to determine the number of different languages and dialects spoken among them.
3. Translation of warning information into the main languages spoken in the country since during emergency, language skills which are normally adequate may be impaired due to stress and pressure.
4. Repetition of warning messages
5. Use of several media to communicate warning information since people who do not speak English fluently may not receive information through mainstream radio, television and newspapers.
6. Use of oral communication: the model recognizes that even the most meticulous disaster preparation cannot guarantee that communication efforts in times of emergency will be effective. Serious disasters may disable infrastructure such as telephone lines or television and radio transmission. There may remain a small number of people who do not receive critical information, and as such, the model takes into consideration the need to convey information by alternate means.
7. Use of simple terminology in the body of the warning message to ensure that the message will be understood by all groups in society regardless of educational attainment.
8. 3D simulation of residents' behavioral output. The realistic visual output of the simulator makes it a great tool for encouraging residents to take appropriate measures to cope with disasters.

3.0 Delineation of the Tsunami Scenario Simulation Model

The Tsunami Scenario Simulator model consists of three components:

i. Information Transmission Simulation Model
ii. Evacuation Transmission Simulation Model
iii. Tsunami Transmission Simulation Model
iv.

i. Information Transmission Simulation Model

The information transmission simulation model provides warning and other relevant information from the authorities to the public, through various communication media (Figure 1). The model also depicts informal means of communication between residents by expressing the communication that occurs by means of telecommunication (i.e. cellular phones and telephones) and face-to-face contact.

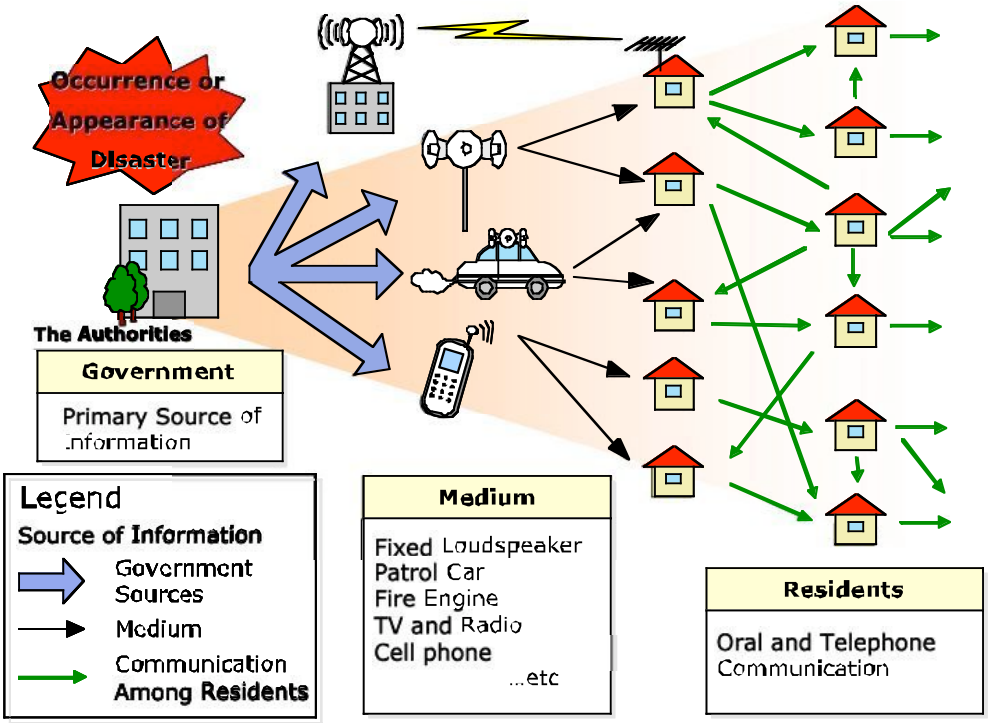

Figure 1: Information Dissemination Framework

The model also takes into consideration spatial distribution of information and the elapse of time of information communicated. The basic structure of this simulation model is constituted according to the Biased Net Model (Rapoport 1979). The information transmission model developed for Providenciales in the TCI takes into consideration:

1. Use of cell phones by government authorities to transmit risk/warning information to residents via SMS (Short Message Services) and an Emergency Ring Tone.
2. Simultaneous transmission of warning messages in the 3 main languages (English, French-Creole and Spanish) spoken in the country
3. Face to Face oral and Tel-communication (fixed line and cellular phones) by residents
4. Use of fixed loudspeakers to transmit a warning sound
5. Use of Patrol Car Speakers to disseminate warning information

ii. Evacuation Transmission Simulation Model

This aspect of the model expresses residents' evacuation behavior from their houses to the nearest shelter after the transmission of evacuation information. The model can also express the preparation time for evacuation, that is, the time that it takes residents to begin evacuation

from the time the evacuation order was issued. The Evacuation model takes into consideration residents' decision-making processes with regard to evacuation i.e. whether or not to undertake evacuation. The model also takes into consideration other factors that might impinge on residents' evacuation behavior and the status of the threat situation at the time residents begin their evacuation to the shelters.

The model expresses residents' evacuation behavior in terms of a family unit, allowing users to establish the family's structure, evacuation speed, evacuation start time and destination. The model assumes that each family evacuates from their house to the nearest shelter at a constant speed. The shortest path from residence to shelter along an existing road network is used as the evacuation route by the simulator. The evacuation simulation has the capability to calculate the time required to undertake evacuation by identifying the shortest evacuation route, impassable routes due to fallen trees or utility poles and traffic congestion that might impede evacuation speed or movement. Therefore, integrating these various elements together, the time frame required for each resident to evacuate safely based on the calculated time that the tsunami will make landfall can be established, as well as variations in the distribution of evacuees due to changes in time flow.

iii. Tsunami Transmission Simulation Model

This component of the model uses a GIS-based framework to calculate the number of casualties that are likely to result from the occurrence of the tsunami, the location of potential evacuees at the onset and during the impact of a tsunami and the areas that would have been inundated by the tsunami. This tsunami simulation works independently from the two simulations previously discussed. This model simulates possible wave height and flood velocity by taking into consideration the geophysical characteristics (such as bathymetry) of the impact zone, during the occurrence of the tsunami. The model is mindful that the tsunami impact will be influenced by the magnitude and location of the hypocenter of the earthquake that caused the tsunami and the existence of prevention infrastructures (e.g. seawalls) in the area. In that regard, the model allows simulation of different scenarios involving earthquake characteristics, human interventions and behavior to mitigate impact.

4.0 DISCUSSION

4.1 Suitability of the TCI for Application of the Model

The Turks and Caicos Islands (TCI) is a small British Dependency covering 430 square kilometers and is situated at approximately 21 degrees latitude and 71 degrees longitude (Figure 2).

Figure 2: Location of the Turks and Caicos Islands

With a national population of only 11,750 people, the TCI is unable to fill much of its human resource demand for educators, medical practitioners etc, from local sources and as a result, relies heavily on the active recruitment of skilled and unskilled migrant workers to fulfill these needs. The TCI is also deficient in physical resources such as agricultural land and fresh water supply. In spite of these deficiencies, the country has maintained a standard of living that surpasses many of the neighboring Caribbean islands, owing to vibrant tourism and offshore banking industries. In essence, the relative prosperity of the TCI has served as a pull factor for migrants throughout the Caribbean region and other countries outside the region (Clerveaux 2005). Currently, the migrant population of the TCI accounts for approximately 65 percent of the 33,202 people living in these islands (DEPS 2006). Although English is the official language of the TCI both Spanish and French-Creole are commonly spoken owing to the influx of migrants from neighboring Dominican Republic and Haiti.

4.2. Multilanguage Concerns in the Turks and Caicos Islands

The issue of Multilanguage is one of the emergent paradigms in disaster management, especially within the context of risk information and risk communication for hazard/disaster risk reduction. The Caribbean region is no stranger to multiculturalism and Multilanguage and even before the formation of the Caribbean Common Market (CARICOM), significant intra-regional movement of people occurred. The recent strengthening of CARICOM through the establishment of the Caribbean Single Market and Economy (CSME) is resulting in even greater movement and resettling of people and languages in host destinations. In a region that is among the most disaster prone in the world and where the multicultural mix involves not only people with different languages, but also differences within the same language, the issue of communicating disaster-related information in an efficient and effective way becomes particularly relevant.

Over the years, the migrant population of the TCI has been increasing steadily. This trend is likely to continue in the foreseeable future especially in light of the increasing economic development based on one of the most vibrant tourism industries in the Caribbean region and the continued shortage of local sources of labor. Since it is the responsibility of the national government of the TCI to facilitate the safety of visitors and migrants alike, and in light of the ever-increasing numbers of visitors and migrants, there is extreme urgency for the formulation and implementation of measures that will ensure the safety of all during an emergency. As such, the need for strategies that will allow timely and effective communication of disaster-related information within the context of the Multilanguage environment cannot be overstated. Warning and evacuation information are most critical in that regard as ineffectiveness in their communication can make the difference between life and death during hazard emergencies such as a tsunami occurrence. The proposed application of the Tsunami Simulation Model on the island of Providenciales in the TCI attempts to address the need for a mechanism that can ensure effective information dissemination and communication, predict the impact of a tsunami on Providenciales and reinforce the need to plan and implement appropriate evacuation measures. The tsunami disaster simulator that is proposed for application in Providenciales has three interrelated components:

1. Transmission of evacuation information
2. The Residents' evacuation behavior
3. Number of casualties in relation to residents' response time

The integration of the above 3 simulators make this tool effective for:
i. Communicating disaster risk information
ii. Analyzing the processes involved in disseminating risk information in Multilanguage society
iii. Analyzing different levels of responses to warnings
iv. Identifying the limitations of present disaster mitigation strategies and,
v. Educating residents on the consequences of their various responses to warning information.

4.3. Aptness of the Island of Providenciales for the Application of the Model

Providenciales is the urban centre of the Turks and Caicos Islands and is situated on the west side of the Caicos archipelago. Providenciales has an area of 38 square miles and is the most developed island in the Turks and Caicos Islands owing to a vibrant tourism industry. Prior to 1960, the island had a population of 500, but today, with a population of approximately 24, 358 (DEPS 2006), it has the largest population concentration in the TCI, accounting for 73% of the resident population of the country. This island also accounts for the largest concentration of non-native population, consisting primarily of Haitians and Dominicans with a recent increase in the number of migrants from within the Caribbean region and outside the region such as from China, Philippines and India. In that regard, Providenciales consist of the largest number of Multilanguage groups in the Turks and Caicos Islands.

In addition, the bulk of the tourism infrastructure of the TCI is concentrated on Providenciales, specifically in Grace Bay which features the famous 12 mile Grace Bay Beach (Clerveaux 2005). Approximately 60 percent of the employment in Providenciales is derived directly or indirectly from tourist-related services and the island has a tourist-to-resident ratio of 10.02 to 1. Grand Turk, which is the capital and the second most developed island in the TCI, and South Caicos, the third most economically vibrant island, and the other islands have a tourist-to-resident ratio of approximately 0.97, 0.62 and 2.88 to 1 respectively. In 2003, Providenciales accounted for 94 % of total tourist arrivals to the TCI. In essence, in the absence of appropriate and effective communication of related risk information to the population of Providenciales and the design of related evacuation measures, the impact of a tsunami or high magnitude hazard on this island would spell unparalleled economic disaster for the rest of the country. In light of the recent focus of Caribbean disaster managers on coastal evacuation planning in the aftermath of the Asian Tsunami and the limited horizontal evacuation options offered by the low topography of Providenciales, the time is opportune for the application of a model that not only ensures effective risk communication but also provides measures for smooth and efficient evacuation during and after the occurrence of a tsunami.

5.0 RESULTS

5.1. Application of the Tsunami Simulation Model to Providenciales

A. Basic Settings Outlined

1. Information Transmission Model

The transmission of information in this model can be described as a 'web of communication' since there is communication taking place between official and informal sources. However, it is worth nothing that the government is the primary source of dissemination of warning information to the public (Figure 1). In this model, the government will utilize a number of media as a means of communicating risk information to the public. These media are loudspeakers, patrol cars, cell phones, and the mass media. On the other hand, residents will engage in face-to-face communication and communication via cell phones and fixed line telephone as a means of verifying the authenticity of the risk information received and in deciding if they should evacuate.

i. Use of loudspeakers:

In the scenario analysis for Providenciales, a proportionate sampling technique was used to determine the optimum number of fixed loudspeakers that should be located in each of its 15 districts. The methodological approach was to first determine the total population of each district as well as the proportion of the population accounted for by the major non-English speaking ethnic groups. Based on population density and sound-range information it is considered appropriate to install 3 loudspeakers for districts with populations exceeding 1000, 2 for districts with populations between 600-999 and 1 loudspeaker where the district population is less than 600. Therefore, a total of 31 loudspeakers would need to be strategically installed throughout the island of Providenciales, assuming a range of 250 meters for each loudspeaker (Figure 3).

Figure 3: Strategic Positioning of Fixed Loudspeakers and Patrol Routes to be used during an emergency situation

The proposed warning sound is a unique one and involves the transmission of three distinct sounds or pitches recorded from the blowing of a conch shell, which in itself is a very distinct sound. Each pitch will be used to communicate 3 main phases of warning information to residents. For example:

Pitch 1: A large earthquake has just occurred.

Pitch 2: There is a possibility that the TCI might be affected by a tsunami, make preparation to evacuate.

Pitch 3: Evacuate Immediately!

It is a known fact that issues such as language differences can hinder the communication process. This may even be the case where two people speak the same language but are of different nationalities: this may lead to the possibility of misinterpretation of information. It is for this reason that the model proposes the use of sound via its fixed loudspeakers. The use of sound,

instead of language, via the fixed loudspeakers ensures that, regardless of primary language, there is no ambiguity or misinterpretation of the risk information being communicated. The information conveyed by the pitch of the conch shell is a universal one as long as people learn the meanings of the different pitches and are sensitized as to what actions are expected following each pitch alert. To accomplish this, a major educational campaign and mock-drills, at regular intervals, will be conducted to enhance preparedness levels. Pitch alerts during a mock drill will differ in length from alerts during an actual hazard occurrence. The former alerts will be short and a one-off sound. However, during an actual hazard pitch alerts would be long and repeated at regular intervals.

The efficiency of the fixed loudspeakers was measured on both resident and tourist population segments in terms of the number of people that can be expected to be reached through this medium. It was found that using this medium, approximately 45 percent of the resident and 30 percent of the tourist population would be able to be reached via this medium. If loudspeakers are to be efficiently located without transmission overlap, some areas will be peripheral to the transmission range and will therefore not be covered. Therefore, patrol cars are proposed to be used to provide information to these areas (Figure 3).

ii. Use of patrol cars:

A total of 8 patrol cars will be dispatched from designated locations along paved roads to disseminate disaster information to the public, especially in those areas not covered by the loudspeakers. Patrol cars will be required to cover a maximum distance of 11 kilometers at a speed of about 20 km per hour. As in the case of the loudspeakers, the patrol cars will also be able to broadcast information at a distance of approximately 250m. For each district, the population size, nationality and primary language of each household was ascertained and plotted on the map. This information is important in order to determine the location of ethnic/language groups, since there is a tendency for persons from similar language/cultural backgrounds to cluster together, and would allow emergency managers to better customize the risk information. Also for each district, the primary language of each household was tabulated and the various languages were then grouped as: English, French-Creole, Spanish and Other (Figure 4†). These languages were then assigned ranking based on prevalence and the rank was used to determine the order in which the patrol cars would relay the warning information to residents in various communities. For instance, if the dominant language in a district is French-Creole, this language would be given priority in transmission followed by the next dominant language

Figure 4: Agglomeration of Population by Primary Language in Providenciales

. *Further investigation proves that the above map closely represents the actual situation which exists in Providenciales in terms of where ethnic groups are presently clustered.

Given the fact that approximately 60 percent of the migrants in the TCI originated from Haiti and owing to the fact that the majority of Haitians are more eloquent in speaking French-Creole rather than standard French, it was deemed prudent that the information being relayed by the patrol car speakers should be disseminated in French-Creole. Additionally, given the absence of data on migrants' educational attainment, it was decided that the information relayed to the residents be simple and brief. This would ensure accuracy and efficiency in the timing of information dissemination from the disaster officials' standpoint and easy comprehension and hopefully prompt responses from residents.

iii. Use of cellular phones*:*

Use of cellular phones to transmit short messages with warning information to the public is another method employed in this simulation. It is estimated that the TCI has a techno-density of two cell phones per person (Oral Communication with Telecommunication Providers, 2007).

Therefore, it was felt that the use of such a communication medium would aid the relevant government officials in transmitting information quickly and in multiple languages. The message that will be relayed via the cellular phone will be tailored to ensure that it is straightforward but informative as to what action is required by residents. An advantage of using short message services (SMS) during a disaster is that it takes less time for the information to be transmitted than using dialogue. Therefore, this medium can prove to be effective during the warning stages of the disaster. Prior to an emergency the government and telecommunication providers on the island would need to cooperate to implement such a system that would allow the transmission of a designated warning tone and the dissemination of risk information in the form of SMS in multiple languages simultaneously via this medium. Such an arrangement would allow the government to transmit the warning sound and text message to all cellular phone holders during an emergency. It would also be required that this sound be heard even if the cellular phone instrument is turned off or is on silent mode by allowing the telecommunication providers to automatically override the codes in the cell phones in order to transmit that warning message or tone. This would therefore further increase the chance of warnings being received by all members of the society.

iv. Use of the mass media

Use of the mass media (radio and television) to communicate disaster information, especially during the onset of a disaster, is one of the oldest media used worldwide. In order to effectively utilize this medium during an imminent threat from a hazard, prior collaboration with local broadcasters would be required. This collaboration can take the form of the disaster office providing personnel who will go on the air to directly relay the warning message from the disaster office to the public or allowing the disaster office to tailor the content as well as the language order in which the information will be broadcasted. The information that will be disseminated through this medium can be very informative, informing residents about the imminent threat, what measures they should be presently undertaking and perhaps, if possible, how much time they have to safely evacuate. This message can also be site specific that is, informing the public of which areas are likely to be impacted first or the expected hardest hit areas and any new development that occurred re the hazard. The use of the mass media is very important because if individuals are located outside the audible range of both the loudspeakers and the patrol car speakers' routes, then the mass media can be relied upon for transmission of risk information to those residents.

v. Use of oral communication

Another medium utilized for information/warning transmission in the model is the use of oral communication. In the context of this model, communication takes place between residents via

telecommunication and face-to-face contact. This parameter was incorporated because in many societies, and especially those that contain large mixed groups, where not only culture is different but also language, there is a tendency for the agglomeration of people either by nationality or language and additionally for mistrust of government. In this model, oral communication is said to take place between residents as a means of verifying the warning message issued and in deciding what action to take. According to Katada et al. (2006), "during a disaster there is increased oral communication between residents. In fact, communication parameters, such as distance of each contact, number of contacts (receivers) and timing of each contact, which usually exist during normal days (i.e. days when there is no imminent threat from a hazard occurrence) tend to increase during a disaster, a factor that explains jammed telecommunication circuits during emergencies. Therefore, it is assumed that oral communication will take place not only between closest neighbors but also with distant friends." This type of communication is especially significant among persons from similar cultural and language backgrounds. During a disaster there is an increased demand by residents for relevant information. However, there is the possibility that communication systems could be damaged and, because of this, oral communication networks will prove to be an effective medium (Katada et al. 1996). Having established a communication web for the dissemination of risk information, disaster managers can therefore determine the information-receipt time for each district in Providenciales (figure 5).

Figure 5: Estimated Information Receive Time by District in Providenciales

They are then in a better position to determine the likely impact a delay in information will have on households.

2. Evacuation Transmission Model

Based on the topography of the island it was decided that all areas below 10 meters could be vulnerable to a tsunami or high magnitude flooding. The inundation level was decided by the authors after taking several factors into consideration such as:

1. Maximum wave height of past tsunamis in the Caribbean.
2. Geographical relief of the seabed near and in the TCI
3. Maximum distance traveled by past Caribbean tsunamis
4. Geographical relief of Providenciales

It is important to note that the inundation depth chosen for Providenciales is not fixed and can be easily modified with the availability of new data or to reflect current situations. Nonetheless, the model in its existing state acts as a type of benchmarking tool that allows disaster managers to simulate different disaster scenarios based on the earthquake characteristic and the origin of the earthquake, and local characteristics of the country etc allowing better preparation for various hazard scenarios. Analysis of the current available data for hazard vulnerability of the TCI suggests that a tsunami hazard is not a significant threat as other hazards such as flooding, hurricane, and storm surge. While tsunamis are not publicly recognized as a major hazard for the TCI, the country is not immune from such threats and sea level changes. It is a well known fact that the earthquake that occurred in Lisbon Portugal in 1755 did travel great distances generating tsunami waves that crossed the Atlantic Ocean, reaching as far as the Lesser Antilles. According to James Lander (1997), the Lisbon Earthquake, in Portugal, "… sent waves into the Caribbean with amplitudes of 7m at Saba, 3.6m at Antigua and Dominica, 4.5m at St. Martin, and 1.5-1.8m at Barbados." Therefore, the Caribbean region is not only vulnerable to tsunamis generated within the region but is also vulnerable to teletsunamis, which may have their origin outside of the region. Given this reality, the implementation of mitigation measures against a possible tsunami occurrence in the TCI can be considered foresightedness and the tsunami model proposed in this study will allow disaster managers to achieve this goal.

In the scenario analysis site for Providenciales there are 15 Government-designated emergency shelters (schools, churches, and community centers) (Figure 6). However, all of these shelters are currently sited below the 10m line. Providenciales has a total of 4926 households but

only 886 households are located in areas of 10m height or above. In other words, approximately 79% of households in Providenciales are below the 10m line and will need to be evacuated in the event of a tsunami or high magnitude meteorological hazard.

Figure 6: Current Location of Shelters and the Emergency Operation Center

Using the model it was determined that, given the current location and number of shelters, if residents were to evacuate by foot, it would take the majority of the population more then 30 minutes to complete evacuation (figure 7) and that the population density in the shelters would be high.

Figure 7: Estimated Evacuation Time by District in Providenciales for Current Shelters

Currently, all the government-designated shelters and the Emergency Management Center, from which disaster mangers are expected to relay warning information, are below the 10m-height level. The model was therefore, able to suggest suitable areas for the strategic relocation of the current shelters, the Emergency Center and the proposed additional 19 shelters, to higher ground throughout the island of Providenciales (Figure 8).

Figure 8: Proposed Relocation of Shelters and the Emergency Operation Center to Higher Ground

Care was taken to ensure that, as far as possible, a shelter would be located in each district. However, this parameter was difficult to achieve given the fact that not all districts had areas of 10m or higher. In order to resolve this problem, shelters were located as near as possible to each district in areas that are 10m or higher. In addition, the time factor required to evacuate quickly from a tsunami was taken into consideration when siting the shelters. However, given the relief of the land, a few shelters had to be located approximately 5 kilometers away from residents in particular districts and therefore evacuation by foot, though the desired mode in order to prevent traffic congestion, would be impossible in light of the time factor involved in evacuating from an imminent tsunami.

Re-simulation of the time required to safely evacuate to shelters based on the relocation of the shelters and the availability of additional shelters indicated that there is a significant decrease of 10 minutes in the time that would be required to complete evacuation on foot by residents. This variance in time can be the difference between life and death in an emergency situation (figure 9).

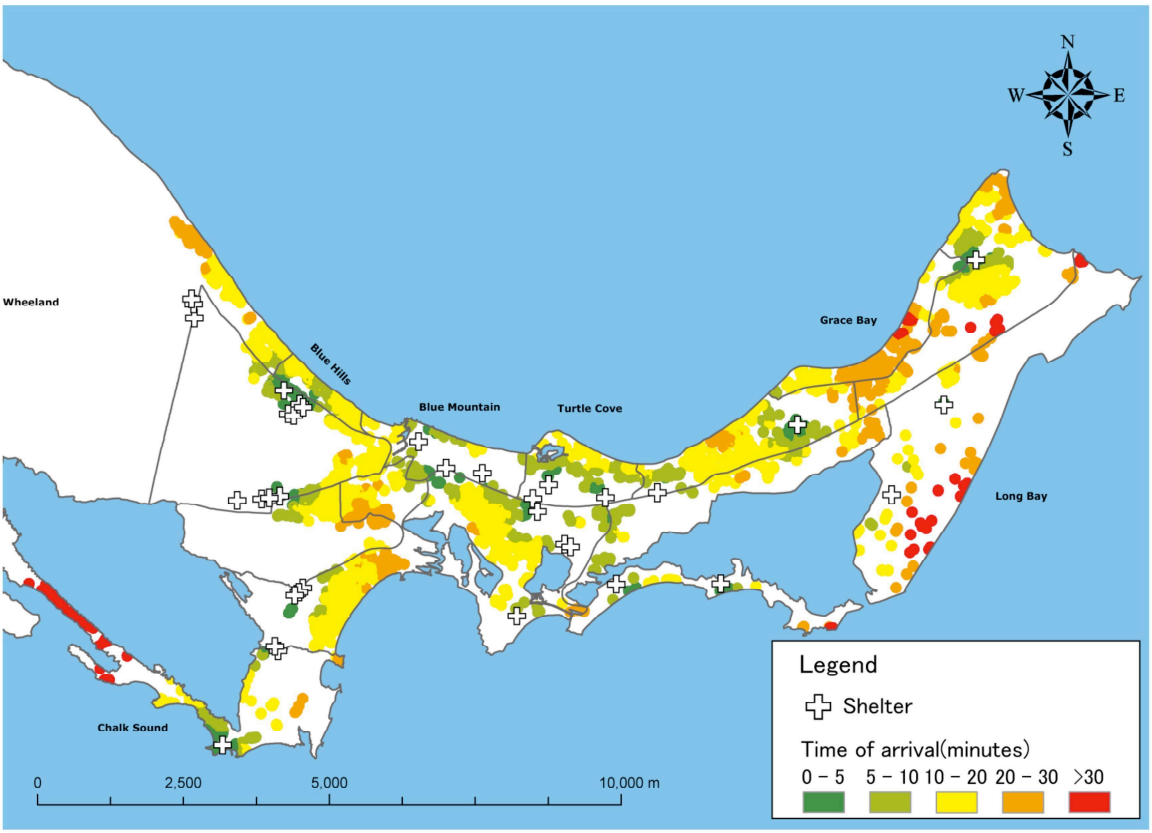

Figure 9: Estimated Evacuation Time by District in Providenciales for Amended Location of Shelters.

In addition, tsunami towers, able to accommodate a higher number of persons, were placed in areas that had a high population density and where the siting of the nearest shelter would still be difficult based both on the parameters of relief and shortest distance to a shelter. Currently, the areas where the tsunami towers have been sited have approximately a combined total population of 4,547 residents and 1,891 hotel room occupancy. It therefore means that shelters would possibly have to be provided for all persons. Of equal importance is the fact that the tsunami towers will be sited near the coast as, according to NOAA (2006), beaches are most vulnerable to loss of life and a 2 meter tsunami would result in high mortality near sea level. Research indicated that in Providenciales approximately 97% (Figure 10) of the hotels are located on relatively low-lying areas (lower than 10m) and of these hotels, only a few are multi-storey.

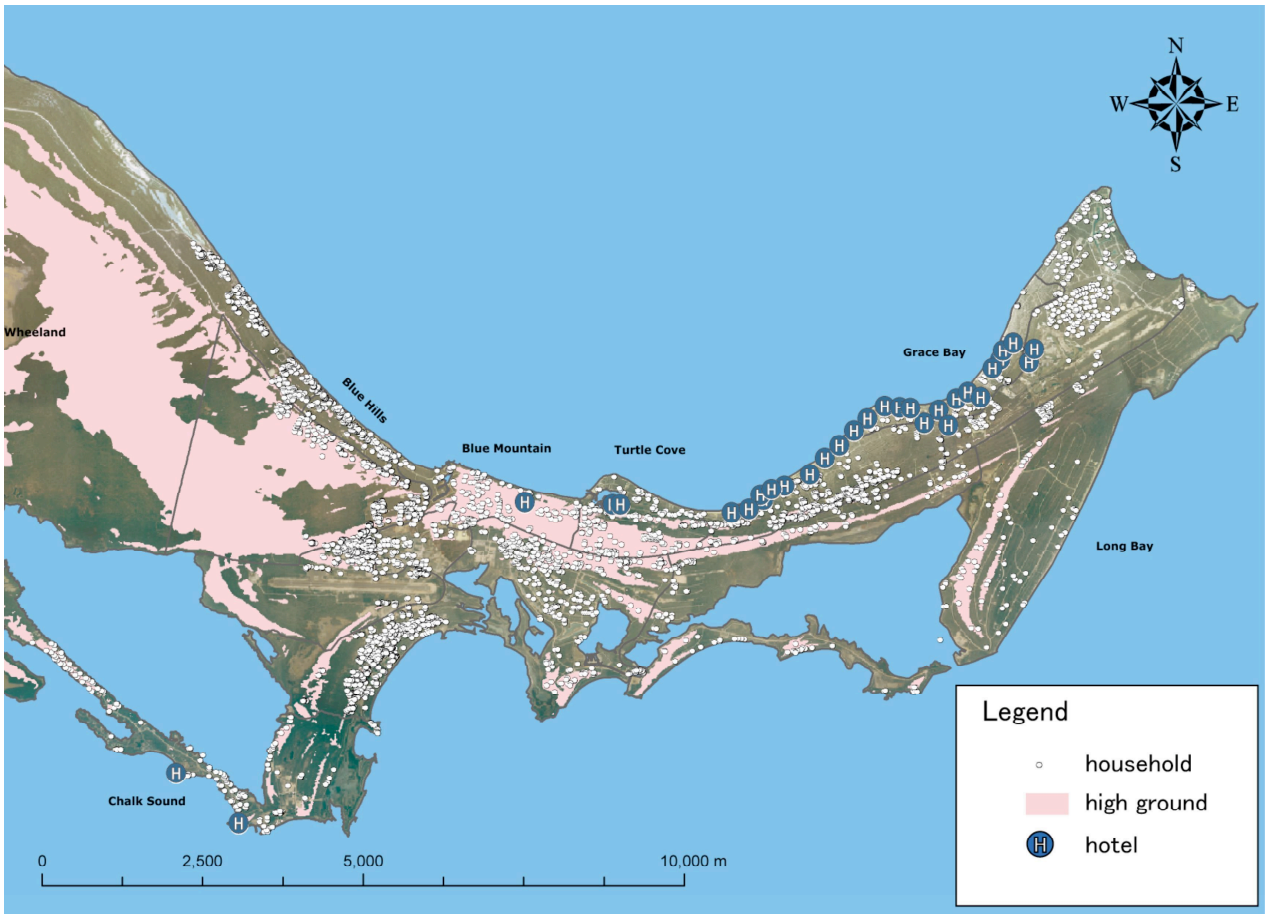

Figure 10: Location of Hotels in Providenciales

Another criteria set up in the simulator was that most households would evacuate to the nearest emergency shelter on foot at a speed of approximately 80 meters per minute. However, persons in areas that are substantially distant from the nearest shelter would have to evacuate via car. For example, the distance from Chalk Sound to the nearest shelter is 5 km, and if residents were to evacuate on foot at 80 meters per minute it would take them approximately 60 minutes to complete evacuation, a potentially dangerous scenario.

3. Tsunami Simulation Model

The tsunami simulator component of the model was used to simulate the different impact scenarios that are possible based on the characteristics of the earthquake and the geological features of the sea floor around Providenciales. The model was used to simulate both a worst and a best-case scenario of a tsunami occurrence in the Caribbean with different possible wave heights estimated reaching the shores of the TCI. Based on these various scenarios/estimates gaps in current disaster management policies were highlighted. Additionally, the range of probable

damage was simulated and the location of vulnerable populations and infrastructures in the island identified. The model will therefore allow the relevant authorities to establish and put in place relevant and essential mitigation strategies for use against the impact of a tsunami. Use of this model will also enable smooth and orderly evacuation of persons located along the coast or other vulnerable sites. In addition, the model can be used to inform land use planning by encouraging the construction of hard measures against tsunamis such as the construction of sea walls or other types of embankment. However, it is important to note that employment of hard measures alone will not stop the tsunami though it may help to reduce its impact. Therefore, a balance between the use of hard measures and soft measures, such as investing in information transmission and educating residents on tsunamis, will be effective in saving lives.

6.0 CONCLUSIONS

The model can be considered a type of dynamic digital "hazard map" as it informs, educates and identifies vulnerable populations. Utility of the model is enhanced by its capacity to depict various scenarios in three-dimensional or graphical formats. This makes presentation of the results more realistic and thus more appealing to residents, irrespective of language differences. The realistic nature scenarios in the model should better persuade residents of the need to take appropriate measures to protect themselves, their family and property from various disasters. The wide range of devices/media used to communicate risk information should ensure maximum and comprehensive coverage of all residents in the Providenciales Multilanguage landscape thus allowing for effective communication of risk information that should result in prompt evacuation from vulnerable areas in the face of an imminent threat. From the disaster managers perspective the tsunami model can be considered as a type of digital disaster manual as it can be used to assess the effectiveness of current disaster management strategies that are in place.

6. REFERENCES

Clerveaux, I. Virginia (2005) Migrants and Resource Utilization in the Turks and Caicos Islands. MPhil Thesis. The University of the West Indies, Mona Jamaica. Unpublished

Cross, T., Bazron, B.J., Dennis, K.K., & Isaacs, M.R. (1989). Towards a culturally competent system of care. Washington, DC: Howard University Press

Department of Economics Planning and Statistics (DEPS).(2006, Turks and Caicos Islands. depstc.org/pressreleases/2006/jun06/0629a.html

Fararo, T.J. (1981. Biased networks and social structure theorems. Social Networks, 2, 1-18.

Green, J.W. (1995). Cultural awareness in the human services. Second Ed. Toronto: Allyn & Bacon.

Imamura, F. (1996. Review of tsunami simulation with a finite difference method. In Long Wave Run-up Models (H. Yeh, P. Liu, and C. Synolakis Ed.) 25-42.

Katada, Toshitaka, Noriyuki Kuwasawa, Harry Yeh, Cherri Pancake (2006) Integrated Simulation of Tsunami Hazards. EERI's Eighth U.S. National Conference on Earthquake Engineering (8NCEE), Paper No.1727.

Katada, Toshitaka, Kuwasawa, Noriyuki, Kanai, Masanobu and Hosoi, Kyohei (2004). Execution and the Evaluation of Disaster Prevention Teaching to the Owase City people using Tsunami Disaster Scenario Simulator Social technological Research Paper Collection, Vol.2, pp.199-208, and October.

Katada, Toshitaka Junsaku Asada, Noriyuki Kuwasawa and Yasushi Oikawa (2000) Development of Practical Scenario Simulator for Dissemination of Disaster Information Journal of Civil Engineering Information Processing System, Vol.9, pp.129-136,

Katada, T., Aoshima, S., and Oikawa. Y. (1996) Oral Communication Network Model for Refuge Warning against Disaster. Proceedings of Japan Urban Planning Society, 31, 757-762. (Japanese)

LaFromboise, T.D., & Foster, S.L. (1992) Cross-cultural training: scientist-practitioner model and methods. Counseling Psychologist, 20(3), 472-489.

James F. Lander and Lowell S. Whiteside (19972) Caribbean Tsunamis: An Initial History. http://www.eird.org/deslizamientos/pdf/eng/doc10729/doc10729.htm. Retrieved December 10, 2007.

Lin, P., Chang, K. -A., & Liu, P. L.-F. (1999) Runup and rundown of solitary waves on sloping beaches, Journal of Waterway, Port, Coastal and Ocean Engineering, ASCE, 125, 247-255.

Martin, F. LaTanya (2003) Cultural Differences in Risk Perception: An Examination of USA and Ghanaian Perception of Risk Communication. MSc. Thesis. Virginia Polytechnic Institute and State University.

Rapoport, A. (1979) A probabilistic approach to networks. Social Networks, 2, 1-18.

Smith Warner International (2006) Turks and Caicos Islands Hazard & Vulnerability Assessment.

Solis, Y. Gabriela, Henry C. Hightower, June Kawaguchi et.al (1995).Guideline on Cultural Diversity and Disaster Management. Final Report Produced within the Canadian Framework for the International Decade for Natural Disaster Reduction. www.epc-pcc.gc.ac/pub/manuals/en_cult.htm. Retrieved October 12, 2005.

Sue, D.W., Arredondo, P., & McDavis, R.J (1992) Multicultural counseling competencies and standards: a call to the profession. Journal of Multicultural Counseling and Development, (20), 64-88.

Sue, D.W. & Sue, D. (1990) Counseling the culturally different. Toronto: Wiley.

Titov, V. V. & Synolakis, C. E. (1998) Numerical modeling of tidal wave run up. Journal of Waterway, Port, Coastal and Ocean Engineering, ASCE, 124(4), 157-171.

FIELD SURVEY OF THE DECEMBER 16, 2004 TSUNAMI AT KANYAKUMARI, INDIA

Arun Bapat,
Seismological Consultant, Pune (India),
Tad Murty,
Department of Civil Engineering, University of Ottawa, Ottawa, Canada.

arun_bapat@vsnl.com

Abstract

The tsunami of 26th December 2004 in the Indian Ocean impacted the town of Kanyakumari at the very southern tip of India. On a coastline of about 4.8 km in length, the tsunami amplitudes varied from about 1.5 m to about 9.5 m. The horizontal extent of inundation ranged from a few meters to about 1,000. The large tsunami run-up variations over such a short distance were caused by wave convergences and divergences due to local shoreline geometry, its orientation and the near shore bathymetric gradients. Apparently, the physical process of quarter wave resonance amplification also played a significant role in enhancing the tsunami run-up at certain locations. The present study reports on the results of the field survey as well as on information gathered through eyewitness accounts.

Figure 1. The Tamil Nadu State in Southeast India.

1. Introduction

The magnitude 9.3 Sumatran Earthquake of 26 December 2004 generated a huge tsunami and caused extensive destruction in Indonesia, Malaysia, Thailand, India, Sri Lanka and other countries bordering the Indian Ocean. The east coast of India was severely affected. Coastal locations as Nagapattanam, Kaddalur were severely affected, while the coastal region of Kanyakumari was struck by a moderate size tsunami. Kanyakumari is a popular tourist destination; therefore it is essential that a suitable tsunami disaster mitigation and management plan be drawn to avert future impact. The National Safety Council (NSC) of India authorized our team to examine this issue and devise suitable scientific measures. The present report details the field survey that was conducted at Kanyakumari from 16 to 20 December 2007. Respectively, Figures 1 and 2 show the Tamil Nadu State in South India and the town of Kanyakumari.

Figure 2. The Town of Kanyakumari in the State Tamil Nadu.

2. **The Inundation Survey**

The extent of inland inundation by tsunami waves is an indication of the level of destruction they can inflict. The collection of such data helps with plans for future mitigation measures. For this reason 4.8 km of the coast of Kanyakumari were surveyed. Survey locations were selected at 50 m intervals along the coast and positioning was determined by GPS (Table 1). Whenever possible, interviews were conducted with eyewitnesses that had been present at that location during the 2004 tsunami event. The details of the interviews are given in Annex I. The collected data were analyzed and summarized with graphs. Figure 3 shows the heights of the tsunami at different locations. Figure. 4 depicts the horizontal extent of inundation.

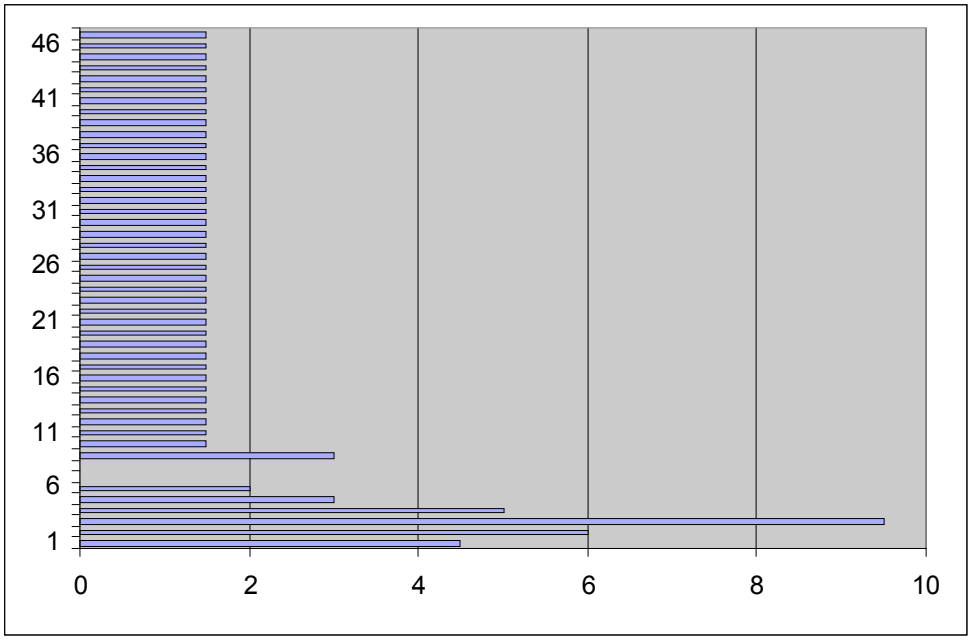

Figure 3. The height of Tsunami at different locations. Observation Points on Vertical axis and Tsunami height (m) on horizontal axes

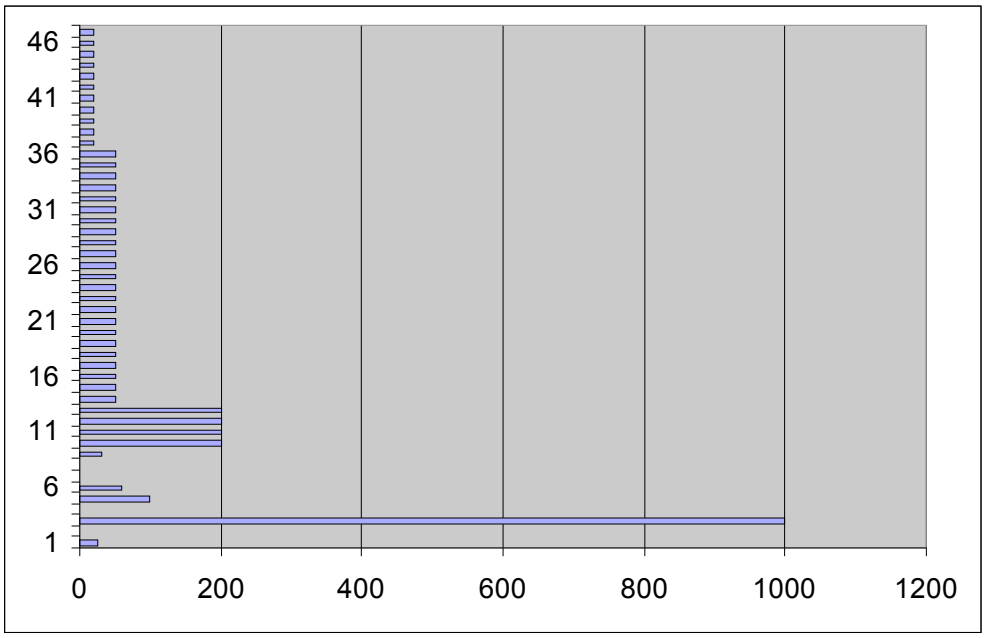

Figure 4. Horizontal extent of Inundation at different points. Observations Points on vertical axis, inundation (m) on horizontal axis.

3. Discussion and Conclusions

The Table, figures and photos (shown in the appendix) provide detailed information about the physical characteristics of the tsunami on the coast of Kanyakumari. The main results from this survey are:

(a) The tsunami run-up height at the majority of the points along the Kanyakumari was about 1.8 m.

(b) At locations 1 to 9 the tsunami run-up heights ranged from 3 to 9.5 m.

(c) The Kanyakumari shoreline appears to have experienced minimum tsunami amplitude of 1.5 m. The Vivekananda Rock Memorial and the Thiruvalluvar Statue might have given partial protection. The tsunami waves hit these two locations first and then arrived at Kanyakumari shoreline.

(d) The horizontal extent of inundation varied from 50 m to 1000 m. It was about 200 m at locations 14 to 36 and about 50 m at points 37 to 46. At some locations where the tsunami height was up to 1.5 m and inundation extent was about 200 m, is an area where numerous of fishermen live and a large number of fishing boats are anchored. At these two locations and other similar locations where extensive tsunami inundation was observed, Gabions could be placed to protect the coastline.

(e) During the survey, the team observed a young coconut tree with color markings on the trunk that clearly indicates the tsunami's height (Photo 1).

(f) Mrs. Muttama Palmani, a 50-year old lady, was struck by the tsunami and got stuck up on a tree. Her nephew Selvaraj was also washed away and got stuck up on another tree (Photos 2 and 3). These observations were useful in determining the height of the tsunami at this location.

(g) A church (shown in Photo 4) has been subsequently repaired. However, the height reached by the tsunami at that location was obvious.

(h) In addition to the placing Gabions, suitable pre-tsunami warning mechanism may be worked out. In addition to the announcements on radio and television, it would be most effective if the tsunami warning were sent by SMS. At present it is possible to send SMS by one operation to about 3000 to 5000 Cell phone users. Suitable mechanism may be worked out with cell telephone companies.

(i) Creation of awareness about tsunami may be taken up as a part of school and community learning activities.

(j) Kanyakumari is about 130 to 150 minutes away from the probable epicentral locations in Indonesia as far as tsunami travel is concerned. If a Tsunamigenic earthquake occurs in Indonesia, it will be known through various websites and through telephone contacts almost immediately. The Tamil Nadu state Disaster Management should establish contacts with Andaman and Nicobar (A & N) Administration. Indonesian Tsunami may hit Andaman within about 20 to 30 minutes. The A & N should immediately inform the District Collector of Nagercoil, which is the headquarters of the district in which the town of Kanyakumari is located.

(k) Periodic assessment of the situation may be routinely undertaken every six months. This will help in reviewing the progress and also help in modifying the mitigation measures. A suitable permanent committee for this purpose may be formed.

Table 1: Location of observation points, GPS Position, tsunami height, inundation and remarks.

Location No.	Latitude (N)	Longitude (E)	Tsunami height (m)	Horz. Inundation (m)	Remarks
01	08° 04.714′	077° 31.895′	4.5	25	Sun set Pt
02	08° 05.403′	077° 29.035′	6	On back water	Keelamanakudi Bridge
03	08° 05.416’	077° 28.588′	9.5	1000	Sothavilai Beach
04	08° 04.761′	077° 32.430′	5	Nil	Old Beach Road
05	08° 04.678′	077° 33.067′	3	100	16 Pillar Mandapam
06	08° 04.896′	077° 33.165′	2	60	Boat Jetty
07	08° 06.134′	077° 32.952′	-	-	Kumarisalkulam. (Panchayat limit on North side)
08	08° 07.577′	077° 33.914′	-	-	Vattakottai (For Ref.)
09	08° 05.654′	077° 33.835′	3	30	Chinnanuttym Muttom (CM)Tample. (KKTP limit Starts on East Beach)
10	08° 05.541′	077° 33.840′	1.5	200	50 m from CM
11	08° 05.525′	077° 33.814′	1.5	200	100 m from CM
12	08° 05.520′	077° 33.789′	1.5	200	150 m from CM
13	08° 05.510′	077° 33.766′	1.5	200	200m from CM
14	08° 05.505′	077° 33.743′	1.5	50	250 m from CM
15	08° 05.498′	077° 33.718′	1.5	50	300 m from CM
16	08° 05.491′	077° 33.694′	1.5	50	350 m from CM
17	08° 05.483′	077° 33.672′	1.5	50	400 m from CM
18	08° 05.477′	077° 33.650′	1.5	50	450 m from CM
19	08° 05.469′	077° 33.630′	1.5	50	500 m from CM
20	08° 05.463′	077° 33.609′	1.5	50	550 m from CM
21	08° 05.453′	077° 33.588′	1.5	50	600 m from CM
22	08° 05.438’	077° 33.568′	1.5	50	650 m from CM
23	08° 05.423′	077° 33.549′	1.5	50	700 m from CM

Location No.	Latitude (N)	Longitude (E)	Tsunami height (m)	Horz. Inundation (m)	Remarks
24	08° 05.412′	077° 33.531′	1.5	50	750 m from CM
25	08° 05.402′	077° 33.508′	1.5	50	800 m from CM
26	08° 05.391′	077° 33.486′	1.5	50	850 m from CM
27	08° 05.379′	077° 33.467′	1.5	50	900 m from CM
28	08° 05.366′	077° 33.449′	1.5	50	950 m from CM
29	08° 05.351′	077° 33.425′	1.5	50	1000 m from CM
30	08° 05.341′	077° 33.405′	1.5	50	1050 m from CM
31	08° 05.331′	077° 33.383′	1.5	50	1100 m from CM
32	08° 05.313′	077° 33.362′	1.5	50	1150 m from CM
33	08° 05.297′	077° 33.338′	1.5	50	1200 m from CM
34	08° 05.274′	077° 33.319′	1.5	50	1250 m from CM
35	08° 05.254′	077° 33.299′	1.5	50	1300 m from CM
36	08° 05.233′	077° 33.282′	1.5	50	1350 m from CM
37	08° 05.209’	077° 33.272′	1.5	20	1400 m from CM
38	08° 05.184′	077° 33.259′	1.5	20	1450 m from CM
39	08° 05.168′	077° 33.213′	1.5	20	1500 m from CM
40	08° 05.072′	077° 33.143′	1.5	20	1550 m from CM
41	08° 05.039′	077° 33.137′	1.5	20	1600 m from CM
42	08° 05.010′	077° 33.142′	1.5	20	1650 m from CM
43	08° 04.985′	077° 33.139′	1.5	20	1700 m from CM
44	08° 04.957′	077° 33.130′	1.5	20	1775 m from CM
45	08° 04.934′	077° 33.125′	1.5	20	1850 m from CM
46	08° 04.908′	077° 33.117’	1.5	20	1925 m from CM
47	08° 04.759′	077° 33.083′	1.5	20	2000 m from CM
48	08° 05.286′	077° 32.819’	-	-	Railway Station (For Ref.)
49	08° 05.235′	077° 32.672′	-	-	Pillar Hospital Road (For Ref.)
50	08° 05.539′	077° 32.610’	-	-	South Kundal Village (Panchayat Border)
51	08° 06.092′	077° 32.456′	-	-	Microwave station (For Ref.)
52	08° 06.135′	077° 32.491’	-	-	Nagarcoil KKRoad
53	08° 06.287′	077° 32.393′	-	-	KK Fire Station
54	08° 05.733′	077° 31.683′	-	-	Railway Crossing
55	08° 04.918′	077° 32.586’	-	-	KK Bus Stand
56	08° 04.911′	077° 32.660′	-	-	St. Michel Community Center for Shelter
57	08° 04.896′	077° 33.021’	-	-	Panchayat Office

Appendix - I

The team begun the tsunami field survey on 17th Dec 2007. The survey was confined to the municipal limits of Kanyakumari and its immediate shoreline of about 4.8 km.

The survey commenced at Sunset Point (GPS Location 08° 04.714′ N and 077° 31.895′ E), identified as KW001. The following information was deduced from interviews with eyewitnesses.

Mr. J. Anthony, age 75, fisherman.

(a) The first tsunami wave arrived at 0930 (Indian Standard time, 5 hours 30 minutes ahead of Universal time) and then the sea receded by 4.0 to 5.0 km.
(b) His boat was washed away by the waves.
(c) The tsunami wave inundated about 10 m from the high tide line, to a height 4 to 5 m above mean sea level.
(d) After the tsunami inundation, the remaining seawater had a bad smell and caused allergies with blisters to local residents.

Mr. Domni, age 40, Fisherman.

(a) A small wave arrived at 0800 hours. At 1000 the sea receded.
(b) The big tsunami wave arrived at 1015 with a height of 5 m.
(c) The previous day, there was high fish catch. In the days following the tsunami the fish catch was reduced.
(d) There was a continuous warning by local church authorities by ringing the church bell.
(e) There was a rise in skin diseases after the tsunami.

Mr.. Christraj Kennedy, Age 45, Fisherman.

(a) At 0800 hours, a slightly higher wave than normal arrived.
(b) At 1000 hours, the sea receded up to 2.5 km.
(c) At 1115 hours a large tsunami wave struck the shoreline.

The second point of observation was at Keelamanakuda (East Manakkudi, GPS Location 08° 05.403′ N and 077°29.035′ E). This has been identified as KW002. The observations here are as follows.

At this site there was a prefabricated bridge of two segments of 30 m length each resting on 4 pillars and the side bunds having a span of 15 m each. The two segments were dislodged by the tsunami. The western segment was thrown up to 30 m towards the western bank and the other was thrown to about 8 m on the eastern side. (Photo 5)

On the western side of the bridge, inside a house compound, a coconut tree had discoloration (Photo 1) up to a height of 6 m. This mark could be correlated to the tsunami height at that location (plus ground height of about 3 m).

The third point of observation was at Sothaivavilai Beach (GPS location 08° 05.416′ N and 077°28.588′ E). This has been identified as KW003. The observations are as follows.

Mrs. Mutthammal, wife of Palmani, age 48 provided the following observations:

(a) She was in a thatched shed, which accommodates 20 persons, where she serves breakfast and lunch.
(b) At 0610 hrs the seawater reached up to the road. At 0810 a slightly higher wave was observed. At 1100 hrs the sea receded up to 3 km.
(c) At 1120 hrs a huge wave struck. She was lifted, her head hit a lamppost and she lost a tooth by the impact. She became unconscious and was carried up to the top of a palm tree (Photo 2) situated about 10 m from her shop. Her sister's 30-year son Silvaraj was also washed away and got stuck up at a coconut tree located at about 25-30 m from the shop (Photo 3). Her husband was in bathroom and could not move out as he had suffered injuries. Both of them were in the hospital afterwards for 42 days (wife) and 45 days (husband).
(d) After about 20 minutes, the sea level came down. Selvaraj shouted for help and people came and rescued them. The heights of both trees positively indicate that the tsunami run-up height was about 7-8 m (plus ground to sea level of 2 m).
(e) The tsunami run-up height is corroborated by the corrosion of the electrical fittings on the nearby lamppost.
(f) The spiral staircase of the sun set view tower in that location was washed away and the water level was up to the bottom brim of the flooring. It is understood that a person who was on the top of the tower jumped into the water. His body could not be retrieved.
(g) In the Manakkudi village enroot to the beach, a Church located at about 2m above sea level has undergone repair about 6 m from ground through out the sea side wall (Photo 4).

The fourth point of observation was at 100 m east of KW001 (GPS location 08° 04.764′ N and 077°32.430′ E) near Kamaraj Mandapam. This has been identified as KW004. The observations at this point are as follows.

Mr. Perumal, age 35, street side goggle seller, had the following observations:

He saw waves at 0600 hrs, 0900 hrs and 1100 hrs. The wave at 0900 hrs receded about 2 km. The tsunami height at this location was about 5 m.

The fifth point of observation was at sixteen-piller mandapam (GPS location 08° 04.678′ N and 077°33.067′ E) near Kamaraj Mandapum. This has been identified as KW005. The local observations are as follows.

Mrs. Joyce Mery, age 39, fruit seller, reported:

(a) At 0700 the sea receded about 500 m.
(b) The first wave came at 0930 up to mandapam. The next wave came from the Thiruvalluar Statue to Bhagavati Amman Kovil (temple). The third wave came at 1200 hrs. The wave height was 3 m.

Observations of Mr. Krishna Pillai, President of Taxi Owners' Association:

(a) At 0900 on 26 December 2004 he saw people crying and running and their numbers were rapidly increasing. He saw crowds at the Vivekanand rock memorial from the Sea View Hotel. His relative and friends in Andaman and Chennai telephoned him that the sea was unusually rough.
(b) At around 0945 the sea begun to recede and there was no water between the jetty and Vivekanand Rock Memorial and the Thiruvalluar statue. A similar situation had never occurred in the past.
(c) Around 1100 large sea waves started hitting the coastline and destroyed a number of ships and other structures. The waves continued to hit for about 20 to 25 minutes. The whole event lasted for about two and half hours.
(d) One boat at Kanniyakumari jetty was swept away and was found after two months at Earnakulam.

Observations by Mr. C. Swarnapandian, Manager, Phoompuhar Shipping Corporation (Govt. of Tamil Nadu Enterprise):

(a) At around midnight on 25th December 2004, it was reported by the security guard that a powerful wave struck the coast and that small boats were damaged. (See Photo No.6 of damaged boat).
(b) His son informed him on the telephone about the rough sea conditions at Chennai. At about 0900 hrs he went out and saw that the seawater was highly muddier than normal and that the wave heights were higher than usual.
(c) He immediately stopped the ferry, which was about to start. The shipping corporation has two ferryboats.
(d) At 0945 hrs the first tsunami wave arrived from east. This was followed by several more waves of increasing heights. The most powerful wave of 8.0 m height occurred at 1110 hrs.
(e) Both ferryboats were lifted up by the tsunami waves and were placed on the jetty.

Photo 1. Shows the tsunami mark on the coconut tree and metallic part on the electric lamppost, which have been corroded.

Photo 2. Trapped lady in center

Photo 3. Selvaraj was stuck up at the tree where he is standing. The distance between this tree and the tree on which Muttama was hanging is about 15 m.

Photo 4. The repairs on first floor indicate damage during tsunami and the level of Tsunami height.

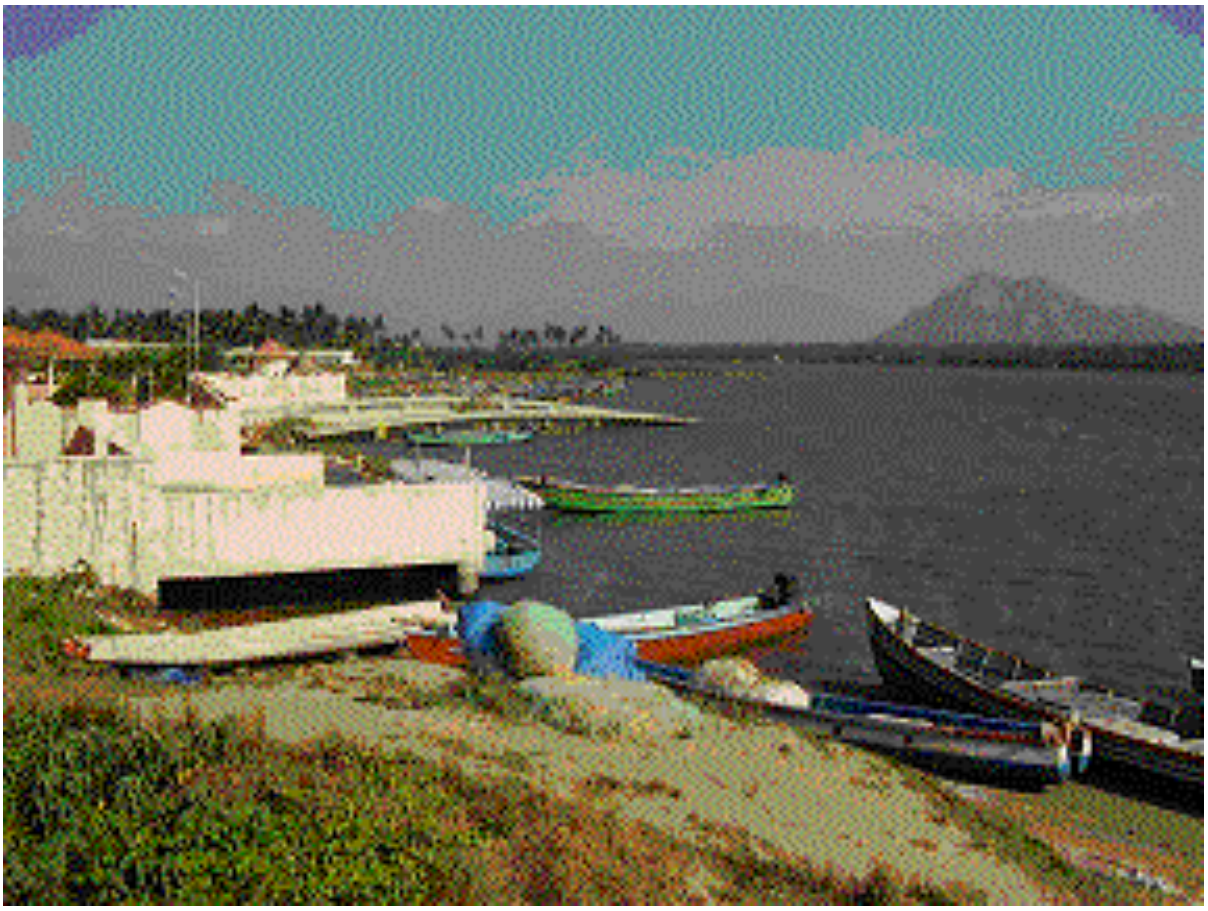

Photo 5. Damaged part of the bridge seen at left of center and boats.

Photo 6. Damaged bridge is seen at rear center. Bridge on right is the new bridge.

The Tsunami Society
P. O. Box 2117
Ewa Beach, HI 96706-0117, USA

WWW.TSUNAMISOCIETY.ORG